



Technical University of Crete
Bachelor's thesis in Production Systems

Use of UAV for 3D visualization of air pollutants in urban areas.

Thesis by
Antonios Koutroumpas

July 2017

Supervisor: Spiros Papaefthimiou





Acknowledgements

This quantitative research was carried out in Technical University of Crete, Chania, Greece. It is part of a larger study that aimed to evaluate the air quality using Unmanned Aerial Vehicles. I take this opportunity to express my gratitude to several people for their aid and support. I am grateful to Spiros Papaefthimiou, for bringing up the idea to us and inspiring us to work through his motivational feedback. Moreover I thank him for supervising, guiding and supporting me during the process of this research. Thanks are also given to my co-researchers Loukakis Konstantinos, Kanelakis Konstantinos and Nikoloudakis Giorgos for the execution of this research, as well as to my fellow students for screening and helping me throughout the build-up of this report. Last, I would like to express my gratitude to the Technical University of Crete for providing the services and equipment needed to carry out this experiment.

Antonios Koutroumpas,

July 2017, Chania, Greece



Abstract

The evaluation of air quality has been traditionally conducted by ground based monitoring, through the use of manned aircrafts and/or satellites. Nevertheless, fast performing, comprehensive and cost efficient data collection is not always possible due to the complexity of the ground, and moving sources or physical barriers. Therefore Small Unmanned Aerial Vehicles (UAVs) equipped with various sensors have been recently introduced for in-situ data acquisition, as they can offer new approaches and research opportunities in many fields. The main purpose of my thesis is:

- i. To visualize air pollutant emissions, measured through sensors located on UAV,
- ii. Create a 3d visualization mesh of the acquired data and
- iii. Visualize data on a geo-referenced 3d layer/model of an urban area or building.

The sensors would be able to measure: Temperature, Atmospheric pressure, Carbon, Sulphur and Nitrogen oxides. The location of the investigation was carried out on the campus of the Technical University of Crete. This study also has the potential to be extended to areas such as airports, harbors and industrial zones. Furthermore, an application of this thesis was carried out as part of my practical training at the Mediterranean Institute of Chania, where the detection and the spread of the Tristeza virus was studied in a citrus crop (Appendix A).

Περίληψη

Η αξιολόγηση της ποιότητας του αέρα παραδοσιακά γινόταν από συστήματα εδάφους, μέσω επανδρωμένων αεροσκαφών και δορυφόρων. Παρ' όλα αυτά, η γρήγορη, πλήρης και οικονομικά αποδοτική συλλογή δεδομένων δεν είναι πάντα επιτεύξιμη λόγω της πολυπλοκότητας του εδάφους, των κινούμενων πηγών ή λόγω φυσικών εμποδίων. Τα μη επανδρωμένα ιπτάμενα οχήματα (UAV) εξοπλισμένα με αισθητήρες διαφόρων τύπων έχουν εισαχθεί για την επί τόπου απόκτηση δεδομένων, καθώς μπορούν να προσφέρουν νέες προσεγγίσεις και ερευνητικές δυνατότητες σε πολλούς τομείς. Κύριος σκοπός της παρούσας διπλωματικής ήταν:

- i. η απεικόνιση εκπομπών αερίων ρύπων που μετρώνται μέσω αισθητήρων που βρίσκονται σε UAV,
- ii. η δημιουργία ενός 3D πλέγματος για την απεικόνιση των δεδομένων και
- iii. η οπτικοποίηση των δεδομένων σε ένα γεωαναφορικό 3D μοντέλο μιας αστικής περιοχής ή κτιρίου.

Οι αισθητήρες μπορούν να μετρήσουν: θερμοκρασία, ατμοσφαιρική πίεση, αέριες εκπομπές οξειδίων άνθρακα, θείου και αζώτου .Η περιοχή μελέτης ήταν η



πανεπιστημιούπολη στο Πολυτεχνείο Κρήτης. Η μελέτη αυτή μπορεί να εφαρμοστεί σε περιοχές όπως αεροδρόμια, λιμάνια και βιομηχανικές ζώνες. Επιπλέον, πραγματοποιήθηκε εφαρμογή αυτής της διατριβής στο πλαίσιο της πρακτικής μου άσκησης στο Μεσογειακό Ινστιτούτο Χανίων, όπου μελετήθηκε η ανίχνευση και η εξάπλωση του ιού της Τριστέτσας σε καλλιέργεια εσπεριδοειδών (Παράρτημα A).



Table of Contents

Acknowledgements.....	iii
Abstract.....	iv
Περίληψη	iv
Table of Contents.....	vi
List of Figures	viii
List of Tables.....	xii
Chapter 1	1
1.1 Motivation.....	1
1.2 Objectives and scope.....	2
1.3 Structure of the thesis	2
Chapter 2	3
2.1 UAVs.....	3
2.1.1 Introduction to UAVs	3
2.1.2 Classification of UAVs.....	4
2.1.3 Advantages and limitations in the use of UAVs.....	6
2.1.4 Regulation.....	6
2.2 Fundamentals and Applications of 3D Modeling	8
2.2.1 Definition of 3D Modeling	8
2.2.2 Procedural 3D Modeling.....	9
2.3 Air pollution	10
2.3.1 Definition of Air pollutants and polluting effects.....	10
2.3.2 Causes of Air pollution	11
2.3.3 Effects of Air pollution	11
2.3.4 Toxicity of Pollutants	12
i. Sulfur Dioxide (SO ₂).....	12
ii. Nitrogen Dioxide (NO ₂)	13
iii. Carbon Dioxide (CO ₂)	13
iv. Carbon Monoxide (CO).....	14
v. Ozone (O ₃).....	14
Chapter 3	15
3.1 Platform: DJI Phantom 4.....	15
3.1.1 Quadrotor flight control.....	16
3.1.2 Hardware and Sensors	17
3.1.3 Onboard Intelligence.....	19
3.1.4 Operational capacity	20
3.2 Aerial Photography	20
3.2.1 Study area.....	21
3.2.2 Flight planning.....	21
3.2.3 Customization of data	23



3.2.4 Data Procedure.....	27
3.3 Air Data Measurements	28
3.3.1 System Architecture.....	29
3.3.2 Wasp mote and Meshlium.....	30
3.3.3 Gas Sensor Board	32
3.3.4 Assembly of the sensors with the Phantom 4	38
3.4 Data Processing.....	41
3.4.1 Visualization tools	41
3.4.2 Surface Interpolation Algorithms	41
3.4.3 2D visualization.....	44
3.4.4 3D visualization.....	48
Chapter 4	55
4.1 Final 3D model and Orthomosaic.....	55
4.2 2D maps of data visualization	56
4.3 Geo-referencing junction of 3D model and 3D layers	66
Chapter 5	72
5.1 Conclusions	72
5.2 Future Work	73
5.3 Other areas of application	73
References	75
Appendix A	80



List of Figures

Figure 3.1: DJI Phantom 4	15
Figure 3.2: DJI Phantom 4 Antenna Range Booster.....	16
Figure 3.3: Free body diagram of a quadrotor helicopter	17
Figure 3.4: DJI Phantom 4 onboard 4K camera.....	19
Figure 3.5: Study area	21
Figure 3.6: Pix4dCapture	22
Figure 3.7: Double Grid Mission	22
Figure 3.8: Circular Mission	23
Figure 3.9: Processing options of the first stage	24
Figure 3.10: Point Cloud Options.....	25
Figure 3.11: 3D Textured Mesh options.....	26
Figure 3.12: Dsm, Orthomosaic and Index options.....	27
Figure 3.13: The final 3D Triangle Mesh.....	28
Figure 3.14: Outside of the fixed station to monitor air pollution at Laranjeiro, Lisbon.....	29
Figure 3.15: Functional diagram of the air quality monitoring station	30
Figure 3.16: Libelium Waspmove	31
Figure 3.17: Libelium Meshlium Xtreme.....	32
Figure 3.18: Gas Sensor Board Pro	33
Figure 3.19: The CO sensor.....	33
Figure 3.20: The CO ₂ sensor	34
Figure 3.21: The SO ₂ sensor.....	35
Figure 3.22: The O ₃ sensor	35
Figure 3.23: The NO ₂ sensor	36
Figure 3.24: The NH ₃ sensor.....	37
Figure 3.25: The Temperature, Humidity and Pressure sensor	38
Figure 3.26: The printed boxes of the sensors and the batteries.....	38
Figure 3.27: The assembly with the Phantom 4	39
Figure 3.28: Side view of the assembly	39
Figure 3.29: DJI's GO application.....	40



Figure 3.30: The database which collects the air-measurements.....	40
Figure 3.31: Inverse Distance Weighted	42
Figure 3.32: Natural Neighbor.....	43
Figure 3.33: Spline.....	43
Figure 3.34: Kriging	44
Figure 3.35: Initializing the data in 2D	45
Figure 3.36: Point Cloud.....	45
Figure 3.37: Exporting data to a shapefile	46
Figure 3.38: Adding a base-map	46
Figure 3.39: The IDW Spatial Analyst	47
Figure 3.40: The result of the IDW method.....	47
Figure 3.41: Initializing the data in 3D	48
Figure 3.42: Point Cloud.....	48
Figure 3.43: The IDW Spatial Analyst	49
Figure 3.44: The result of the IDW method.....	49
Figure 3.45: Exporting 3D layer into .wrl format.....	50
Figure 3.46: Importing the 3D mesh.....	50
Figure 3.47: Setting the position of the mesh at the beggining of the axes.....	51
Figure 3.48: Applying the .jpg file to the.wrl file	51
Figure 3.49: Selecting the image file from the Material editor	52
Figure 3.50: Setting transparency to the layer.....	52
Figure 3.51: The geo-referenced layer above the 3D model.....	53
Figure 4.1: The created 3D mesh	55
Figure 4.2: The created mesh from another view.....	55
Figure 4.3: The created Orthomosaic.....	56
Figure 4.4: CO measurements at 30 meters	57
Figure 4.5: CO measurements at 40 meters	57
Figure 4.6: The two CO layers attached	58
Figure 4.7: CO ₂ measurements at 30 meters	58
Figure 4.8: CO ₂ measurements at 40 meters	59



Figure 4.9: The two CO ₂ layers attached	59
Figure 4.10: O ₃ measurements at 30 meters.....	60
Figure 4.11: O ₃ measurements at 40 meters.....	60
Figure 4.12: The two O ₃ layers attached.....	61
Figure 4.13: Temperature measurements at 30 meters	61
Figure 4.14: Temperature measurements at 40 meters	62
Figure 4.15: The two temperature layers attached.....	62
Figure 4.16: Humidity measurements at 30 meters	63
Figure 4.17: Humidity measurements at 40 meters	63
Figure 4.18: The two humidity layers attached.....	64
Figure 4.19: Atmospheric pressure measurements at 30 meters	64
Figure 4.20: Atmospheric pressure measurements at 40 meters	65
Figure 4.21: The two atmospheric pressure layers attached	65
Figure 4.22: Top view of CO	66
Figure 4.23: Angle view of CO	66
Figure 4.24: Left view of CO	66
Figure 4.25: Top view of CO ₂	67
Figure 4.26: Angle view of CO ₂	67
Figure 4.27: Left view of CO ₂	67
Figure 4.28: Top view of O ₃	68
Figure 4.29: Angle view of O ₃	68
Figure 4.30: Left view of O ₃	68
Figure 4.31: Top view of Temperature	69
Figure 4.32: Angle view of Temperature.....	69
Figure 4.33: Left view of Temperature	69
Figure 4.34: Top view of Humidity	70
Figure 4.35: Angle view of Humidity	70
Figure 4.36: Left view of Humidity	70
Figure 4.37: Top view of Pressure.....	71
Figure 4.38: Angle view of Pressure	71



Figure 4.39: Left view of Pressure.....71



List of Tables

Table 2.1 – Different types of drones on the basis of weight.....	6
Table 2.2 – Example of military classification	6
Table 2.3 – Differences between recreational and commercial use (FAA, 2014).....	9
Table 3.1 – CO sensor characteristics	33
Table 3.2 - CO ₂ sensor characteristics.....	34
Table 3.3 - SO ₂ sensor characteristics	34
Table 3.4 - O ₃ sensor characteristics.....	35
Table 3.5 - NO ₂ sensor characteristics.....	36
Table 3.6 - NH ₃ sensor characteristics	36
Table 3.7 - Electrical characteristics and Temperature sensor characteristics	37
Table 3.8 - Humidity and Pressure sensors characteristics	37

Chapter 1

Introduction

This Chapter underlines the motivation, the objectives and the structure of this thesis.

1.1 Motivation

The content of the surrounding air changes every day, owing to not only natural but also anthropogenic emissions which, when released into the atmosphere as aerosols, alter the air quality and human health [1]. Nevertheless, it is well known that air pollution has been recognized as the ninth largest health risk factor globally [2]. Besides, atmospheric pollution not only reduces agriculture yields, visibility, sunlight at ground level and snowfall, but also increases atmospheric heating as well [3,4]. Due to these impacts, it is major importance the continuous air quality assessment. In order to quantify the effects of air pollutants on human health and the environment, accurate information on the components of aerosol distribution is needed [5,6]. Nevertheless, spatial and temporal resolution of data from ground, manned aircraft [7,8] and satellite measurements is relatively low and often inadequate for local and regional applications. Moreover, satellite and airborne sensors can be extremely costly and as a result limit the use of these platforms for routine analysis. Furthermore, collect measurements close to pollutant sources it is not always achievable and can be dangerous or risky for manned aircrafts [9,10]. All these reasons encourage the use of small, lightweight UAVs for a wide range of applications, including atmospheric measurements. From this point of view, the small, lightweight UAVs are very interesting tools, as they can provide more precise data on gas emissions throughout the atmospheric column and give the opportunity to better understand air quality and its composition in specific atmospheric layers [11,12]. In addition, UAVs are quickly deployable, cover large areas and can monitor remote, dangerous or inaccessible locations, increasing operational flexibility and resolution over land-based methods [13,14]. Since the use of UAV for research purposes is relatively new, the aims of this thesis were to: (1) visualize the air pollutant emissions, which were measured through sensors located on UAV, (2) create a 3d visualization mesh of the acquired data and (3) visualize data on a geo-referenced 3d model of an urban area. By and large, this configuration of the



two 3D models (acquired air data and geo-referenced model), contribute to detect and better understand the distribution of gas emissions in the atmosphere and gives the opportunity to interfere where is necessary.

1.2 Objectives and scope

This research was motivated by the current problems that are faced due to air pollution worldwide. The area of investigation of this thesis was the Technical University of Crete (TUC). Although, the University is an area of minor importance as regards the air pollutants, this thesis suggests an alternative methodology, of acquiring and visualizing data, that can be applied in many fields, like harbors and industrial zones. Without doubt the result of this research could serve as a reference for further investigation.

1.3 Structure of the thesis

This Bachelor's Thesis consists of introduction, theoretical part, a practical part, results and summary. This thesis starts with the introduction which gives an overview of the topic, stated aim and the structure of this thesis. The theoretical part of this thesis is divided into three sections. The first part analyses the technology of UAVs, states the advantages of UAVs in remote sensing and classify them into categories. The second one describes the fundamentals and applications of 3D modeling whereas the last one illustrates the nature of air pollutants, their effects and what causes them. The practical part of this thesis is focused on 3D modeling of rural areas. As final result of the practical part, a 3D model of the Technical University of Crete (that is located near the city of Chania) was created. Thus, the measurements of a sensor, located on the drone, were processed via ArcGis software for 3D visualization. This part of the thesis starts with a chapter about the case study area. It includes a description of the chosen area and of the data which were used for modeling. The next chapter explains the data processing and the modeling process. It covers the steps of data preparation before the import into modeling software and the data import, then explains the steps of procedural modeling and describes the problems which occurred and their solutions. After the practical part, follows an overview of the results. There two types of results, 2D and 3D, where the 2D data were visualized on a map and the 3D data on a 3D geo-referenced 3D model. The last section of this Bachelor's thesis is the summary. It consists of conclusion and gives suggestions for improvement and further research.



Chapter 2

Related Work and Background

This Chapter describes the theoretical part of this thesis, giving an introduction to the technology of UAVs, the fundamentals of 3D modeling and the air pollutants.

2.1 UAVs

2.1.1 Introduction to UAVs

Unmanned Aerial Vehicle is an aircraft without a pilot or like van Blyenburgh states “UAVs are to be understood as uninhabited and reusable motorized aerial vehicles.” [15]. Furthermore, these vehicles are remotely controlled, semi-autonomous, autonomous, or have a combination of these capabilities. In a technological context, a drone is an unmanned aircraft, like a flying robot. The aircrafts may be remotely controlled or can fly autonomously through software-controlled flight plans in their embedded systems working in conjunction with onboard sensors and GPS. Although, UAVs have been used for over a hundred years now, the term drone became to existence only after 1930s. At first, UAVs were used only for target practice and it was after the 60s that operated for military reconnaissance missions. It was only after the 70s that drones were equipped with live video cameras and the ability to send photos back to the base. Furthermore, the technological advancements of military drones have led to the development of the civil drones. The first civilian UAVs were in the form of airplane and helicopter models and they flew by radio controls with no autonomy on-board. Fortunately, the development of technology has made it possible to have autonomous drones at home, extending their applications in many fields. As regards the shape of a drone can be almost anything, like “fixed wing, rotorcraft, tilt rotor, or airship” [16]. Merriam-Webster dictionary states that a rotorcraft is “an aircraft (as a helicopter) whose lift is derived principally from rotating aero-foils”. The term Rotorcraft is a bit fuzzy, since it includes everything gaining lift from rotating aerofoils. In order to separate helicopters from the differently working aircrafts using rotors directed upwards only, the term multicopter was invented [17]. Thus, the term multicopter (or quadcopter to be more specific) is used in this thesis to emphasize the particular type of the drone used. Some other drones



types are usually airplanes which are used for long distance flying, but cannot have as big payload compared to the multicopters.

2.1.2 Classification of UAVs

As the use of drones for civil purposes is relatively new, there is no much of legislation existing yet. However, in order to conduct legislation, a classification is needed to figure out the different kind of necessities. This chapter describes the current status of drone classification as European Parliamentary Research Service [18] (EPRS), European Aviation Safety Agency (EASA) [16] and National Aeronautics and Space Administration (NASA) [19] have proposed.

Table 2.1 - Different types of drones on the basis of weight

Type of drone	Current and potential future uses	Current regulation
Small (<20/25kg) Price 140-28000€	Leisure and commercial use (e.g. surveillance, inspection, photography)	Falls under Member State regulations
Light (20/25-150kg) Price 55000-420000€	Used in geospatial surveying and wide-area surveillance. Potential to inspect pipelines and power cables, spray crops, search and rescue, control borders and monitor forest fires	Falls under Member State regulations
Large (>150kg) Price 670000€ and above	Used by the military and defense forces. Potential to carry cargo and passengers	Civil drones with an operating mass of more than 150 kg fall under Regulation 216/2008/EC and EASA competency, unless operated by a state agency

To begin with, there is need to classify drones in a board and simple way. As drone is an ‘aircraft and its elements which are operated with no pilot on board’, EPRS categorizes UAVs in two classes:

- Remotely piloted aircraft systems (RPAS): where the aircraft system is piloted from a distant pilot station
- Autonomous UAS: Unmanned: unmanned aircraft system which operates autonomously without pilot intervention.

Nevertheless, a detailed classification with high accuracy seems to be hard to achieve, which can be witnessed from the amount of classification listed by NASA [20]. Some of the parameters are take-off weight, speed, operational



altitude, distance and environment, purpose of use and kinetic energy. Especially the kinetic energy is major importance as it defines the probable damage caused by a collision. Subsequently, these parameters are combined differently with weight being the fundamental factor. Table 1 illustrates a primal example of a classification from EPRS. The following table (Table 2.2) classifies drone into the three most common parameters and considers also the smaller drones. In addition, it is worth mentioning, that only micro and mini classes are likely to be used in civilian use.

Table 2.2 - Example of military classification

Class	Mass Range [kg]	Operating Area	Operating Altitudes [m], flight level [FL]
Micro	<1	Local	<150
Mini	1-14	Local	30-3000
Tactical	14-455	Regional	460-5500
Medium altitude	455-13600	Regional/National	5500-FL600
High altitude	455-13600	Regional/National/International	>FL600
Heavy	>13600	National/International	5500-FL450

Additionally, EASA [\[21\]](#) has suggested a three category classification based on the risk for the operation of drones. These categories are:

- a. 'Open' category (low risk). No authorization is required to operate, as long as forbidden or restricted drone zones, as defined by the national aviation authority (NAA), are respected.
- b. 'Specific' category (medium risk). Authorization is required by a national aviation authority (NAA), following a risk assessment performed by the operator. Some standard scenarios will be published by EASA providing the evaluation of the risk of that specific operation and the list of the required mitigation measures.
- c. 'Certified' category (higher risk). Here the requirements are comparable to those for manned aviation. Oversight by NAA (issue of licenses and approval of maintenance, operations, training, ATM/ANS and aerodromes organizations) and by EASA (design and approval of foreign organizations) will be required according to a process similar to manned aviation.

Moreover, the military classifications differ from the civilian. Even though, some of the parameters are the same, e.g. weight, maximum altitude and range, their



values are different (EASA, 2015). For instance, civilian classifications define operational weight over 150 kg, whereas military classifications define it over 2000 kg [22].

2.1.3 Advantages and limitations in the use of UAVs

As far as the advantages in the use of UAVs are concerned, UAVs give the opportunity to operate at high risk situations without endangering a human life and reaching inaccessible areas, at low altitude and at flight profiles close to the objects where manned systems cannot be flown. These areas can be for example natural disaster sites, e.g. mountainous and volcanic areas, flood plains, desert areas and scenes of accidents. In these places, where the access is difficult and no flight permission is given to manned aircrafts, UAVs sometimes are the only practical alternative. Moreover, even at cloudy and drizzly weather conditions, UAVs can still acquire data, as long as the distance to the object permits flying below the clouds. On the contrary, manned aircrafts cannot collect data at the same weather conditions with large format cameras due to high flight altitude. Furthermore, UAVs are not loaded with physiological limitations and economic expenses of human pilots. In addition, unmanned aircrafts provide in-situ data measurements, since they transmit image, video and orientation data in real time to the ground control station. Nowadays UAVs are less expensive than before, thus they have lower operating costs compared to manned aircrafts. As cost efficient tools, can be applied also for photogrammetry purposes like creating high resolution texture maps on existing DSMs or 3D-models. There is no disputing the fact that, the implementation of GPS/INS systems combined with the stabilization and navigation units allow precise flights, and simultaneously assure sufficient image coverage and overlap, giving the opportunity to the user to estimate the expected product accuracy preflight. As regards the limitations of UAVs, are mainly technical issues. Low-cost UAVs, in order to limit their payload in weight and dimension, are equipped with low weight sensors and small or medium format amateur cameras. As a result, UAVs have to acquire more images in order to obtain the same image coverage and comparable image resolution whereas less stable sensors result in reduced image quality. Furthermore, low-cost UAVs are normally equipped with less powerful engines, limiting the reachable altitude.

2.1.4 Regulation

Generally, the Radio Controlled (RC) aerial vehicles have not created lots of trouble, as it has not been possible to fly beyond line-of-sight. Besides, without a modern camera and the telecommunication technologies, the only way to control



a RC aircraft is by seeing it with your own eyes. That is the main reason of the limited flight distance. Fixed-wing airplanes have easily flown out of the range of the controller, whereas helicopters have been too unstable to fly far away. Likewise, their lifting capacity has not allowed much of extra equipment on-board. All these made the regulation easy, or even almost unnecessary. Nevertheless, the rapid development of customer electronics has enabled multicopters. Due to the intelligence in the Flight Controller (FC), they are stable enough to stay at the same spot without human intervention. With the use of GPS they can fly by themselves through pre-set waypoints, giving the possibility for multicopter to fly relatively long distances unattended. Multicopters are able to carry even heavy payloads such as digital cameras and video cameras, making them a popular tool to shoot videos on top of audiences. In addition, by using first person view (FPV) setups, the user has the opportunity to pilot the drone with a limited view and information about the surroundings. These new ways of piloting has changed the necessity for legislation completely. Multicopters are being produced in a large scale, simultaneously becoming a consuming product where it is required almost zero knowledge to fly them. This troubles the regulators, who try to protect human lives. Furthermore, EASA lists two more risks groups for drones: "mid-air collision with manned aircraft" and "damage to property". This kind of worries has created a need for regulating the usage of drones all around the world. FAA (Federal Aviation Administration) [23] has already started legislating and restricting the use whereas in China they have already started requiring licenses for the drone pilots [24].

Table 2.3 - Differences between recreational and commercial use

Hobby or Recreation	Not Hobby nor Recreational
Flying a model aircraft at the local model aircraft club.	Receiving money for demonstrating aerobatics with a model aircraft.
Taking photographs with a model aircraft for personal use.	A realtor using a model aircraft to photograph a property that he is trying to sell and using the photos in the property's real estate listing. A person photographing a property or event and selling the photos to someone else.
Using a model aircraft to move a box from point to point without any kind of compensation.	Delivering packages to people for a fee.
Viewing a field to determine whether crops need water when they are grown for personal enjoyment.	Determining whether crops need to be watered that are grown as part of commercial farming operation.



In Greece, the drone regulation conducted and released in 2016. According to the drafts around the world, generally the use of drones for delivering packages, flying over audiences, flying nearby airports etc., is forbidden. Additionally small drones, like toy multicopters and model airplanes, are allowed to be flown without any licenses for recreational use. In the following Table 2 FAA separates recreational use from the non-recreational use. Although recreational use has also strong limitations, like flying only to the visual line of sight, and no flying at all near airports or power stations, some special cases have been made as for instance Amazon, who has already gotten an exemption to test their drones for mail delivery [25]. In Greece the aerial vehicle legislation is done by the Civil Aviation Authority (YPA). The current legislation set the boarders for flying UAVs. According it, flying an UAV is allowed only at the visual line of sight for aircrafts weighted under 25 kg within a safe distance from people at the ground, reaching maximum altitude 400 ft. The law obliges the pilot to inform the Aviation Authority the type of use of the UAV, for example commercial, scientific or recreation activities. Additionally, the airspace, where the UAV is permitted to fly, is chosen according to the AIP GREECE [26]. Furthermore, the aircraft is not allowed to fly within 8 kilometers from the traffic zones of airports. Moreover, it is prohibited flying above people and movable/immovable property assets at a lateral distance of less than 50m in order to protect the personal data. Also it is major importance to register the drone at a special list with name of the holder. The Greek draft does require a drone piloting license, just like the American draft by FAA. Users would also need to take good care of the drone, for example going through a status check-up before every lift-off. In addition, the use of a spotter is allowed. The pilot and spotter must have two separate communication devices available all the time. This restricts the drone going somewhere far away, for example taking a video of a LTE mast and return to the starting point. Likewise, it has been also stated that flying in the night would not be allowed, except for the civil safety like police and firemen. Undoubtedly, it is hard to keep the orientation of the drone in the night [27].

2.2 Fundamentals and Applications of 3D Modeling

2.2.1 Definition of 3D Modeling

As Govil-Pai has stated, modeling is the base of 3D graphics and can be characterized as “*the process of creating a 3D model in the computer*” [28]. This procedure includes three main steps: 3D data acquisition, modeling and rendering. As regards the first step, data about object’s size and depth are collected. There are two main methods of data acquisition – contact



(measurements using tape) and non-contact (laser scanning and measurements taken with total stations). As far as modeling is concerned, it includes clarification of the initial shape, where the main elements of this process are the shape of an object, spatial layout and connectivity of parts that compose the object. In addition, the rendering of the model involves smoothing, morphing and other processing methods to make the final result look more natural. The constructed model in this process is a representation of a factual or abstract entity in order to visualize the structure of it. There are different types of representation:

- Quantitative representation: equations are used in order to illustrate and describe a system's behavior
- Organizational representation: hierarchies are being used to describe classification schemes
- CG (Computer Graphics): models refer to geometrical representation of the entity

Nowadays, 3D modeling has many areas of application, such as animation, architecture, education, design, movies, engineering and others since it allows modeling and simulating the real world.

2.2.2 Procedural 3D Modeling

Overall, Procedural modeling is a term that encloses a number of techniques in computer graphics that create 3D models and textures from sets of rules. Some of the procedural modeling techniques are L-Systems, fractals, and generative modeling, since they apply algorithms for producing scenes. The set of rules may either be embedded into the algorithm, configurable by parameters, or the set of rules is separate from the evaluation engine. Procedural models often exhibit database amplification, meaning that large scenes can be generated from a much smaller amount of rules. If the employed algorithm produces the same output every time, the output doesn't need to be stored. Often, it suffices to start the algorithm with the same random seed to achieve this. Although all modeling techniques on a computer require algorithms to manage and store data at some point, procedural modeling focuses on creating a model from a rule set, rather than editing the model via user input. Procedural modeling is often applied when it would be too bulky to create a 3D model using generic 3D modelers, or when more specialized tools are required.



2.3 Air pollution

2.3.1 Definition of Air pollutants and polluting effects

Air pollution is a major problem in today's societies with increasingly national and international interest. Public awareness and concern continues to rise, and a number of proposals for regulating pollution emissions have been made. Air pollution can be defined as the form that refers to the contamination of the air, irrespective of indoors or outside. A physical, biological or chemical adjustment of the air in the atmosphere can be termed as pollution. It occurs when any harmful gases, dust, smoke enters into the atmosphere and makes it difficult for plants, animals and humans to survive as the air becomes dirty. Furthermore, many pollutants are natural constituents of the air. Plants, animals and natural activity can cause some pollution even without human technology. In other words, animals exhale carbon dioxide, decaying vegetation produces methane, decaying animals produce ammonia and volcanic activity outlets sulphur dioxide in the atmosphere. Moreover, air pollution can be categorized into two sections- Visible air pollution and invisible air pollution. Another way of looking at Air pollution could be any substance that holds the potential to damage the atmosphere or the well-being of the living beings surviving in it. Essentially, if any matter that is not normally in the environment or its concentration is greater than the normal can be considered as pollutant. Nowadays, pollutants are introduced into the environment in significant amounts in the form of industrial waste, accidental discharge, domestic waste and sewage or as by-product of manufacturing processes or other human activities. Even the Ozone layer, that is considered crucial for the existence of the ecosystems on the planet, is decreasing due to increased pollution. Global warming, a direct result of the increased imbalance of gases in the atmosphere has come to be known as the biggest threat and challenge that the contemporary world has to overcome in a bid for survival. In order to understand the causes of air pollution, several divisions can be made. Primarily air pollutants can be caused by primary sources or secondary sources. Those pollutants that are a direct result of the process can be called primary pollutants. In other words, a primary pollutant would be the sulfur-dioxide emitted from factories. Secondary pollutants are the ones that are caused by the inter blending and reactions of primary pollutants. Smog created by the interactions of several primary pollutants is known to be, for instance, as secondary pollutant. On the whole, air pollution, as USA Environmental Protection Agency (EPA) states [29], is usually a mix of sulphur dioxide, ground-level ozone, lead, particulate matter, nitrogen dioxides and carbon monoxide.



2.3.2 Causes of Air pollution

In order to better understand air pollutants and how to encounter them, primly it is major importance to investigate the causes, to wit how they diffused at the atmosphere. To begin with, Sulfur dioxide emitted from the combustion of fossil fuels like coal, petroleum and other factory fuels is the number one cause of air pollution. In the same way, pollution emitting from vehicles including trucks, jeeps, cars, trains, airplanes cause immense amount of pollution. Although, today's technology relies on them to fulfill daily basic needs, the overuse devastates the environment as dangerous gases are polluting the environment. Another major pollutant along with Nitrogen Oxides is Carbon Monoxide, which is caused by improper or incomplete combustion and generally is emitted from vehicles, is produced from both natural and manmade processes. In addition, Ammonia is a very common by product from agriculture related activities and is one of the most hazardous gases in the atmosphere. Due to the rising need of large-scale food production, the use of insecticides, pesticides and fertilizers in agricultural activities has grown quite a lot. Hence, harmful chemicals are emitted into the air, causing air and water pollution. Simultaneously, manufacturing industries release large amount of carbon monoxide, hydrocarbons, organic compounds, and chemicals into the air thereby depleting the quality of air. Undoubtedly manufacturing industries can be found at every corner of the earth and there is no area that has not been affected by it. Likewise, petroleum refineries also release hydrocarbons and various other chemicals that pollute both air and land. As regards the mining operations, mining is a process wherein minerals below the earth are extracted using large equipment. During this process dust and chemicals are released in the air causing massive air pollution. Besides, this is the principal reason which is responsible for the deteriorating health conditions of workers and nearby residents.

2.3.3 Effects of Air pollution

A variety of air pollutants have known or suspected harmful effects on human health and the environment. In most areas of Europe, these pollutants are principally the products of combustion from space heating, power generation or from motor vehicle traffic. Pollutants from these sources may not only prove a problem in the immediate vicinity of these sources but can travel long distances. The effects of air pollution are alarming, especially as regards the human health. Air pollutants are known to create several respiratory and heart conditions along with Cancer, among other threats to the body. Several millions are known to have died due to direct or indirect effects of air pollution. Children in areas exposed to air pollutants are said to commonly suffer from pneumonia and



asthma. Furthermore, the State of Global Air 2017 report [30] states that extensive, long term exposure to fine particulate matter contributed to more than four million premature deaths in 2015 worldwide, where around 1.1 million was only in China and India. Another direct effect is the immediate alterations that the world is witnessing due to Global warming. With increased temperatures worldwide, increase in sea levels and melting of ice from colder regions and icebergs, displacement and loss of habitat have already signaled an impending disaster if actions for preservation and normalization aren't undertaken soon. Moreover, harmful gases like nitrogen oxides and sulfur oxides are released into the atmosphere during the burning of fossil fuels. When it rains, the water droplets combines with these air pollutants, becomes acidic and then falls on the ground in the form of acid rain, which can cause great damage to human, animals and crops. As far as eutrophication is concerned, it is a condition where high amount of nitrogen present in some pollutants gets developed on sea's surface and turns itself into algae and adversely affects fish, plants and animal species. The green colored alga that is present on lakes and ponds is due to presence of this chemical only. By and large, just like humans, animals also face some devastating effects of air pollution. Toxic chemicals present in the air can force wildlife species to move to new place and change their habitat. The toxic pollutants deposit over the surface of the water and can also affect sea animals. Ozone exists in earth's stratosphere and is responsible for protecting humans from harmful ultraviolet (UV) rays. Earth's ozone layer is depleting due to the presence of chlorofluorocarbons, hydro chlorofluorocarbons in the atmosphere. As ozone layer will go thin, it will emit harmful rays back on earth and can cause skin and eye related problems. UV rays also have the capability to affect crops [31].

2.3.4 Toxicity of Pollutants

Hazardous air pollutants, also known as toxic air pollutants or air toxics, are those pollutants that are known or suspected to cause health effects, or adverse environmental effects. Every pollutant has different effect on human health. In this thesis, three main pollutants are measured by sensor (SO_2 , NO_2 and CO_2).

1. Sulfur Dioxide (SO_2):

The prime source of SO_2 in the atmosphere is the burning of fossil fuels by power plants and other industrial facilities. On the other hand, smaller sources of SO_2 emissions include: industrial processes such as extracting metal from ore; natural sources such as volcanoes; and engines, ships and other vehicles and heavy equipment that burn fuel with high sulfur content. As regards the human health, short-term exposures to SO_2 can harm the



human respiratory system and make breathing difficult, whereas children, the elderly, and those who suffer from asthma are particularly sensitive to effects of SO₂. Also, SO₂ emissions that lead to high concentrations of SO₂ in the air generally also lead to the formation of other sulfur oxides (SO_x). SO_x can react with other compounds in the atmosphere to form small particles, where these particles contribute to particulate matter (PM) pollution: particles may penetrate deeply into sensitive parts of the lungs and cause additional health problems. As long as the environmental impact is concerned, at high concentrations, gaseous SO_x can harm trees and plants by damaging foliage and decreasing growth. Lastly, SO₂ and other sulfur oxides can contribute to acid rain which can harm sensitive ecosystems [32].

2. Nitrogen Dioxide (NO₂):

In the case of NO₂, it is primarily passes in the air from the burning of fuel and is formed from emissions from cars, trucks and buses, power plants, and off-road equipment. Breathing air with a high concentration of NO₂ can irritate airways in the human respiratory system. Such exposures over short periods can enhance respiratory diseases, particularly asthma, leading to respiratory symptoms (such as coughing, wheezing or difficulty breathing, whereas people with asthma, as well as children and the elderly are generally at greater risk for health effects of NO₂ [33]. The environmental impact of NO₂ is major importance. NO₂ and other NO_x interact with water, oxygen and other chemicals in the atmosphere to form acid rain, which is disastrous for the sensitive ecosystems such as lakes and forests. Besides, the development of NO_x in the atmosphere contributes to nutrient pollution in coastal waters.

3. Carbon dioxide (CO₂):

The fundamental source of carbon dioxide into the air is from living organisms breathing it out, whereas smaller natural sources are forest fires and volcanoes. At the same time, analogous quantities are absorbed by plants. The burning of fossil fuels (coal, oil and natural gas) for industrial, domestic and transport purposes releases significant, though relatively smaller, amounts. At normal environmental concentrations, carbon dioxide has no impacts on human health. Only at extremely high (artificial) concentrations in an enclosed space with the reduction in oxygen levels could lead to suffocation. On a local scale, increased levels of carbon dioxide are unlikely to cause adverse environmental impacts. On the other hand, it has a main impact on a global scale: It is one of the main "greenhouse gases" contributing to global warming and is used as a



reference against which to rate the "global warming potential" of other greenhouse gases [34].

4. Carbon monoxide (CO):

The main source of carbon monoxide is from petrol vehicles which are not fitted with a catalytic convertor. Carbon monoxide levels in urban areas closely reflect traffic density (in combination with weather conditions). Other man-made sources are power stations and waste incinerators. At a domestic level, faulty gas appliances and cigarette smoking are significant sources of carbon monoxide. Natural processes produce relatively small amounts. Inhalation of carbon monoxide at high concentrations can be fatal, because it prevents the transport of oxygen (in blood) around the body. Releases from poorly maintained appliances in poorly ventilated spaces could result in concentrations high enough to cause death. Long-term exposure to lower concentrations (such as through smoking) could harm unborn babies or cause neurological damage. Carbon monoxide reacts with other pollutants in the air to form potentially harmful ground level ozone. This occurs close to the site of emission. It does not have any significant environmental effects at a global level. [35]

5. Ozone (O₃)

Since ozone comes from chemical reactions among ozone precursors in the atmosphere, the sources of ozone are actually the sources of the precursors. Ozone precursors come from fuel combustion and evaporation associated with cars, trucks, buses and equipment or from large stationary sources such as power plants, oil refineries, and factories. Furthermore, it can be released to the atmosphere as an organic compound evaporation from consumer products such as paints, cleaners and solvents. As regards the effects of ozone at the human health, it can irritate the respiratory system, causing coughing, feel an irritation in throat and/ or experience an uncomfortable sensation in chest and can reduce lung function making it more difficult to breathe deeply. Ground-level ozone can have detrimental effects on plants and ecosystems. These effects include: interfering with the ability of sensitive plants to produce and store food, making them more susceptible to certain diseases, insects, other pollutants, competition and harsh weather damaging the leaves of trees and other plants, negatively impacting the appearance of urban vegetation, as well as vegetation in national parks and recreation areas and reducing forest growth and crop yields, potentially impacting species diversity in ecosystems. [36]



Chapter 3

Methods

In this chapter the tools and the method of this thesis is described, giving a detailed report about the characteristics of the equipment and a step by step analysis of the methodology.

3.1 Platform: DJI Phantom 4

The prior step is to choose a suitable robot platform that enables both the development and testing of outdoor aerial methods. Because of that, a direct choice is to use a quadrotor helicopter, commonly designed to be unmanned aerial vehicle (UAV), due to its small size and extremely maneuverability that allows both indoor and outdoor flights.



Figure 3.1: DJI Phantom 4

Nowadays, small quadrotors with on-board stabilization can be bought off-the-shelf at affordable, to the consumers, prices. These quadrotors make it possible to shift the research from basic control of the platform towards intelligent applications. The platform selected is the Phantom 4 quadrotor helicopter. The main advantages of this quadrotor are its durability and its extended flight time.



The Phantom 4 is equipped with 4k camera on an advanced 3-axis gimbal, which takes out unwanted vibration, and provides live video streaming. Furthermore, it has an ultrasound sensor and an inertial unit that measures pitch, roll, yaw and accelerations along all axes. The vehicle is controlled by sending commands over a Wi-Fi connection.



Figure 3.2: DJI Phantom 4 Antenna Range Booster

In this chapter, the Phantom 4 is evaluated as a robotic platform. The flight control of a quadrotor is described, drone's hardware is listed and the intelligent onboard software is described.

3.1.1 Quadrotor flight control

As regards the mechanical structure of a quadrotor, it consists of four rotors attached to a body frame. Furthermore, each pair of opposite rotors (pair 1; 3 and pair 2; 4) is turning the same direction, where one pair is turning clockwise and the other counter-clockwise. Each rotor produces both a thrust T and torque about its center of rotation, as well as a drag force D_b opposite to the vehicle's direction of flight. Thrust T , is a force that is generated by expelling or accelerating mass in one direction. The accelerated mass will cause a force of equal magnitude but opposite direction on that system. Torque is the tendency of a force to rotate an object about an axis. Drag D_b is the force that opposes the motion of an aircraft through the air. This force depends on velocity of the vehicle and de-accelerates the vehicle if insufficient thrust is generated. Together the motors should generate



sufficient vertical thrust to stay airborne, which is indicated by the gravity force mg in the direction e_D .

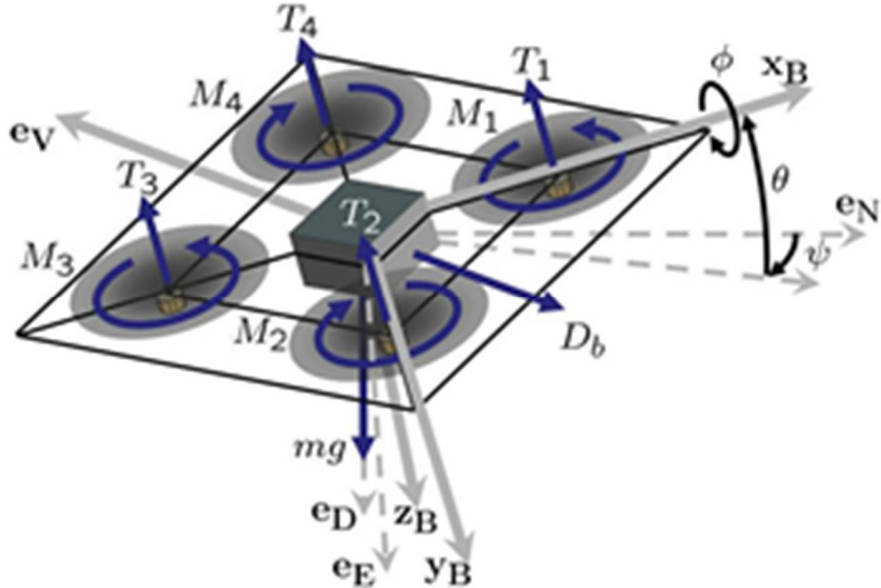


Figure 3.3: Free body diagram of a quadrotor helicopter (Courtesy Hoffman et al. [37]).

As long as the movement is concerned, the quadrotor relies on differential torque and thrust. Pitch, roll and yaw are used in flight dynamics to indicate the angles of rotation in three dimensions about the vehicle's center of mass. If all rotors are spinning at the same angular velocity, the differential torque is zero, resulting in no angular acceleration about the yaw axis. If the total thrust is kept constant, the vertical velocity remains unchanged. A vertical movement is achieved by increasing or decreasing the thrust from each motor by the same amount, so that total thrust changes but differential torque on the body remains zero. A horizontal movement is achieved by maintaining a non-zero pitch or roll angle. Angular accelerations about the pitch and roll axes can be generated separately. Each pair of blades rotating in the same direction controls one axis, either roll or pitch. Increasing thrust for one rotor while decreasing thrust for the other will maintain the torque balance needed for yaw stability and induce a differential torque about the roll or pitch axes.

3.1.2 Hardware and Sensors

The Phantom 4 is a remote-controlled consumer quadrotor helicopter developed by DJI and is a consumer grade product, it has medium cost and it is easy to use. All parts of this quadrotor are replaceable. It comes with a customizable remote controller that is designed with sensitive control sticks, dedicated buttons,



and up to 3.1 mile (5km) range. Phantom 4 consists of a magnesium skeleton that reduces weight while keeping stiffness at a maximum to minimize vibration. The Phantom 4's sleek and aerodynamically designed body minimizes buffeting when flying in strong winds and against gusts from any angle, keeping its movements predictable and precise. The deeply integrated gimbal and the placement of battery lift Phantom 4's center of gravity, improving balance, enhancing agility and adding more accuracy to how it reacts to user's commands. The propellers are powered by four brushless motors (power: 89.2 Wh). Energy is provided by a Lithium polymer battery with a capacity of 5870 mAh, which allows a flight time of approximately 28 minutes [38]. The onboard computer is Wi-Fi enable, which gives the ability to control the drone with any Wi-Fi enabled devices such as compatible smart phones, tablets and PCs. As far as the onboard sensors are concerned, Phantom 4 has different types of sensors. These are Accelerometers, Gyroscopes, Compasses, Barometers, Ultra sonic sensors and Satellite Positioning System. In addition, a high definition camera provides the user with visual feedback from the vehicle. An Inertial Measurement Unit is a single unit in the electronics module which collects angular velocity and linear acceleration data which is sent to the main processor. IMU contains two separate sensors. The first sensor is the accelerometer triad. It generates three analog signals describing the accelerations along each of its axes produced by, and acting on the vehicle. Due to thruster system and physical limitations, the most significant of these sensed accelerations is caused by gravity. The second sensor is the gyroscope, which is an angular rate sensor triad. It also outputs three analog signals. These signals describe the vehicle angular rate about each of the sensor axes. Even though the IMU is not located at the vehicle center of mass, the angular rate measurements are not effected by linear or angular accelerations. The data from these sensors is collected by the IMU and returned to a main processor [39]. Ultrasonic sensors combine with advanced computer vision and processing to give the Phantom active obstacle avoidance that allows it to react to and avoid obstacles in its path. Additionally, they provide altitude measures for automatic altitude stabilization and assisted vertical speed control. The ultrasound sensors are attached at the bottom of Phantom 4. As regards the onboard camera, the Phantom 4 is equipped with a 4k camera, featuring video capture at 30 frames per second and Full HD 1080p at 120 frames per second for smooth slow motion. An aspherical lens with a 94° field of view (FOV) reduces distortion by 36% and chromatic aberration by 56% when compared to previous models. In addition, a hyperfocal length of one meter allows getting closer to objects while keeping them in pin-sharp focus.



Figure 3.4: DJI Phantom 4 onboard 4K camera

The camera has a resolution of 4000×3000 pixels (VGA) and automatically provides video feedback on a screen (e.g., smartphone). Furthermore, a range of video color profiles are available from bright vibrant colors to professional flat profiles including D-Log and Cine-D that are ready for video post-production. Moreover, an advanced 3-axis gimbal takes out unwanted vibration and movement in-flight. This gimbal is accurate to a highly precise $\pm 0.03^\circ$, coupled with custom designed dampers enabling the camera to capture smooth and fluid footage even during complex maneuvers.

3.1.3 Onboard Intelligence

Usually quadrotor remote controls have multiple joysticks and knobs for controlling pitch, roll, yaw and throttle. It generally takes hours of practice to safely perform basic maneuvers like take-off, trimming, hovering with constant altitude and landing. Thanks to the onboard computer and sensors, take-off, hovering, trimming and landing are now completely automatic and all maneuvers are assisted. Because the quadrotor system is unstable, feedback from the sensors to the control system is required. This raises the issue of state estimation. The vehicle's control system must be robust to cope with various disturbances that can be encountered in practice. Redundancy in the state estimation is the solution in this case. The Phantom 4 has multiple methods to compute estimated states. In terms of sensor calibration, Phantom 4 uses sensors, which introduce issues like bias, misalignment angles and scale factors. These errors are not negligible and differ between Phantoms. For this reason, a manual board calibration is performed at the factory. After inertial sensor



calibration, sensors are used inside a complementary filter to estimate the attitude and de-bias the gyroscopes. The de-biased gyroscopes are used for vision velocity information combined with the velocity and altitude estimates from a vertical dynamics observer. The velocity from the computer vision algorithm is used to de-bias the accelerometers, the estimated bias is used to increase the accuracy of the attitude estimation algorithm. Finally, the de-biased accelerometer gives a precise body velocity from an aerodynamics model. To address the problem of state estimation, the Phantom 4 is equipped with embedded sensors that are described in the previously. When combining the sensor measurements in data fusion algorithms, relatively good state estimates are obtained.

3.1.4 Operational capacity

To summarize, Phantom 4 has the ability to fly continuously for approximately 28 minute with a top speed of 20 m/s depending to the user's settings. Furthermore, its maximum transmission distance is 5km using a remote controller. Moreover, Phantom 4 can operate at a surface with clear pattern and adequate lighting (lux>15) and it is also able to fly with maximum wind speed resistance of 10m/s.

3.2 Aerial Photography

The survey of the Technical University of Crete (TUC) was a user friendly procedure due to the fully autonomously. Through Pix4Dcapture the flight plan and the parameters of the flight were chosen. The processing of the data was done with the photogrammetric software Pix4Ddeskop was used. The process consists of 4 main stages. Initially, the program is parameterized to ensure the best quality and speed ratio of data processing. After the Initial Processing process, the process is interrupted to manually import the Control Points. The program continues with 2 stages of fully automated processing and results in the extraction of a series of images and data, depending on what the user has requested. The production process of finished products is based on three subsections:

1. Flight planning through separate software (Pix4D Capture), which determines, the area and flight height, the number of images to be captured (and consequently the overlapping of the images), etc.
2. The flight and receipt of primary data
3. Output results through Pix4D



3.2.1 Study area

The location of the study is as mentioned before the Technical University of Crete, which is 7km from the center of Chania and has five different schools. In this thesis the buildings of the Production and Management Engineering School were chosen, due to their landing space availability. The following figure shows the area of study.

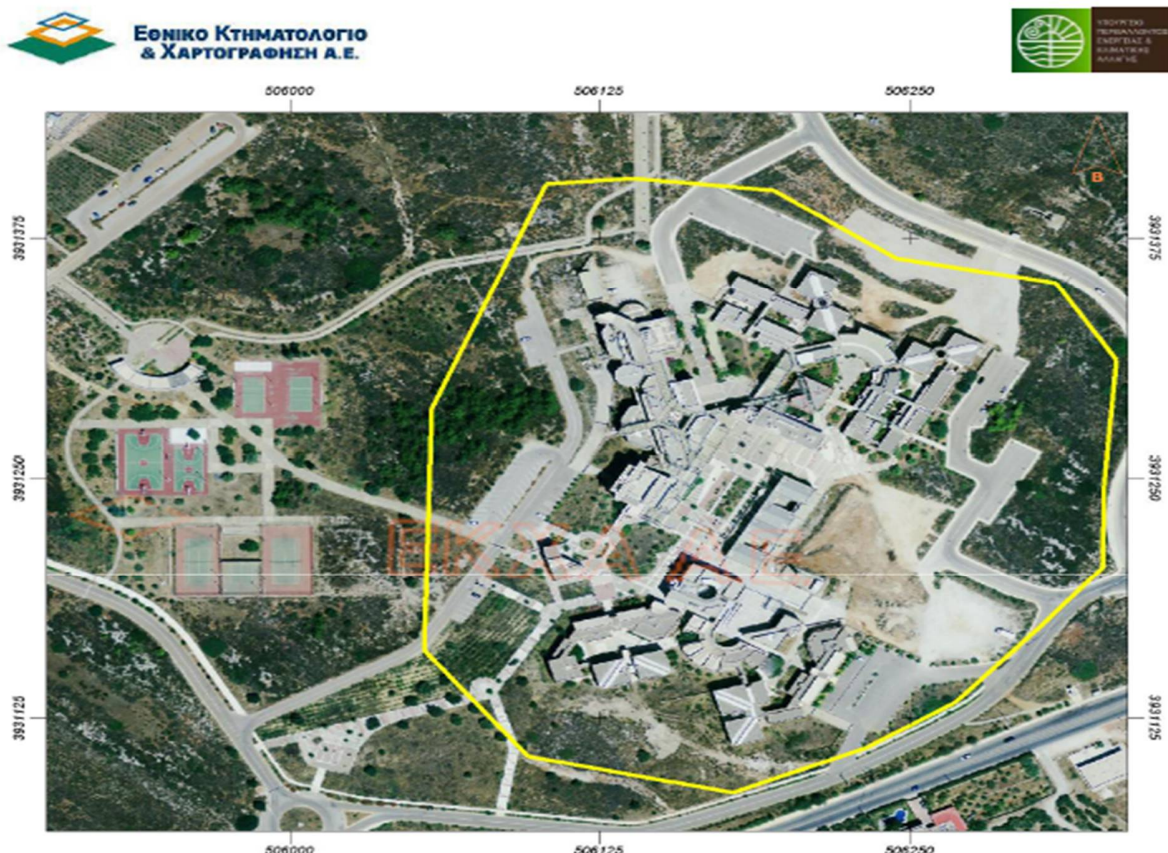
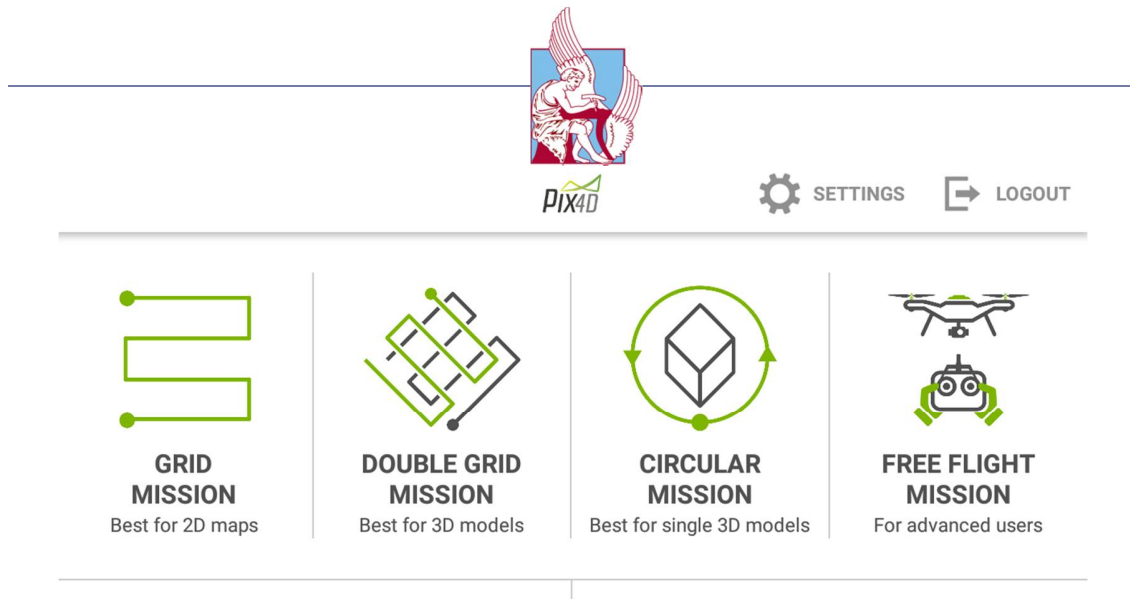


Figure 3.5: Study area

3.2.2 Flight planning

To achieve a good quality of the image data, careful flight planning needs to be conducted. Baring that in mind, different flight plans were applied with different altitudes, overlapping and flight grids, in order to achieve the best result. The software that it was used is Pix4d Capture, a mobile application that allows creating flight plans for capturing image data. Through the Pix4dCapture an area of interest is defined and kml/kmz files can be exported.



PROJECT LIST

TUTORIAL/HELP

Figure 3.6: Pix4dCapture

For the creation of 3D models, the option “Double Grid Mission” and “Circular Mission” is suggested. The options that the user has to set at the “Double Grid Mission” are:

- The boundaries of the area
- The flight height
- The flight speed
- The camera’s angle
- The rate of overlap



Figure 3.7: Double Grid Mission

On the contrary at the “Circular Mission” the user needs to set only:



- The boundaries of the area
- The flight height
- The flight speed
- The degrees between taking each photo



Figure 3.8: Circular Mission

3.2.3 Customization of data

After determining the type of processing, importing the images into the Pix4d's software, and defining the details for the spatial data of the images, continued the adjustment of three basic processing steps. These are:

1. The editing options
2. The Cloud and Point Cloud settings
3. The production of DSM and the Orthomosaics, as well as the options for different types of output files of the results.

Furthermore, the process of customization for the output results began with some basic choices concerning both the type of processing to be performed and the optimization of some camera and image parameters.

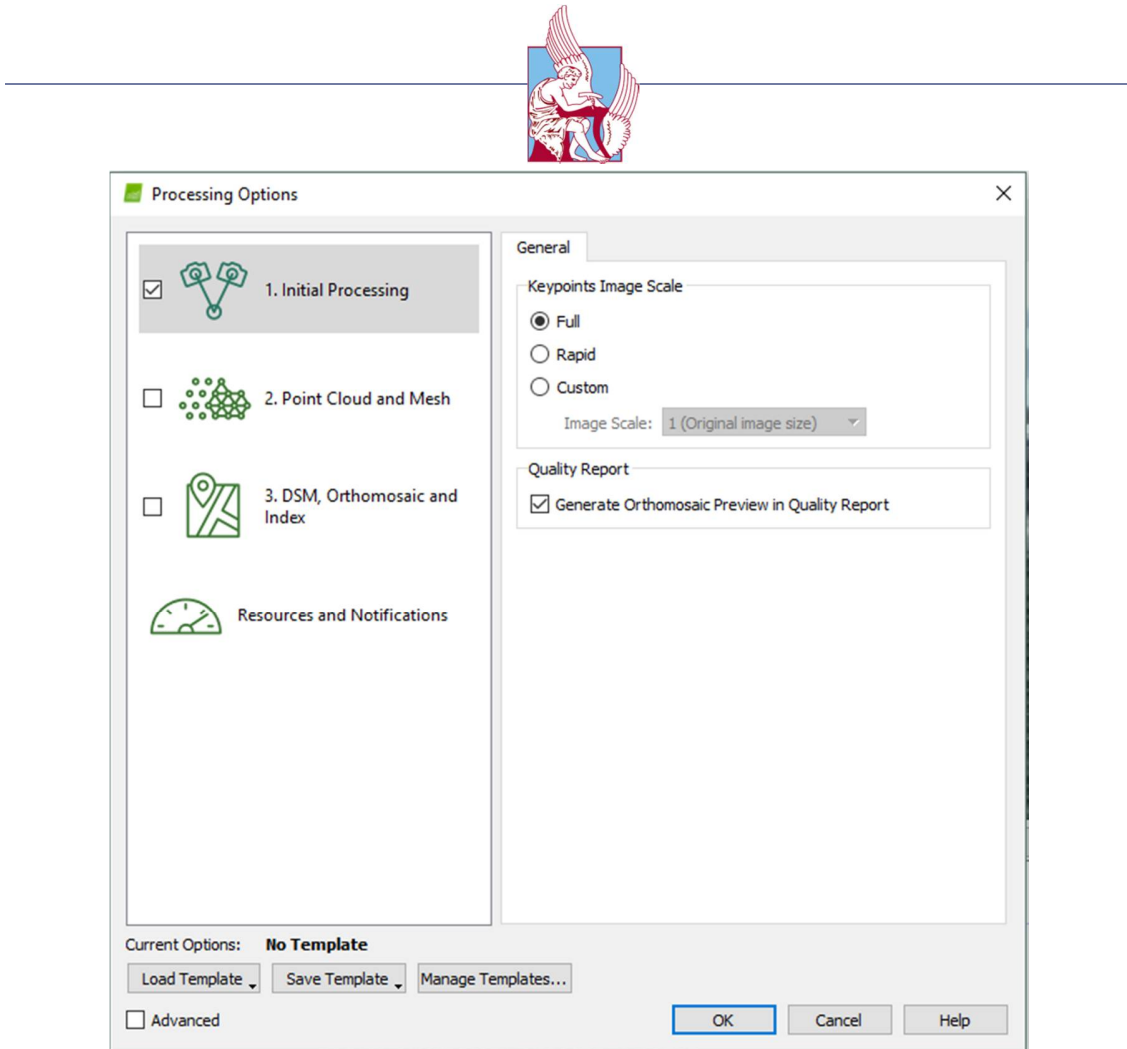


Figure 3.9: Processing options of the first stage

To be more specific, the user has the ability to change the type of processing he had originally selected at the start of the wizard. Then, in the "Key-points Image Scale" field, it is possible to define the scale on which the already-inserted images will be processed. The most common option is also the one that by default selects the software to actually process images in their real size. In some cases where the inserted images have a particularly low resolution (<1MP), it is useful to select the magnification of images 2-3 times, although it might have a major impact on the precision of the outputs. On the other hand, when the inserted images have a particularly high resolution (> 50MP), then a reduction of $1/2$ or $1/4$ is suggested for saving time and processing resources. The last choice in customization is the ability to create a first orthomosaic with low resolution. This mosaic has low precision but is particularly useful as it can give an initial view to the user about the surface. Moreover, at the "Point Cloud and Mesh" stage the options for the production and processing of condensed cloud points had to be determined.

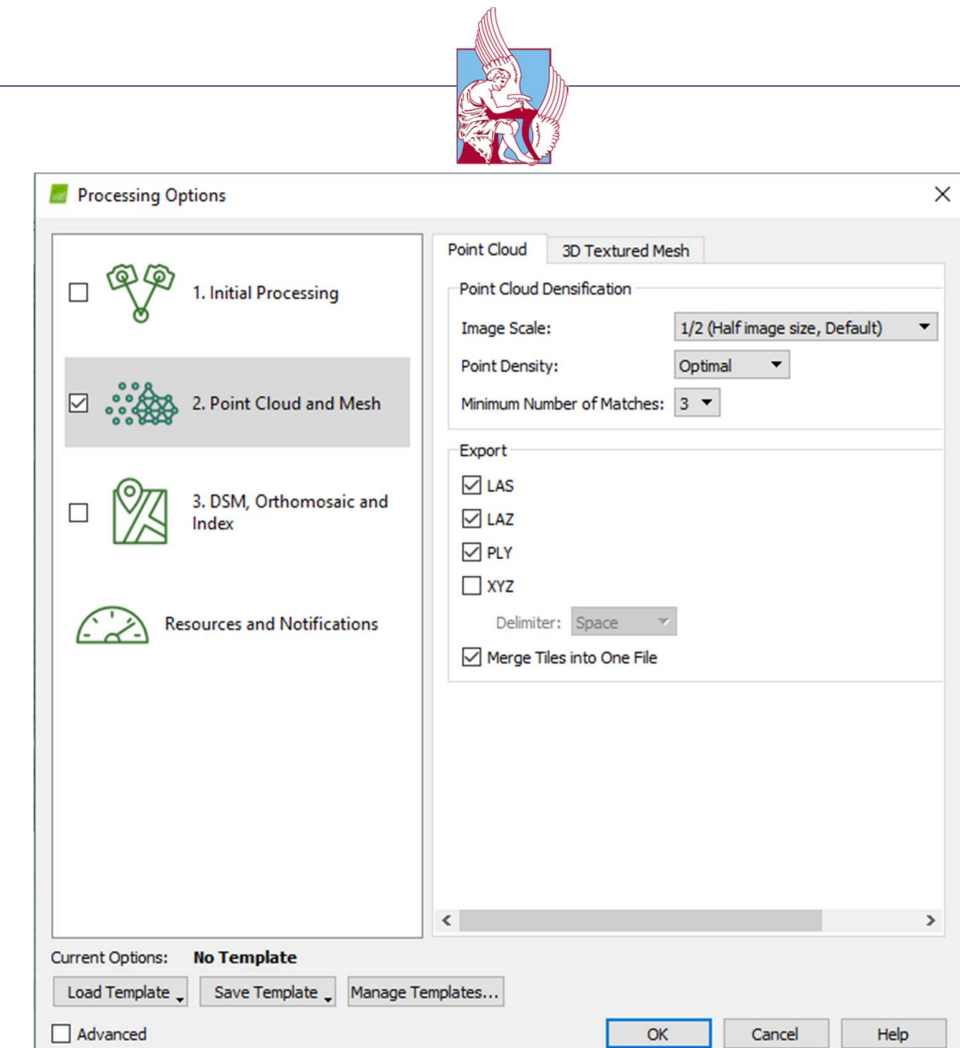


Figure 3.10: Point Cloud Options

Initially, the first block of options has to do with Point Cloud Densification settings. These are the process settings that will essentially convert the calibrated images of the previous stage into a particularly dense cloud of points. In the "Image Scale" field, the scale of the original images was defined, in order to be processed by the algorithm, which creates the pixel associations. Usually, most pixel sensors display optimal processing results when half the size of the image is selected ("1/2 (Half Image size)"). In addition, scale selection also determines the number of points to be produced and, consequently, the display accuracy of the produced model, always in dependence on the processing time. As the scale decreases, the faster the process is processed and the number of cloud points produced is reduced. The next option was about the density of points, where the finishing point is selected optimal ("Optimal"). Density of points is about the spacing between the pixels and is directly related to their number and processing speed. If low density is selected, the number of points and consequently the processing time drastically decreases, and if high density is selected, the



pixels and processing time will be multiplied without however any substantial difference in the information provided.

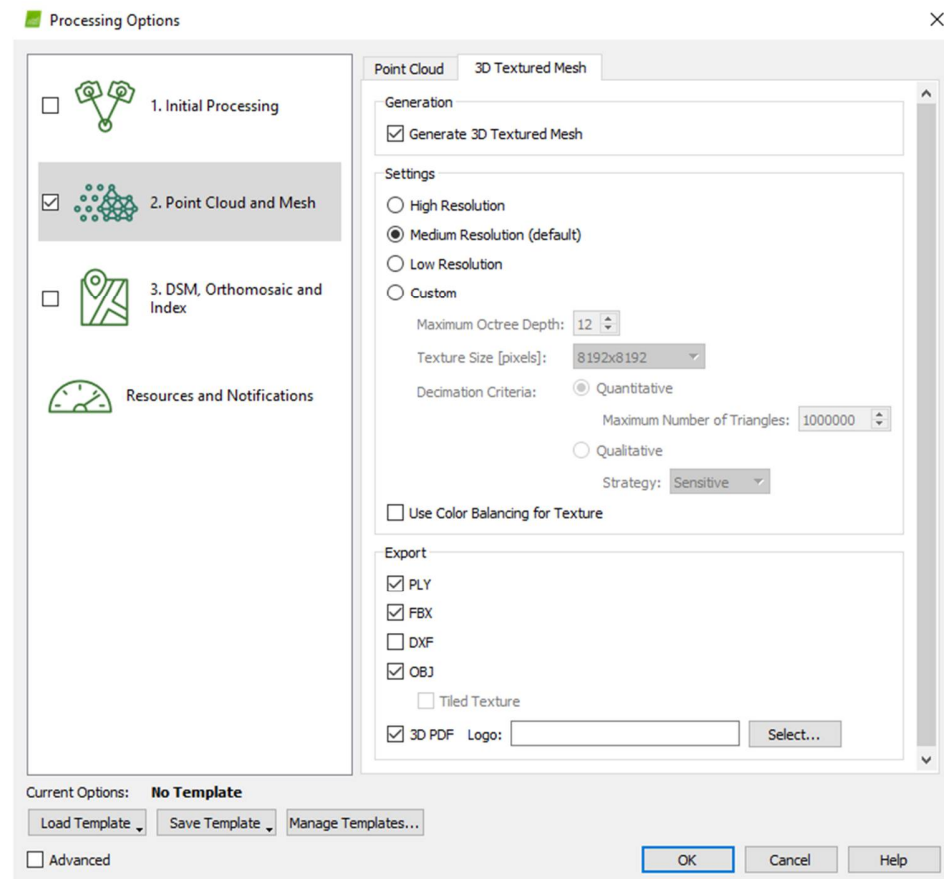


Figure 3.11: 3D Textured Mesh options

As regards the 3D Textured Mesh, the program creates a three-dimensional grid to smooth gaps in pixels. In conclusion, the cloud was requested to be produced in LAS, LAZ and PLY format, while the 3D Textured Mesh in PLY, FBX, OBJ and 3D PDF file format. In the next step, the parameters that are related to the production of both the Digital Surface Model and the Ortho-Mosaic were determined.

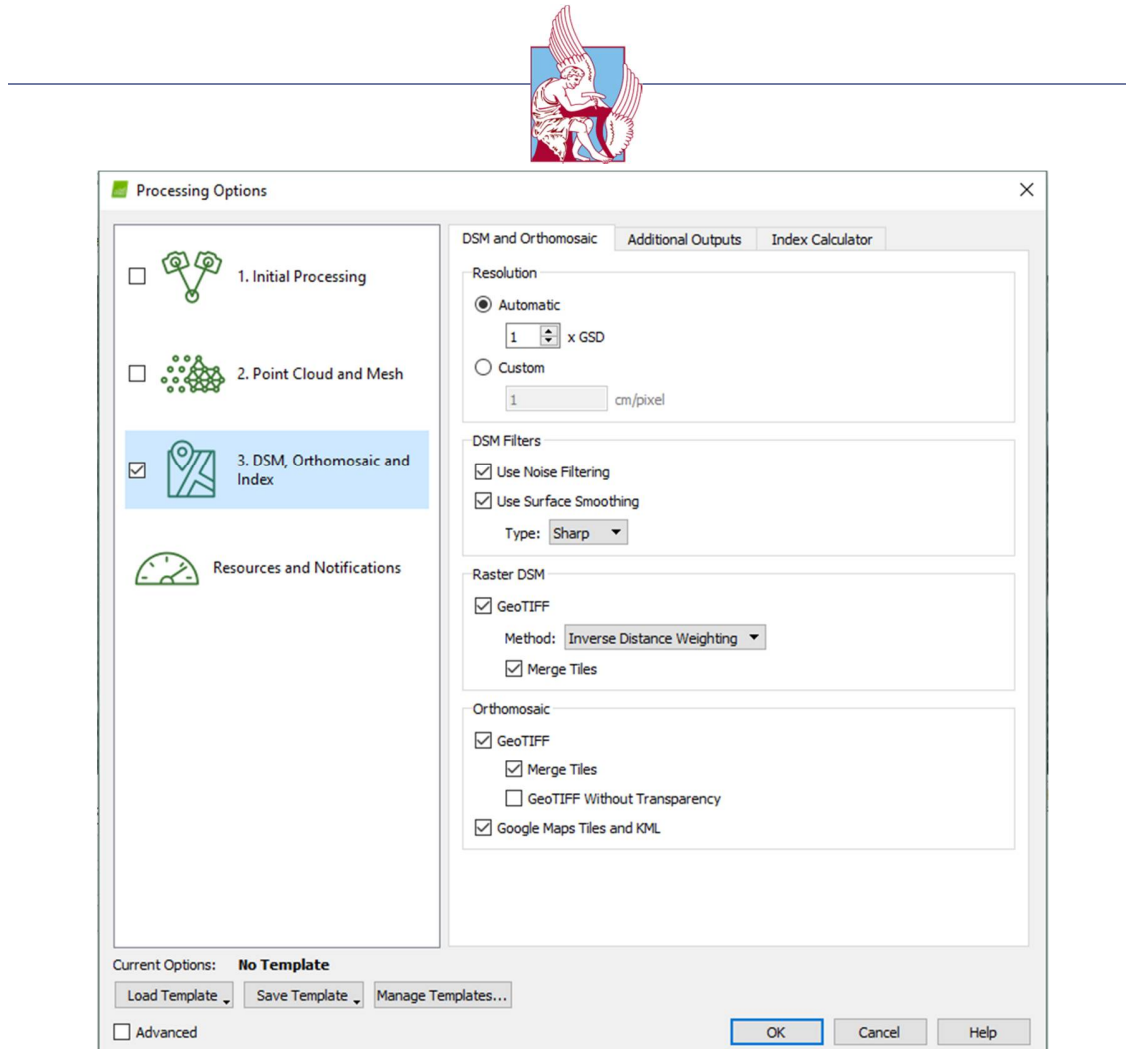


Figure 3.12: Dsm, Orthomosaic and Index options

As regards the DSM filters, are used in DSM to improve its accuracy and ultimate visual result. There are two types of algorithms to achieve this result: a) the Noise Filtering algorithm and b) the Surface Smoothing algorithm. The Noise algorithm will essentially generate statistics for all points and try to identify cases in which one point is very far from another, where the Surface algorithm will remove small details from the surface model since most are usually noise and not real elements on the surface of the ground. The KML file enables direct integration and visualization of the orthomosaic on the Google Earth platform.

3.2.4 Data Procedure

Finalizing the 3-step configuration starts the data processing phase. The order followed by the software is roughly the same as it was parameterized:

1. Initial Processing
2. Point Cloud Densification
3. DSM and Orthomosaic generation



The processing phase starts with "Home Processing". During this phase, the software performs sequential tasks such as computing the correlations between images and creating Automated Tie Points. Then, by calibrating and optimizing by incorporating geospatial data into the images, it proceeds to calculate the Rematches as it was configured to perform. Furthermore, at the point cloud densification phase, the software starts with a relatively time consuming process to produce the points. Then the 3D Mesh was created and a series of processes were implemented, such as Improving - Smoothing - Simplifying, to ultimately lead to the segmentation and creation of the final texture of the grid.

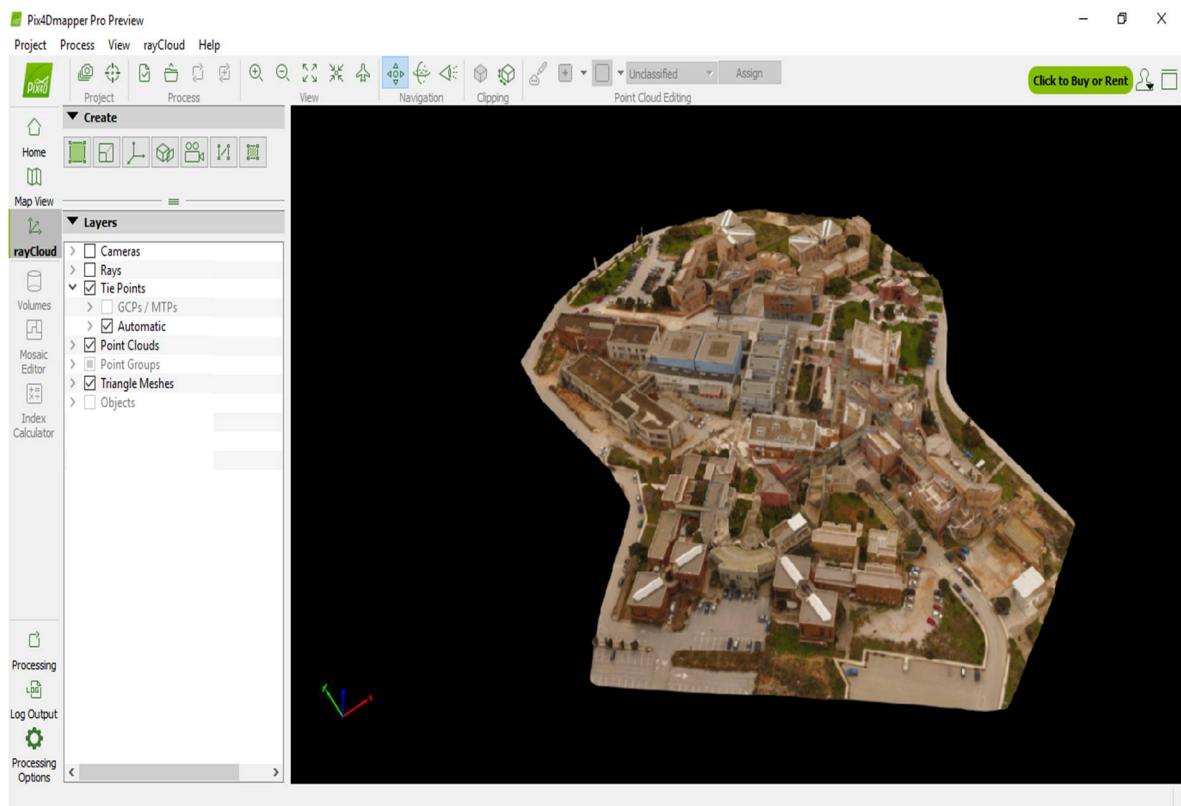


Figure 3.13: The final 3D Triangle Mesh

After the production of cloud and mesh cloud, the process reaches to its third and final stage, the production of DSM and the orthomosaic. The software, at this stage, initially loads the cloud of points produced in the previous stage. Then it produces the DSM in tiles and at the end of this process it joins them into one.

3.3 Air Data Measurements

The conventional systems to monitor air pollution in urban areas are based in container style monitoring stations, or also stations incorporated in a modified



trailer to accommodate the instruments and air circuits. These stations have large size and usually their construction involves a large cost. Most of the data collected by the stations is transmitted to a central database, not requiring personnel to operate the stations, but the methods used usually require some maintenance and calibration process that can be made only by qualified personnel. These stations can acquire very precise and selective data for measurement of different gases, but they collect them at a small range of area.



Figure 3.14: Outside of the fixed station to monitor air pollution at Laranjeiro, Lisbon

On the other hand, UAVs with portable systems can obtain measurements at nearly any point in a three dimensional space including at different altitudes. This fact is interesting not only for reducing the number of sensors and therefore the total cost of such a system but also for obtaining local data for production monitoring, problem detection and local climate control. The company Libelium has stations that are modular. Modules can be assembled to have a system with an 8MHz microprocessor, 8KB RAM, 128 KB flash memory, GPS module, GSM/GPRS module, 802.15.4 zigbee. These stations have a variety of sensors to be mounted. For this thesis CO₂, NO₂, SO₂ sensors were chosen. The sensors used on the Libelium stations are metal oxide semiconductor sensors, which are low cost and compact.

3.3.1 System Architecture

The main requisites for the system were low cost, portability and the capability of storing measurement data locally and transmuting it remotely using a wireless interface. Another requirement was time and location stamping of gas



measurements. A significant computational power was desired for use in future application in volume data fusion and signal processing algorithms. The best way to achieve these goals is by using a digital system that can store sensor data correspondent to large period of time, and that can be integrated with the existent technology to make possible the transmission of the data to a central station. It was determined that the following components had to be used and integrated into a single system:

- Gas Sensors
- Temperature and Humidity sensors
- Analog-to-Digital conversion
- Microprocessor
- Data Storage
- WiFi and GPRS communication systems
- Global Position System receiver module

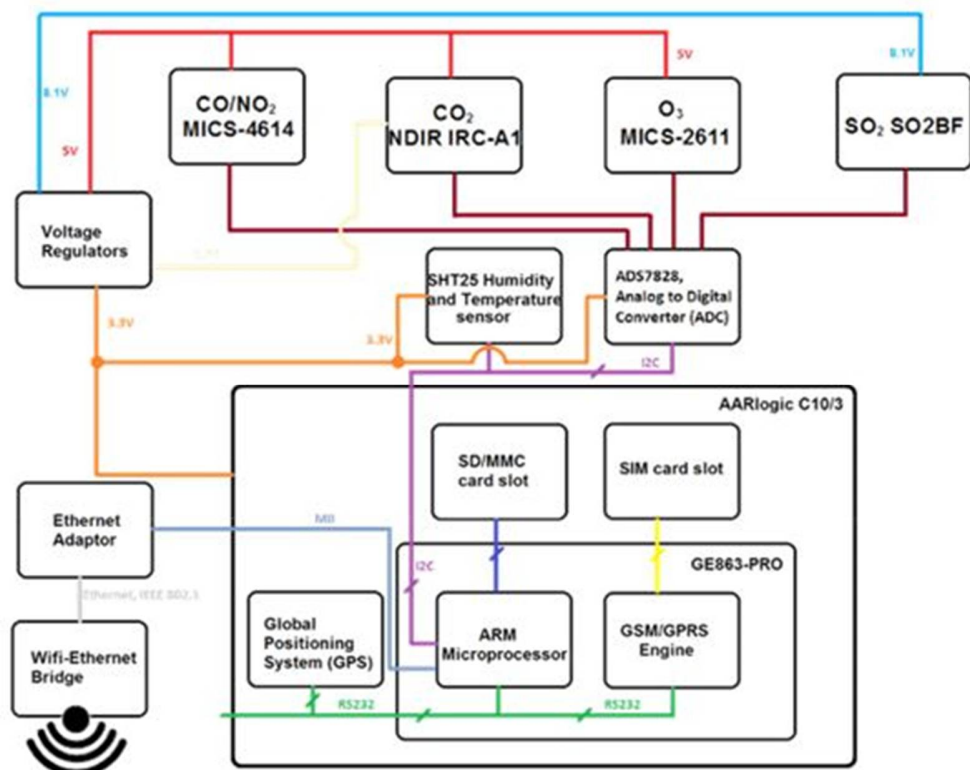


Figure 3.15: Functional diagram of the air quality monitoring station.

3.3.2 Waspmove and Meshlum

The Waspmove [40] is an open source Zigbee and IEEE-802.15.4 sensor platform which is based on a user-friendly modular architecture for rich application development. The classification of the external boards is as follows:



gases, events, agriculture, smart metering, smart parking, and smart cities. These boards hold various types of sensors which are mounted on the Wasp mote to give it this compact feeling and neat touch. In addition, Wasp motes support a number of protocols and standards of communications such as, the IEEE-802.15.4, Zigbee, Digimesh, Bluetooth, and RF-XSC.



Figure 3.16: Libelium Wasp mote

The ability to integrate many protocols into a single node provides capabilities for implementations of multi-WSN architectures where independent communications can exist within a single network. The main features of the Wasp mote node include: module architecture, simple sensor integration, support of numerous communication protocols, secured transmission using AES (Advanced Encryption Standard), long range communication capabilities [41], low power consumption MC (ATmega1281 microcontroller), and support to over the air programming functions (OTAP). Meshlium [42] is a powerful WSN router which combines many communication technologies into one single device. The supported technologies include: Wi-Fi (2.4 GHz and 5 GHz), Zigbee, GPRS, Bluetooth, and GPS. It is based on a 500 MHz processor with 256 MB of RAM and runs a Debian/Linux Operating System (OS). It is designed to withstand harsh environments using an aluminum casing to protect it from dust and water. Furthermore, Meshlium allows a large number of high level services to be managed such as, sending alarm SMS and e-mails, accessing the World-Wide-



Web (WWW) services, and managing MYSQL databases for data storage. The main functions of Meshlium include:

1. Initiating of short and long distance data communication
2. Routing data multiple communication protocols
3. Capturing and storing of data from the sensor network
4. Local network control and link maintenance



Figure 3.17: Libelium Meshlium Xtreme

3.3.3 Gas Sensor Board Pro

The Gas Sensor Board has designed for monitoring environmental parameters like, temperature, humidity, atmospheric pressure and 14 different types of gases [\[43\]](#).

Features of Gas Sensor Board

- Weight: 20gr
- Dimensions: 73.5 x 51 x 22mm (without the sensors)
- Temperature range [-20°C, 65°C]

Electrical Features

- Sensor Board Voltage: 3.3V and 5V
- Sensor Voltage: 3.3V and 5V
- Maximum Current (continuous): 200mA
- Maximum Current (peak): 400mA



Figure 3.18: Gas Sensor Board

CO sensor:

The chosen sensor was the CO-A4.

Table 3.1 – CO sensor characteristics

Performance Characteristics		Operation Conditions	
Nominal Range	0 to 25 ppm	Temperature Range	-30 °C to 50 °C
Maximum Overload	2000 ppm	Operating Humidity	15 to 90% RH-non considering
Long Term Sensitivity Drift	<10% change/year in lab air	Pressure Range	80 to 120 kPa
Response Time	≤20 seconds	Storage Temperature	0 °C to 20 °C
Sensitivity	220 to 375 nA/ppm	Expected Operating Life	3 years in air
Accuracy	As good as ±1ppm		



Figure 3.19: The CO sensor



CO₂ sensor:

The chosen sensor was the INE20-CO2P-NCVSP.

Table 3.2 - CO₂ sensor characteristics

Performance Characteristics		Operation Conditions	
Nominal Range	0 to 5000 ppm	Temperature Range	-40 oC to 60 oC
Maximum Overload	2000 ppm	Operating Humidity	0 to 90% RH-non considering
Long Term Output Drift	<±250 ppm/year	Storage Temperature	-45 oC to 85 oC
Response Time	≤60 seconds		
Resolution	25 ppm		
Accuracy	±50 ppm from 0 to 2500 ppm range ±200ppm from 2500 to 5000 ppm range		



Figure 3.20: The CO₂ sensor

SO₂ sensor

The chosen sensor is 4-SO2-20.

Table 3.3 - SO₂ sensor characteristics

Performance Characteristics		Operation Conditions	
Nominal Range	0 to 20 ppm	Temperature Range	-20 °C to 50 °C
Maximum Overload	150 ppm	Operating Humidity	15 to 90% RH-non considering
Long Term Output Drift	<2% signal/month	Pressure Range	90 to 110 kPa
Response Time	≤45 seconds	Storage Temperature	0 °C to 20 °C
Sensitivity	500± 150 nA ppm	Expected Operating Life	2 years in air
Accuracy	As good as ±0.2 ppm		



Figure 3.21: The SO₂ sensor

O₃ sensor:

The chosen sensor is OX-A431.

Table 3.4 – O₃ sensor characteristics

Performance Characteristics		Operation Conditions	
Nominal Range	0 to 18 ppm	Temperature Range	-30 °C to 40 °C
Maximum Overload	50 ppm	Operating Humidity	15 to 85% RH-non considering
Long Term sensitivity Drift	-20 to -40% change/year	Pressure Range	80 to 120 kPa
Response Time	≤45 seconds	Storage Temperature	3 °C to 20 °C
Sensitivity	-200 to -500 nA ppm	Expected Operating Life	>24 months in air
Accuracy	As good as ±0.2 ppm		



Figure 3.22: The O₃ sensor



NO₂ sensor:

The chosen sensor is 4-NO2-20.

Table 3.5 – NO₂ sensor characteristics

Performance Characteristics		Operation Conditions	
Nominal Range	0 to 20 ppm	Temperature Range	-20 °C to 50 °C
Maximum Overload	250 ppm	Operating Humidity	15 to 90% RH-non considering
Long Term Output Drift	<2% signal/month	Pressure Range	90 to 110 kPa
Response Time	≤30 seconds	Storage Temperature	0 °C to 20 °C
Sensitivity	600±150 nA ppm	Expected Operating Life	2 years in air
Accuracy	As good as ±0.2 ppm		



Figure 3.23: The NO₂ sensor

NH₃ sensor:

The chosen sensor is 4-NH3-100.

Table 3.6 – NH₃ sensor characteristics

Performance Characteristics		Operation Conditions	
Nominal Range	0 to 100 ppm	Temperature Range	-20 °C to 50 °C
Long Term Output Drift	<2% signal/month	Operating Humidity	15 to 90% RH-non considering
Response Time	≤90 seconds	Pressure Range	90 to 110 kPa
Sensitivity	135±35 nA ppm	Storage Temperature	0 °C to 20 °C
Accuracy	As good as ±0.5 ppm	Expected Operating Life	≥1 year in air



Figure 3.24: The NH₃ sensor

Temperature, Humidity and Pressure sensor:

The chosen sensor is BME280 developed by Bosch Sensortec.

Table 3.7 – Electrical characteristics and Temperature sensor characteristics

Electrical characteristics		Temperature sensor	
Supply voltage	3.3 V	Operational range	-40 to +85°C
Sleep current typical	0.1 µA	Full accuracy range	0 to +65 °C
Sleep current maximum	0.3 µA	Accuracy	±1 °C (range 0 °C to +65 °C)
		Response time	1.65 seconds (63% response from +30 to +125 °C)
		Typical consumption	1µA measuring

Table 3.8 – Humidity and Pressure sensors characteristics

Humidity sensor		Pressure sensor	
Measurement range	0 to 100% of Relative Humidity	Measurement range	30 to 110 kPa
Hysteresis	±1%RH	Operational temperature range	-40 to +85 °C
Accuracy	< ±3%RH (at 25 °C, range 20 to 80%)	Full accuracy temperature range	0 to +65 °C
Operating Temperature	-40 °C to +85 °C	Absolute accuracy	±0.1 kPa (0 to 65 °C)
Response time (63% of step 90% to 0% or 0% to 90%)	1 second	Typical consumption	2.8µA measuring
Typical consumption	1.8 µA measuring	Maximum consumption	4.2µA measuring
Maximum consumption	2.9 µA measuring		



Figure 3.25: The Temperature, Humidity and Pressure sensor

3.3.4 Assembly of the sensors with the Phantom 4

The first problem that we faced at this thesis was the assembly of the sensors with the Phantom 4. Phantom 4 is meant for photography use. So we had to adjust this, and create new features to transform it to an air-measurement platform. The first step was to design and print from a 3D printer a base and two boxes, one for the sensors and the second for the battery. The second issue that we had to face was the way to attach them to the Phantom. After hours of investigation we concluded that the best option was as it is shown at the following figure.

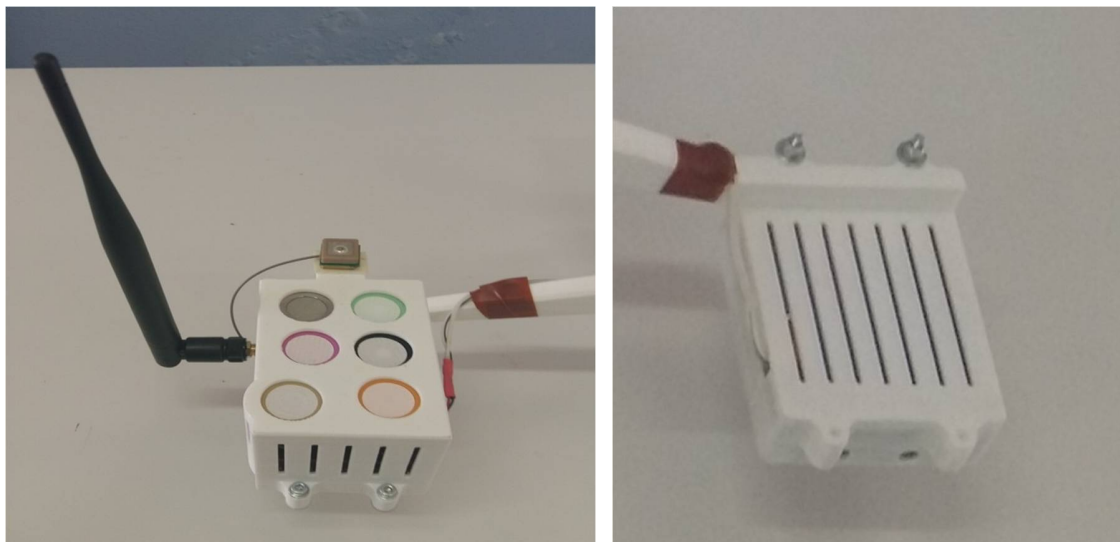


Figure 3.26: The printed boxes of the sensors and the batteries



Figure 3.27: The assembly with the Phantom 4



Figure 3.28: Side view of the assembly

The software that it was used for flying the Phantom 4 with the sensors and take the air measurements was DJI's GO, a mobile application that allows flying manually. It supports auto take-off and land of the aircraft with just a swipe of the



finger at the smart device, thus the user can track the aircraft's position and heading with a glance at a map. Besides, through the application it is possible also to use a map to set a new home point position or even activate the "Return to Home", making flying easy and simple.

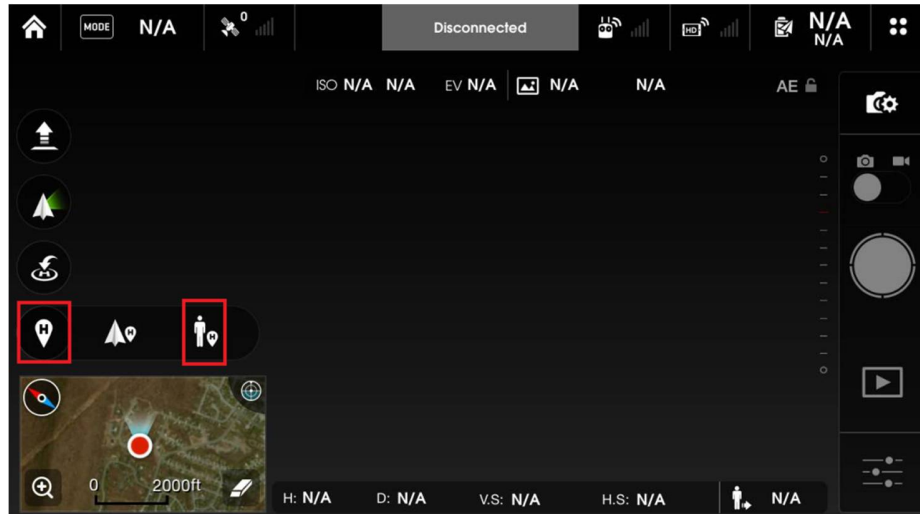


Figure 3.29: DJI's GO application

The sensors send directly the data of the air-measurements at the database and we export them at an .xls format.

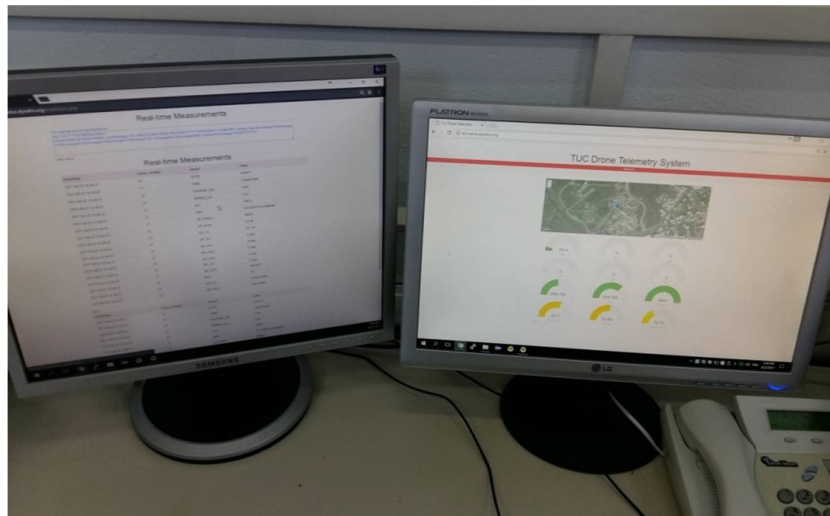


Figure 3.30: The database which collects the air-measurements

3.4 Data Processing

Before import and start to model, it is necessary to make data preparation. This data preparation includes:



- Import data from the data base to an excel file
- Process the excel file by selecting the data of interest and removing any additional information
- Import the data at the ESRI's software

3.4.1 Visualization tools

There are many 3D visualization tools available today. The most commonly used 3D software packages include Google Sketchup, ArcGIS, AutoCAD, 3D Studio Max, Maya, etc. While some software packages are very comprehensive and include 3D visualization and analysis functions (e.g., ArcGIS, AutoCAD), some are 3D-orientied, like Google SketchUp, and 3D Studio Max. ArcGIS developed by the Environmental Systems Research Institute (ESRI) is a Geographic Information System (GIS) software package. There are four products within ArcGIS with some adding higher levels of functionality to the basic package. Nevertheless, only two of them were used in this thesis, ArcScene and ArcMap version 10.4 for desktop. Therefore, ArcScene allows the managing and visualizing of extremely large sets of 3D geographic data from a local or global perspective. Whereas ArcMap is the application used to view, edit and query geospatial data, and creates maps. The ArcMap interface has two main sections, including a table of contents on the left and the data frame(s) which display the map. Items in the table of contents correspond with layers on the map. Furthermore, for the 3D conjunction of the 3d models, the Autodesk 3DS Max 2017 graphic software was used.

3.4.2 Surface Interpolation Algorithms

Interpolation is necessary due to the incomplete measurement of a feature within an area. For the interpolation of ground surface, measurements are taken at a series of locations, then using an interpolation algorithm; the elevation values between the points are estimated. Interpolation of the ground surface is where the theory of spatial auto-correlation, where points closer together are more similar to each other than points further away. The basic two principals of interpolation algorithms based on 1) the definition of neighborhood area and 2) the neighboring values to determine the mathematical algorithm for the interpolation. The choice of algorithm or formula used can influence the estimated elevation surface, which is created from interpolation. Understanding the interpolation algorithms and their assumptions can assist when creating any interpolated surface. Two classifications of interpolation methodologies are Deterministic and Geostatistical. Deterministic models estimate data relationships utilizing priori models, which are directly based on the surrounding



measured values. Geostatistical models utilize the entire dataset to infer similar relationships for use in the neighborhood value interpolation [\[44\]](#).

- *Inverse Distance Weighting (IDW)*: Inverse Distance Weighting (IDW) is a type of Deterministic interpolation method it uses the exact data variables when creating the surface. The parameter setting for IDW is a power function, where the power function illustrates the weight for the values that are proportional to the distance (Lu and Wong 2008). IDW is an appropriate interpolation methodology when interpolating from point datasets that are non-clustered, spatially correlated, contain no data outliers, and are non-directionally dependent. For elevation surfaces, IDW results in flattening peaks and valleys unless these sites have a high point density.

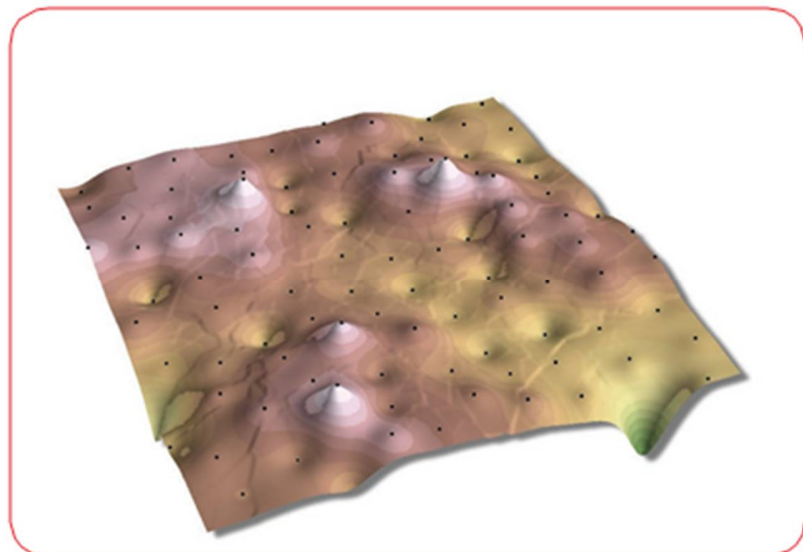


Figure 3.31: Inverse Distance Weighted

- *Natural Neighbor (NN)*: Natural neighbor interpolation has many positive features, can be used for both interpolation and extrapolation, and generally works well with clustered scatter points. Another weighted-average method, the basic equation used in natural neighbor interpolation is identical to the one used in IDW interpolation. This method can efficiently handle large input point datasets. When using the Natural Neighbor method, local coordinates define the amount of influence any scatter point will have on output cells.

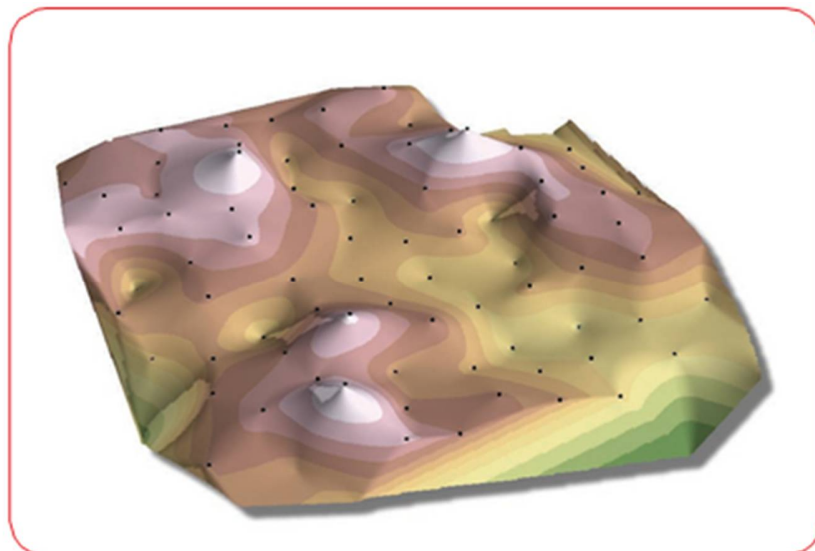


Figure 3.32: Natural Neighbor

- *Spline*: Spline is another Deterministic interpolation method that tries to ensure a smooth surface. This is achieved by finding a function that minimizes the tradeoff between fitting the points and the smoothness of the surface. Both IDW and Spline rely on spatial auto-correlation. In comparison to IDW, Spline is able to predict values above and below the measured values, using the neighboring values as well as not requiring quantification of spatial auto-correlation. Spline functions produce smoother results when the measured points are not rapidly changing or highly dense.

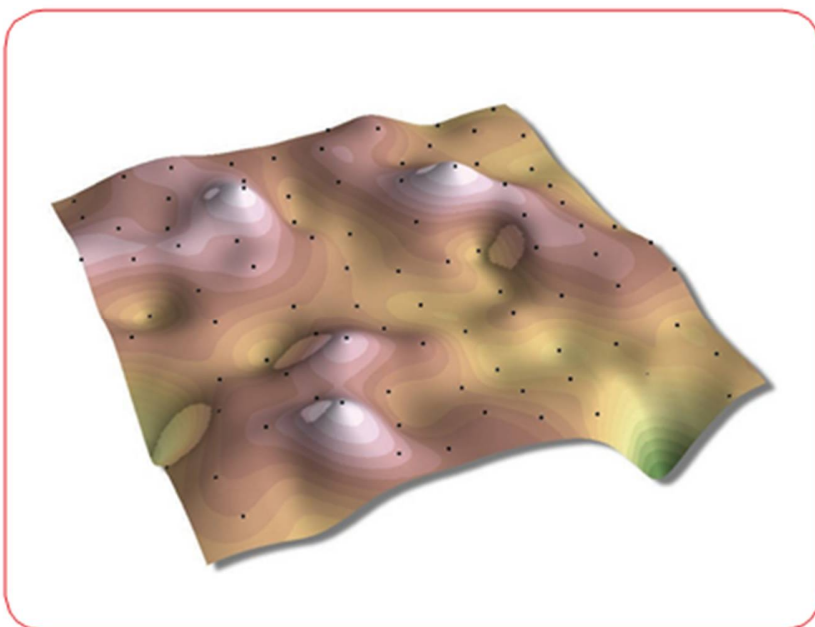


Figure 3.33: Spline



- **Kriging:** Kriging is to produce the most accurate surface not a smooth surface. Kriging is able to provide the prediction of uncertainty. Kriging assumes spatially correlated points, Normally Distributed, Stationarity of the data and does not represent a trend. This interpolation type measures distances between all possible pairs of sample points and uses the information to model the spatial auto-correlation in order to derive the surface. Kriging provides a wealth of variability in the parameter choices and methodologies, but the outputs from this interpolation method can hold to a higher standard due to the uncertainty value the model provides.

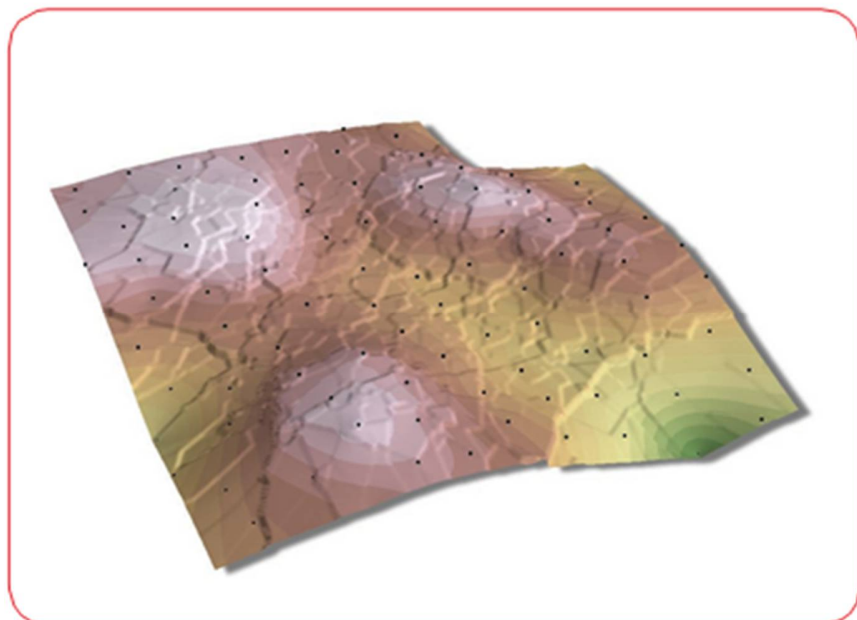


Figure 3.34: Kriging

3.4.3 2D visualization

ArcMap is the main visualization tool for this project. It provides the spatial context and display of the networks. To do this, it uses ModelBuilder processes and Python scripts to manipulate and transform the data. At this point, it is major importance to underline that our air measurements data were collected at two different heights, at 30 and 40 meters. That was done because we wanted to investigate any differences of the air quality at different height, thus to understand how the air pollutants diffuse at the atmosphere. The first step for the data processing is to add the data to the Arcmap. This is done by choosing the “Add XY data” option. At the opening window, we choose the path of the data file, which in our case is an excel file named data, we set our parameters correctly at the X, Y and Z Fields and finally we choose the correct coordinate system, which is “GCS_GGRS_87” for Greece.

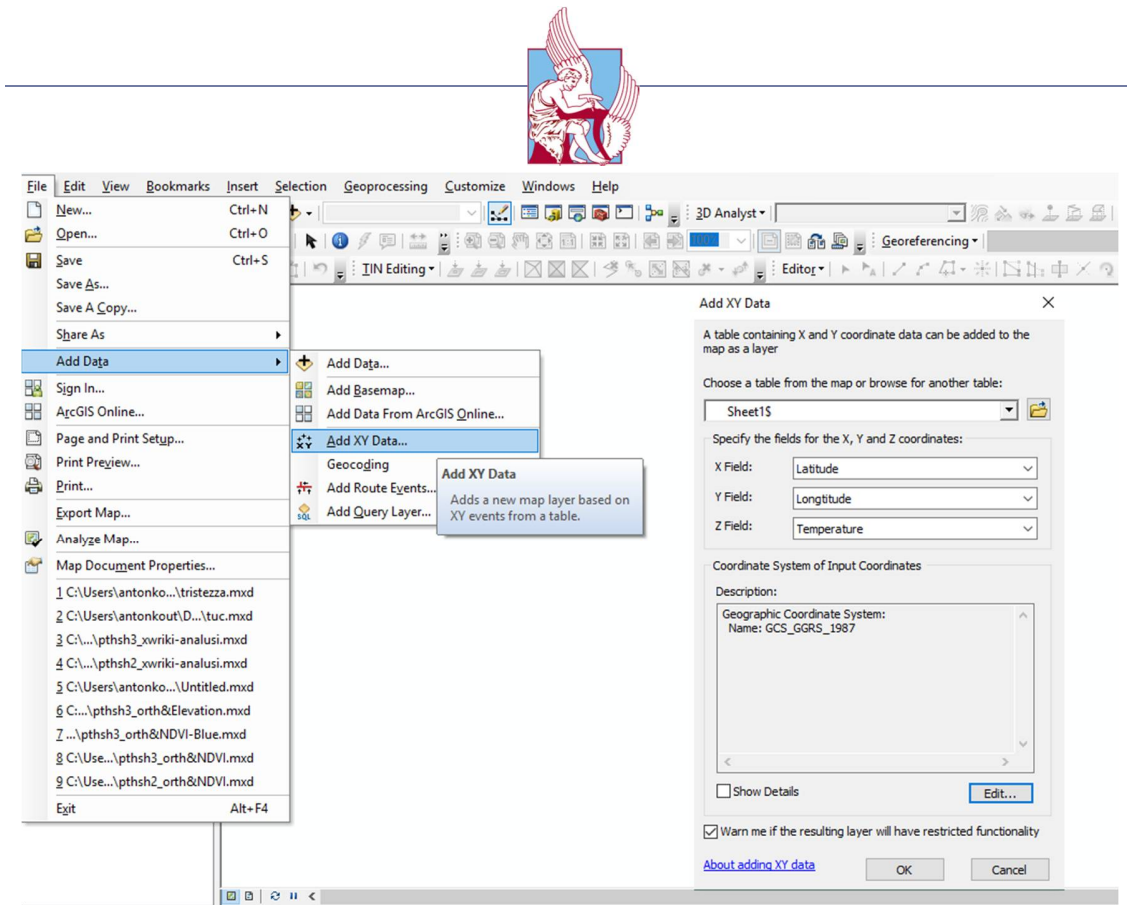


Figure 3.35: Initializing the data in 2D

The importing data are shown as points in our workspace.

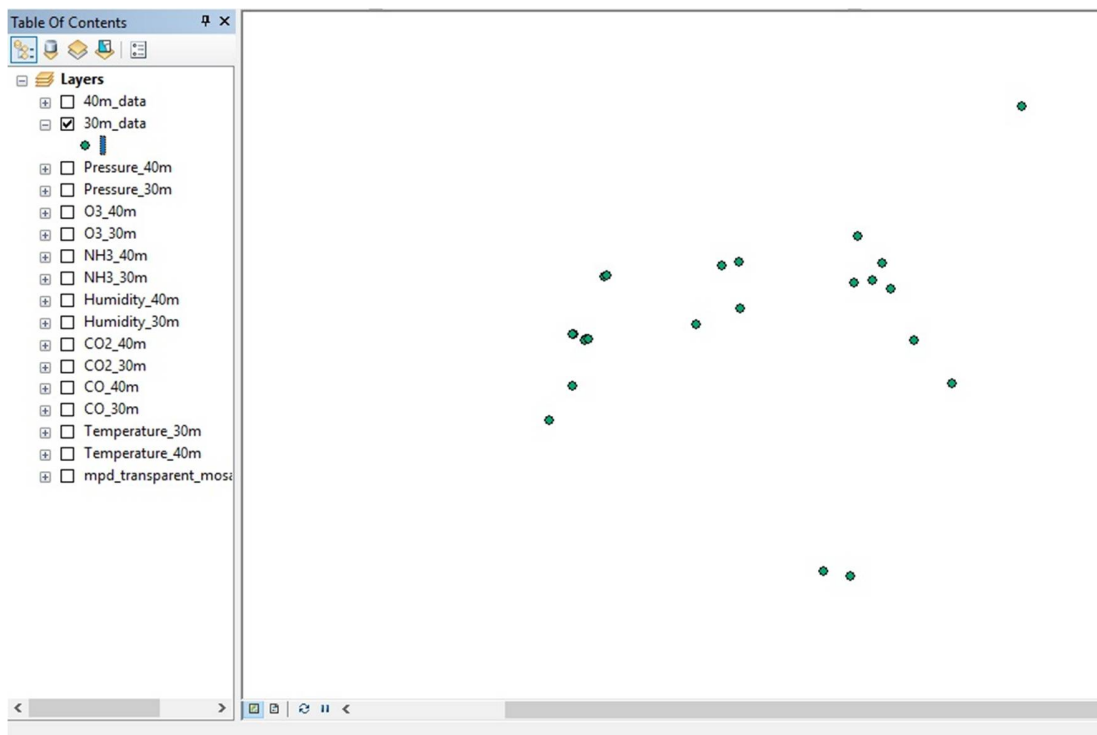


Figure 3.36: Point Cloud



In addition, we have to export our data to a shapefile in order to process them.

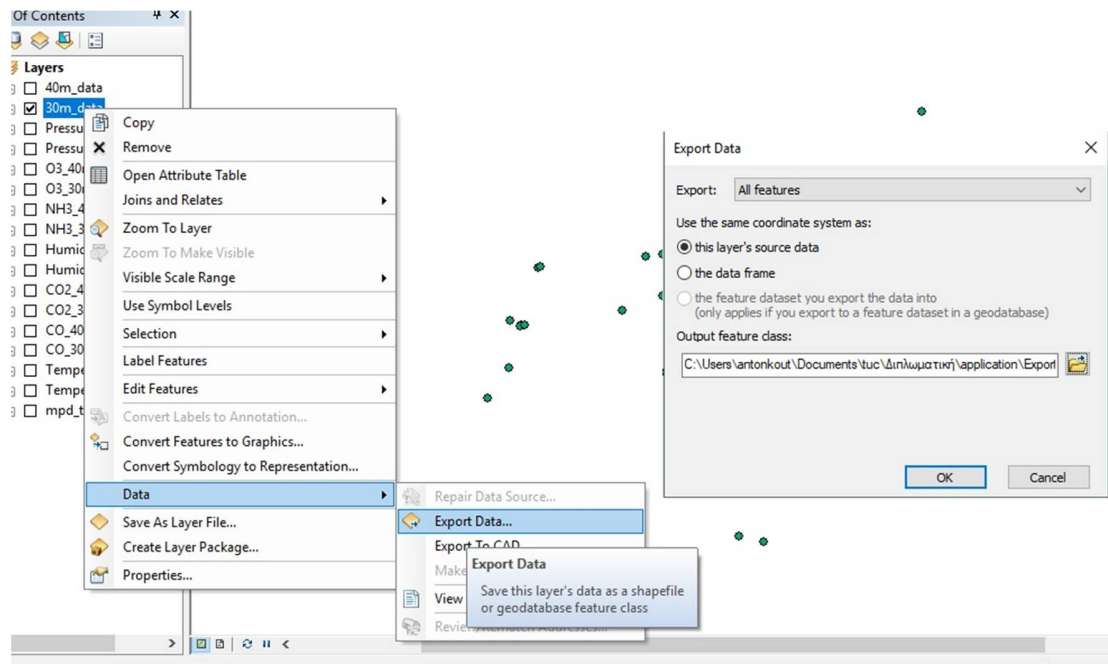


Figure 3.37: Exporting data to a shapefile

Moreover, we import the orthomosaic of the study area from the “Insert picture” option, which was produced through Pix4Ddesktop, as a base-map.

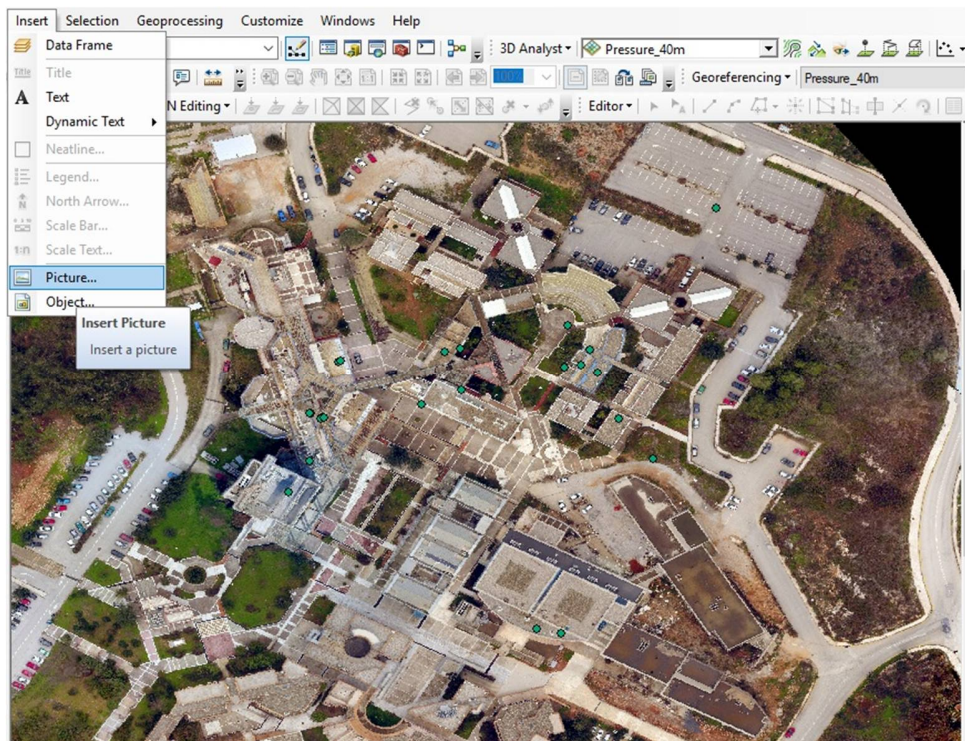


Figure 3.38: Adding a base-map



Finally we process our data with the Inverse Distance Weighting interpolating method (IDW). We chose IDW because gives the best results for visualizing due to our spatially correlated data.

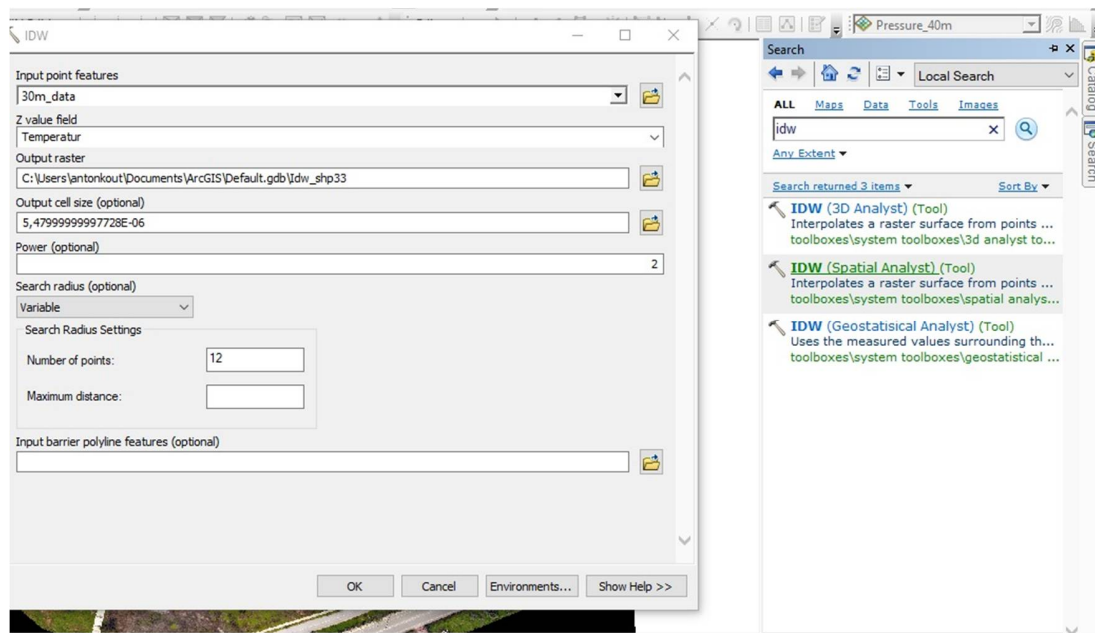


Figure 3.39: The IDW Spatial Analyst

The following figure illustrates the results of the IDW method. At the output layer we set the transparency from the layer properties at 50% in order to see exactly the position of each value at the base map.

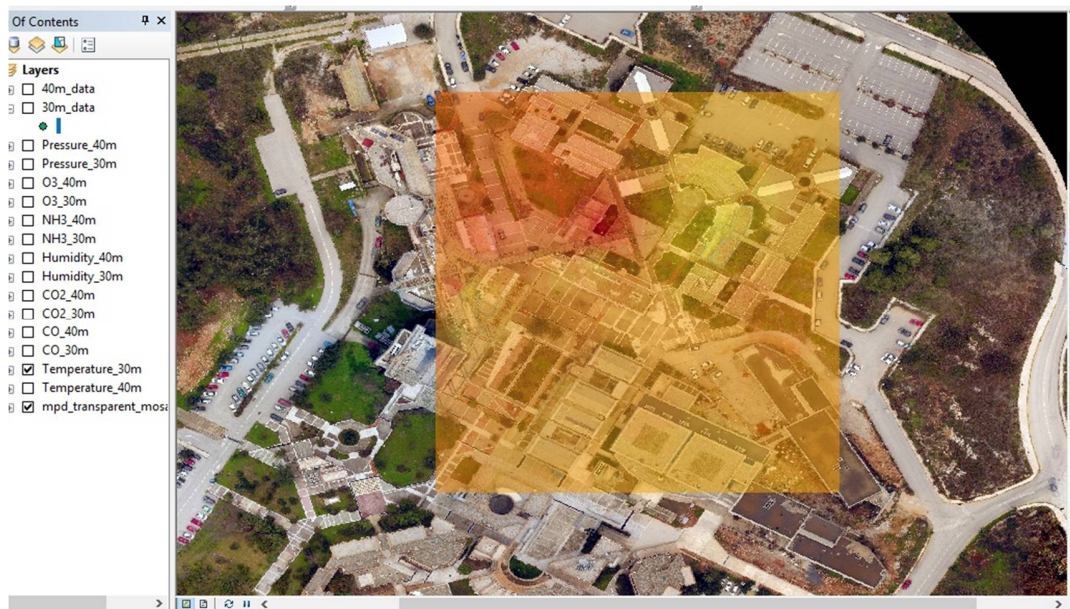


Figure 3.40: The result of the IDW method



3.4.4 3D visualization

As long as the 3D visualization is concerned, we processed our data with the ArcScene software. Essentially, ArcScene is a 3D visualization application that allows viewing the GIS data in three dimensions. Again the first step is to add the data into ArcScene again with the “Add XY Data” option. We add the path to our excel spread sheet and we choose which parameter we want to visualize. Finally we choose the correct coordinate system, which is “GCS_GGRS_1987” for Greece.

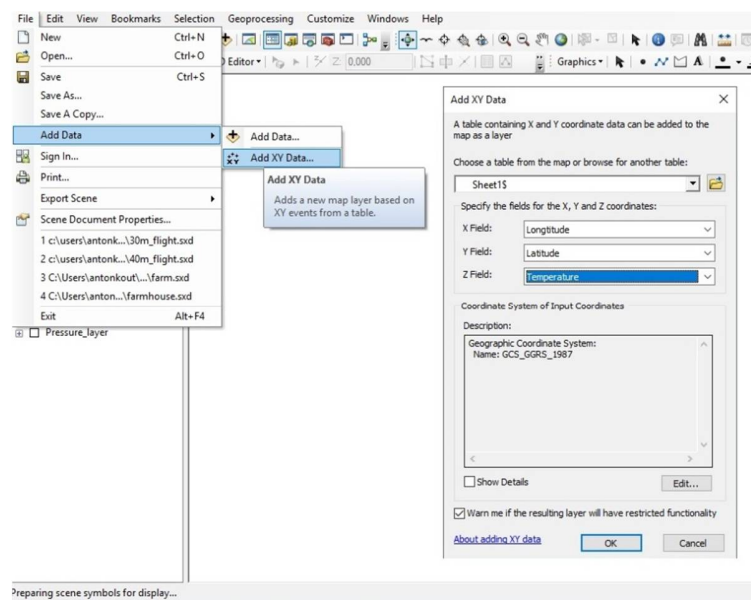


Figure 3.41: Initializing the data in 3D

Our importing data are now in three dimensions in our work space.

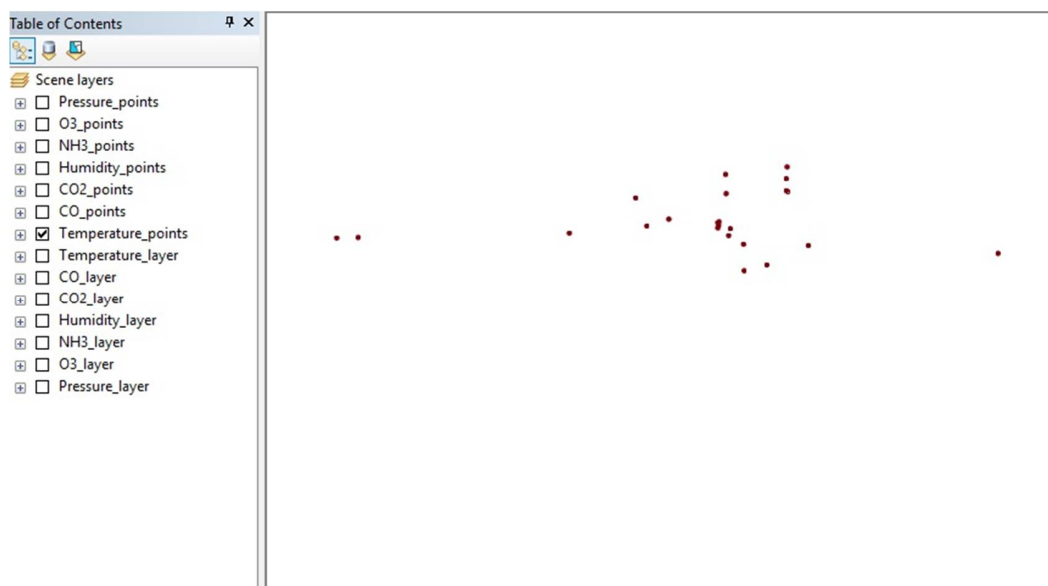


Figure 3.42: Point Cloud



Furthermore, we process our data with the Inverse Distance Weighting interpolating method (IDW) again but for 3D illustration.

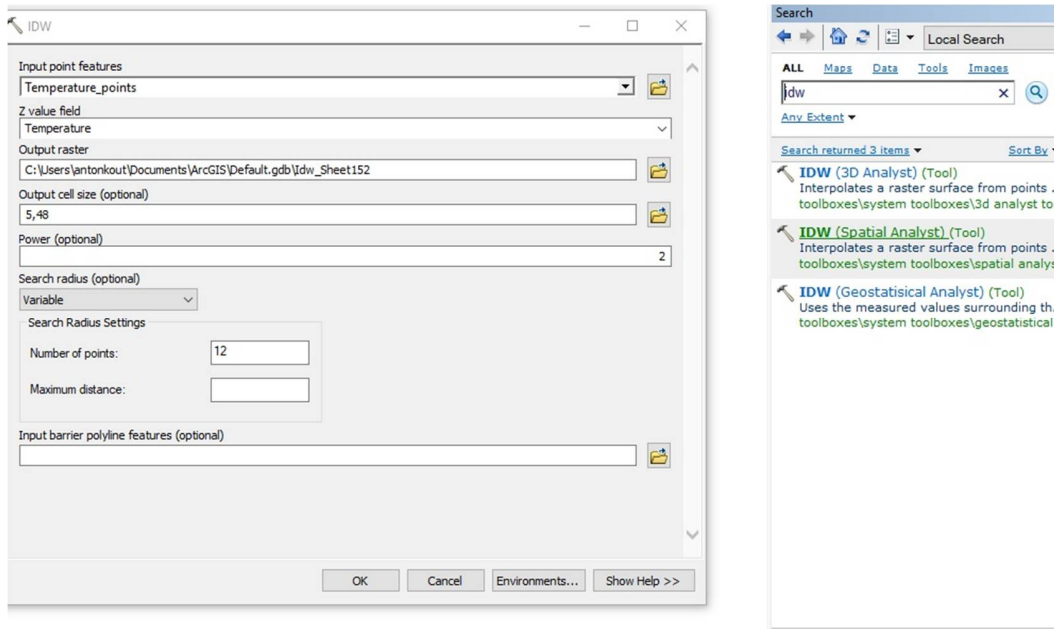


Figure 3.43: The IDW Spatial Analyst

The following figure illustrates the results of the IDW method.

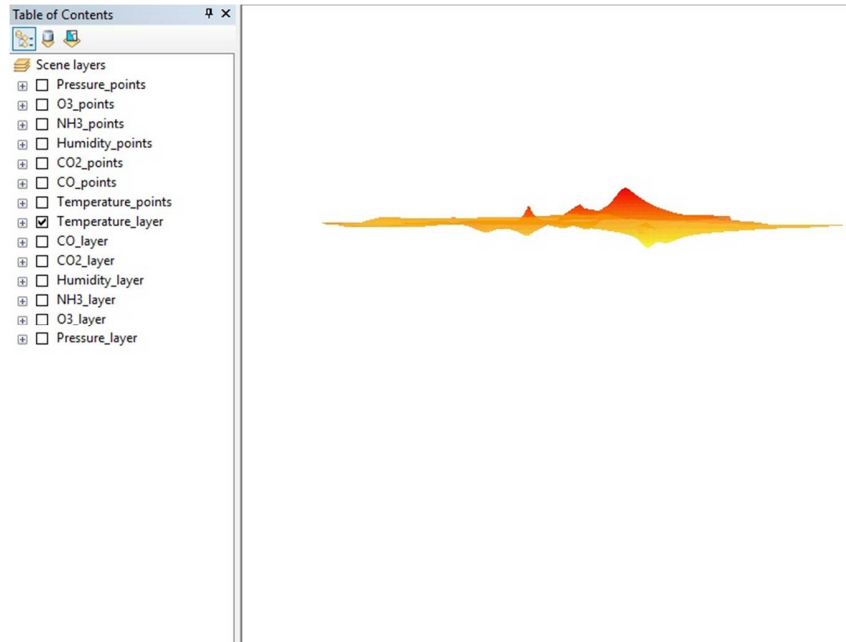


Figure 3.44: The result of the IDW method

In ArcScene there is no need to export the data at a shapefile in order to process them. Moreover, it is worth mentioning that we don't add a base-map to our



workspace in ArcScene, since we will illustrate the 3D layers above the constructed 3D model is in .obj format and it is not supported in ArcScene.

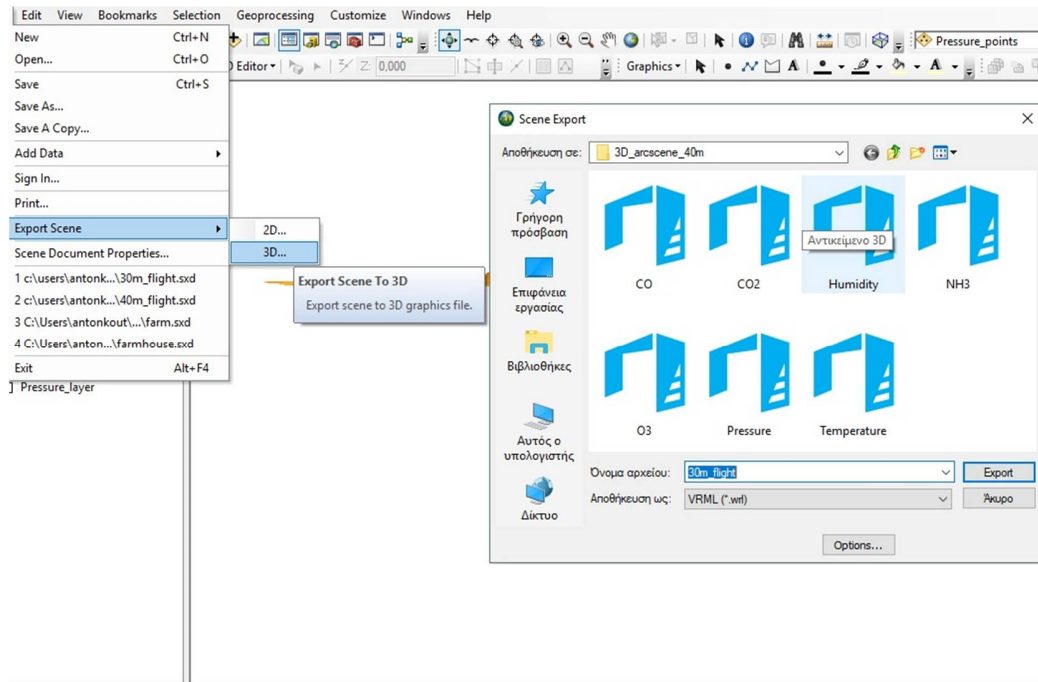


Figure 3.45: Exporting 3D layer into .wrl format

This is done with the 3ds Max, which is a software for 3D modeling, animation, rendering, and visualization. First we need to export our 3D layers into a .wrl format.

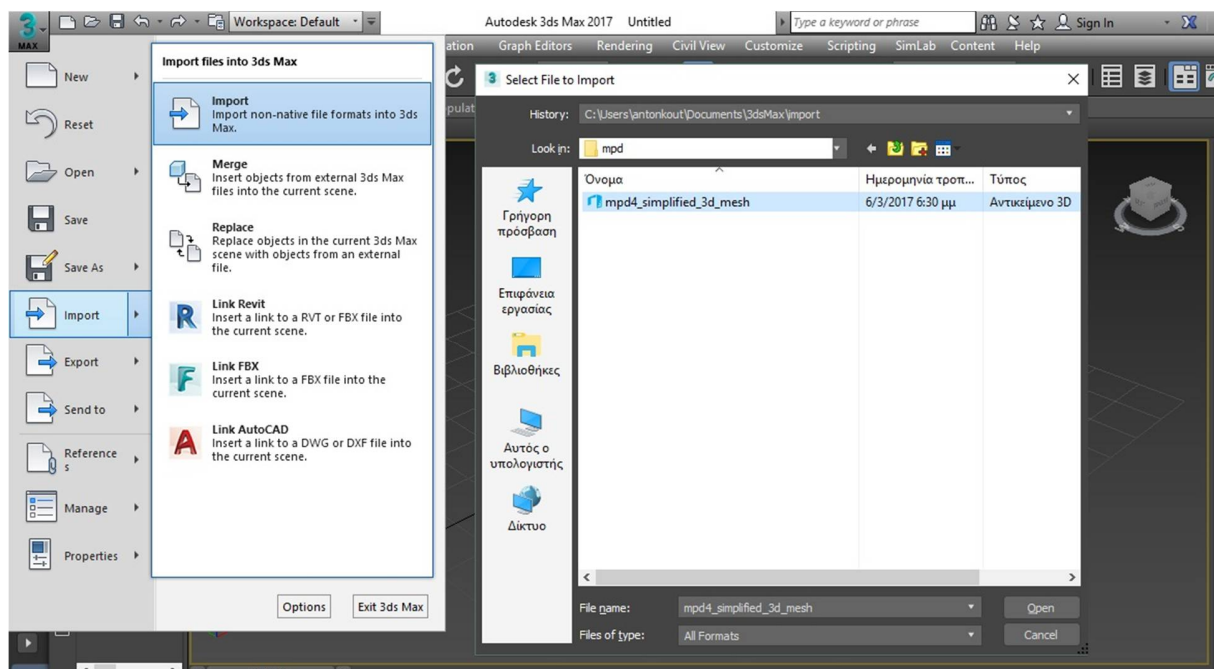


Figure 3.46: Importing the 3D mesh



The exported file has two parts, the .wrl file and the image of the 3d object. To be more specific, a WRL file includes data specifying 3-D details such as vertices, edges for a 3-D polygon, whereas the surface color, image-mapped textures, light and reflection mapping are included at a second JPG file. Then, we import our 3D model, which was created via Pix4Ddesktop software, into the workspace and we set the position of the model at the three axes to 0. This is done by choosing from the basic menu the “Hierarchy” option->Affect pivot only-> Center to object.

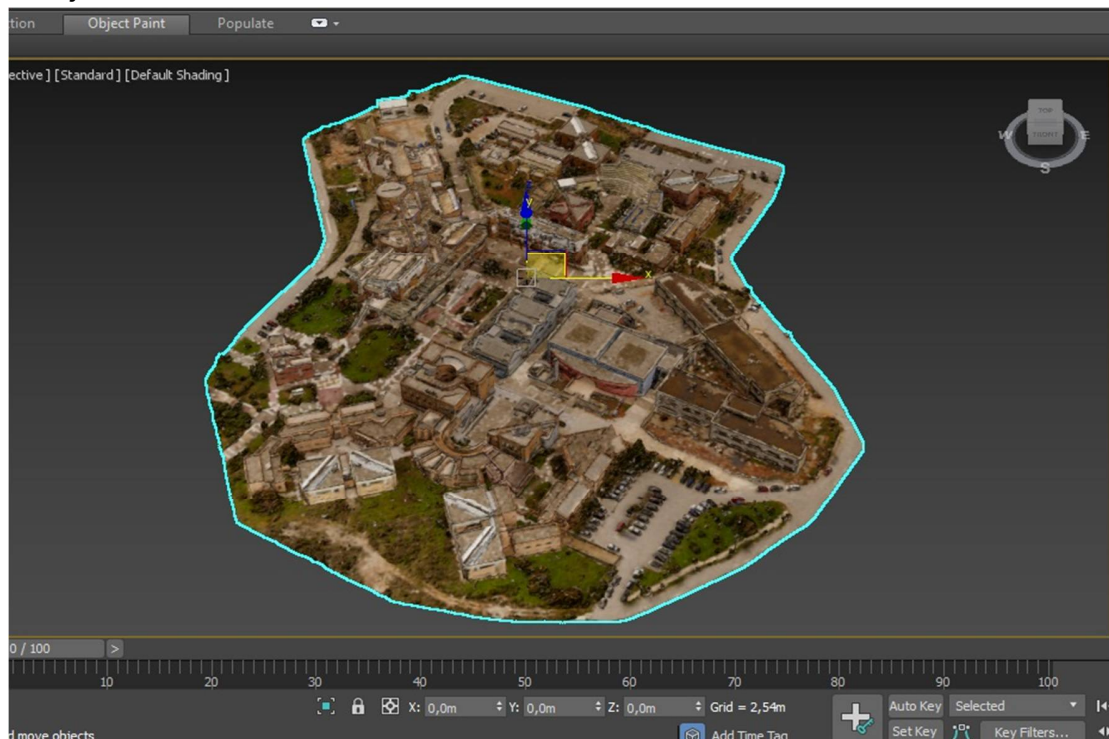


Figure 3.47: Setting the position of the mesh at the beginning of the axes

After initializing our mesh we are ready to import our 3D layer to the workspace. The output of ArcScene, as it was mentioned above is a .wrl file and a .jpg image. After importing the .wrl file into 3ds Max, we need to apply the image to the layer. This is done using the “Material Editor” option. At the material editor we choose the “Material/Map Browser” option. Then from the opening list we choose the “mental ray category”->“Arch & Design”. From the opening window, we double click the title (Arch & Design) and the editing window opens. Through the “Main material parameters”->“Color”->“Bitmap” we choose the image that we want to apply on our layer. After selecting our image, we need to turn on the “Show Shaded Material in Viewport” option that is located at the top bar of material editor in order to appear our image to the workspace.

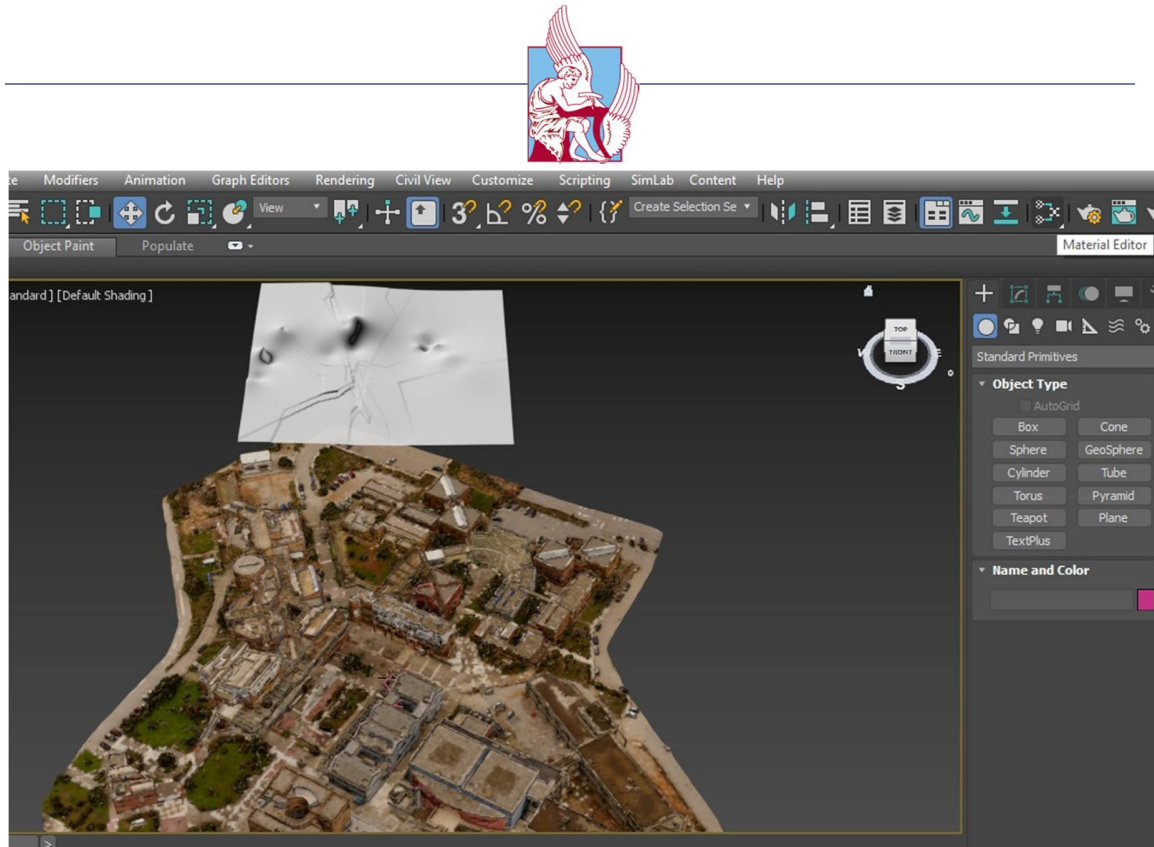


Figure 3.48: Applying the .jpg file to the.wrl file

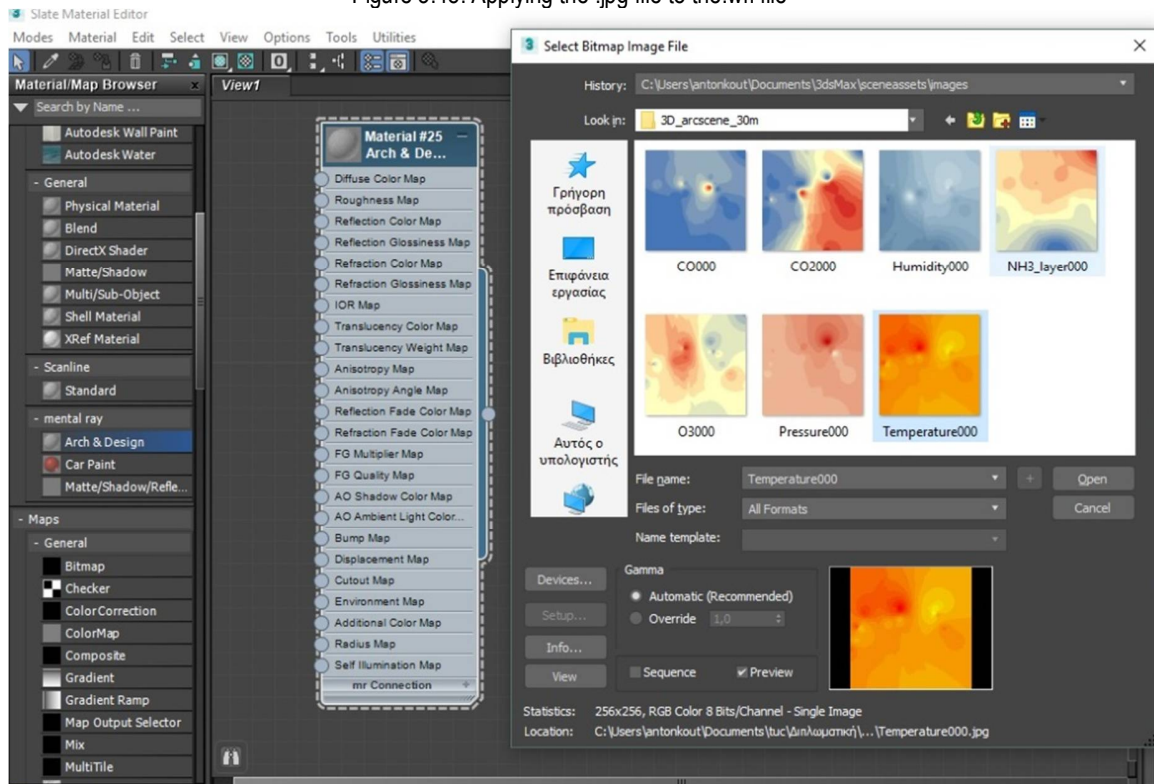


Figure 3.49: Selecting the image file from the Material editor

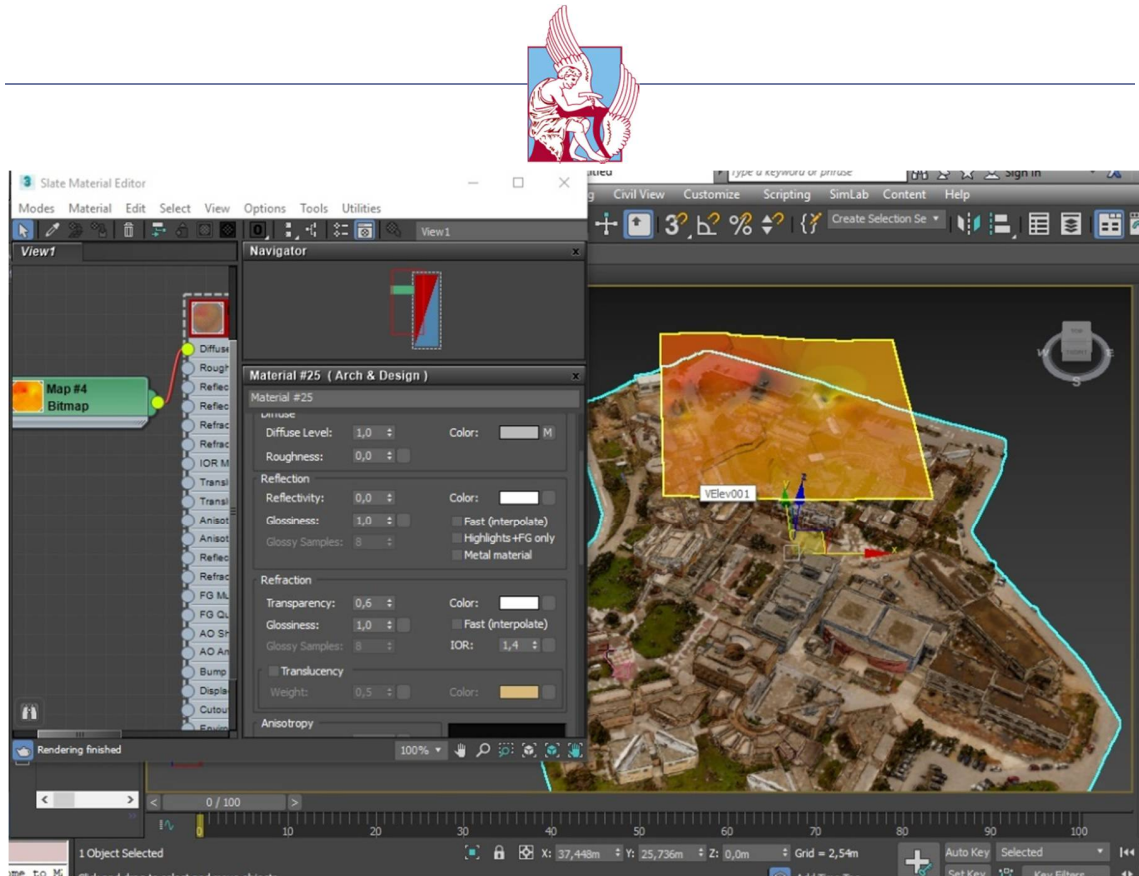


Figure 3.50: Setting transparency to the layer

Again we set transparency to our layer in order to see through the layer the 3D mesh.



Figure 3.48: The geo-referenced layer above the 3D model



Moreover, we need to align these two models and set the layer to its exact position in space. In the 2D visualization with Arcmap this is done automatically, since the orthomosaic is a geo-referenced .png image. This means that the image has also information about the space, having coordinates for each pixel of the image. However, at the 3D visualization, we need to calculate the position of the models manually. The 3D mesh that was created from Pix4Ddeskop is an .obj file, which lacks the information of space. In order to geo-reference these two we just need to find a common point with the same coordinates. After setting the layer at the beginning of the axes, we find the coordinates of the points manually and then we check where these sets of coordinates are corresponding to our layer. With the same methodology we add the second 3D layer that is created from the 40 meter height.



Chapter 4

Results

This Chapter gives an analysis of the final results of the data procedure.

4.1 Final 3D model and Orthomosaic

After the customization of data, the 3D model from the captured photos was created. It took approximately 24 hours to create this 3D model due to the large number of the photos. Furthermore, the created 3D mesh was processed, removing out of the model any noise point cloud (points created illustrating clouds or sky) and adjusting the model at the area of interest. The following figure shows the results of the Pix4D process.



Figure 4.1: The created 3D mesh



Figure 4.2: The created mesh from another view



As regards the orthomosaic , is a 2D map. Each point contains X, Y and color information. The orthomosaic has uniform scale and can be used for 2D measurements (distance, surface). The orthomosaic generation is based on orthorectification. This method removes the perspective distortions from the images using the 3D model. A high number of matches/keypoints (more than 1000) is required to generate the 3D model. This method handles all types of terrain, as well as large datasets. Distances are preserved and therefore the orthomosaic can be used for measurements.



Figure 4.3: The created Orthomosaic

4.2 2D maps of data visualization

The measured gases were CO, CO₂, SO₂, NO₂, NH₃, O₃ as well as the Temperature, Humidity and Atmospheric pressure. Nevertheless, the sensor gave zero results for SO₂ and NO₂ and that was the reason that there is no visualization of these gases. Furthermore, the concentration of ammonia (NH₃) at the atmosphere was almost the same without showing any particular variation, showing differences only after the fifth decimal. After the process of the data through the Arcmap platform, 2D maps for the visualization of the data were created. The export format can be varying. The following figures illustrate the constructed maps. The process was done separately for two different heights (30 meters and 40 meters) and thereafter the two different layers were attached into one map.



- CO air emissions
- CO at 30 meters

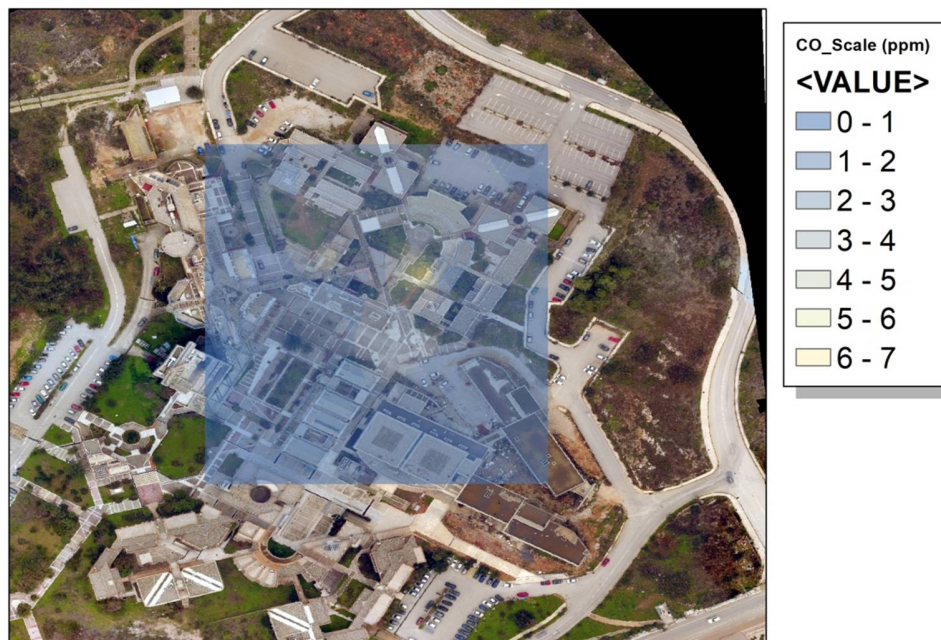


Figure 4.4: CO measurements at 30 meters

CO at 40 meters

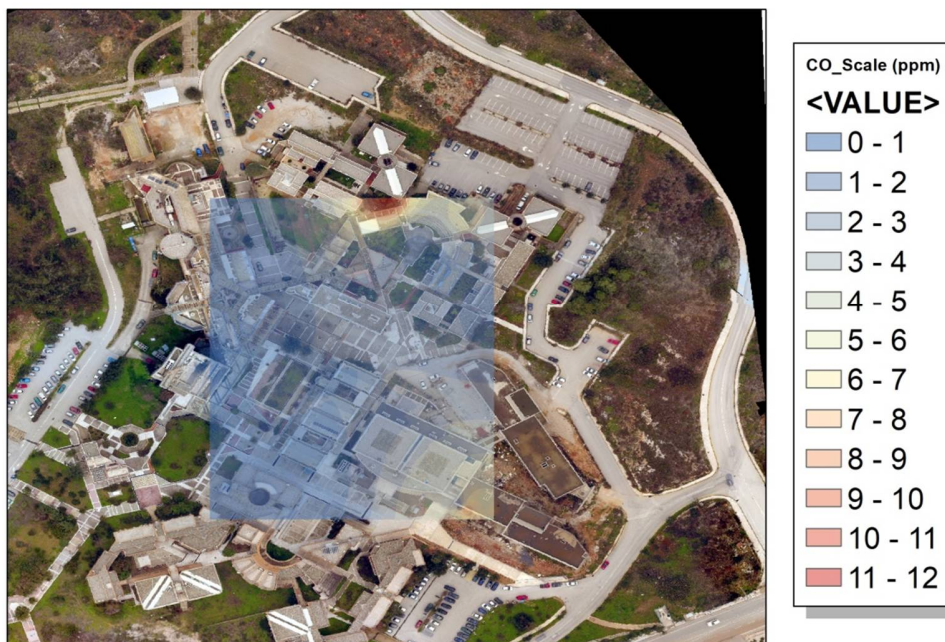


Figure 4.5: CO measurements at 40 meters



CO

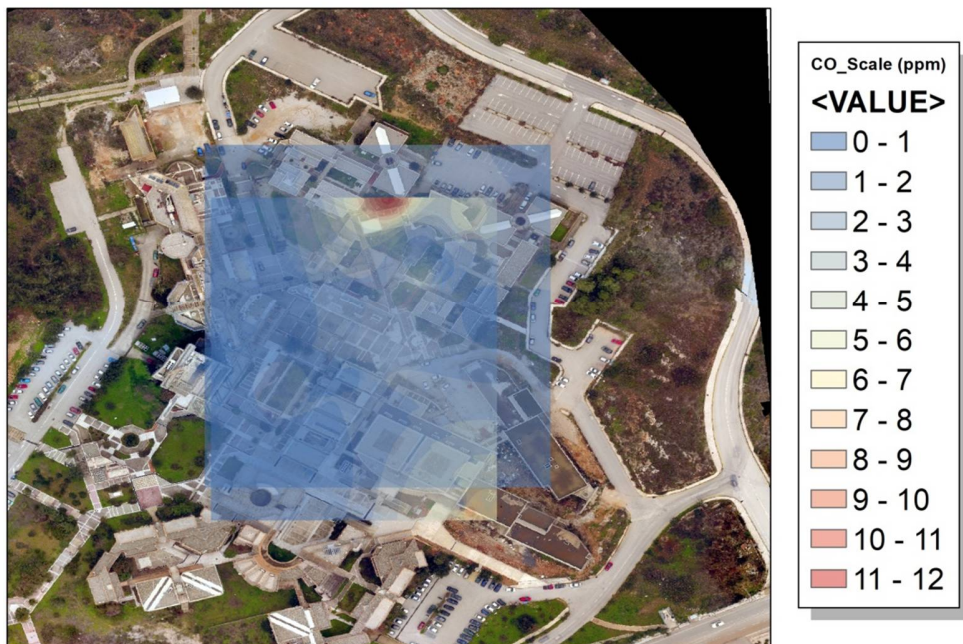


Figure 4.6: The two CO layers attached

As it is illustrated, there are low concentrations of CO at the atmosphere.

- CO₂ air emissions
- CO₂ at 30 meters



Figure 4.7: CO₂ measurements at 30 meters



CO₂ at 40 meters

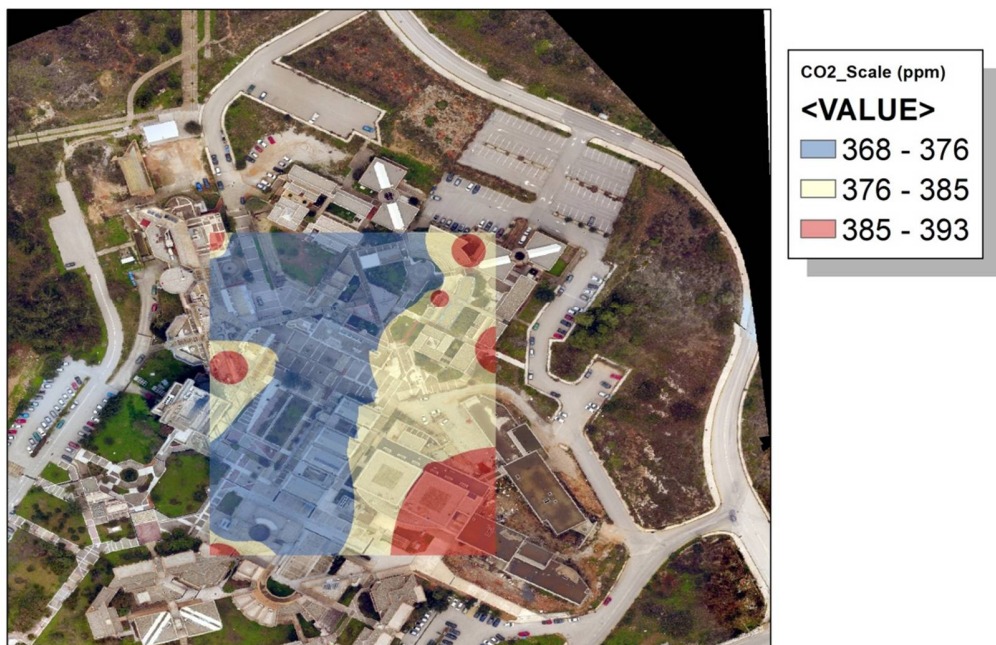


Figure 4.8: CO₂ measurements at 40 meters

CO₂



Figure 4.9: The two CO₂ layers attached

The normal levels of CO₂ at the atmosphere are approximately 380 ppm. We can denote some high concentrations above the parking lot and the chimney of the university's restaurant.



- O₃ air emissions
- O₃ at 30 meters



Figure 4.10: O₃ measurements at 30 meters

- O₃ at 40 meters

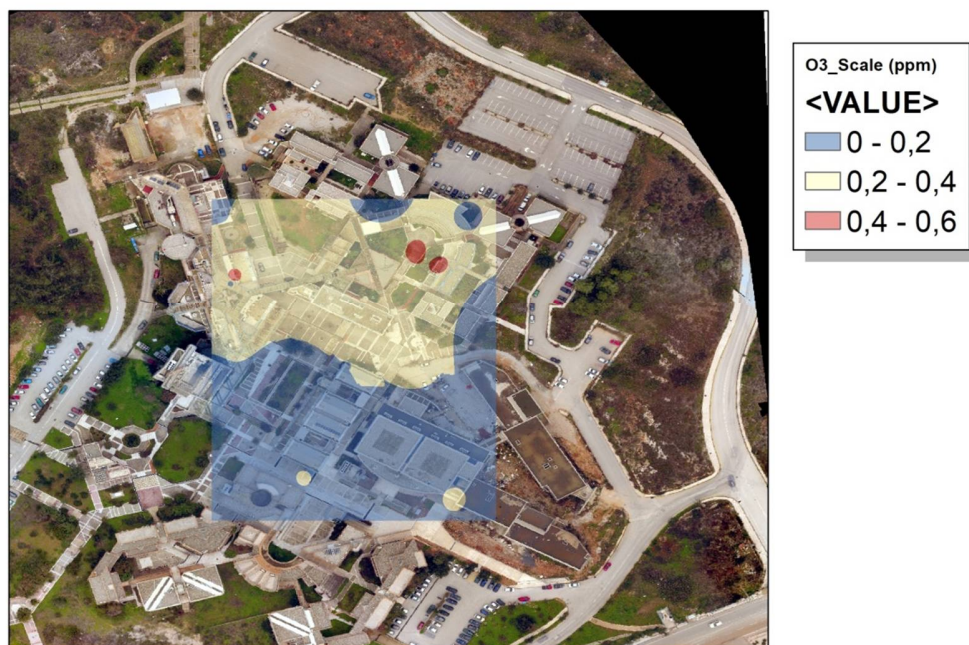


Figure 4.11: O₃ measurements at 40 meters



O3

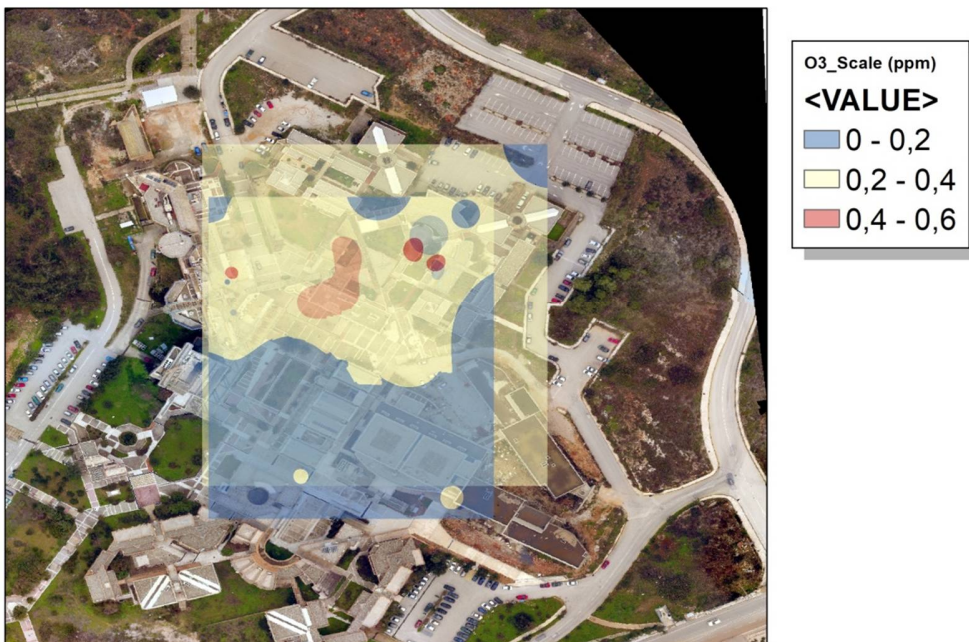


Figure 4.12: The two O₃ layers attached

As regards the O₃ gases, we can underline low concentration at the atmosphere.

- Temperature above the buildings.
Temperature at 30 meters

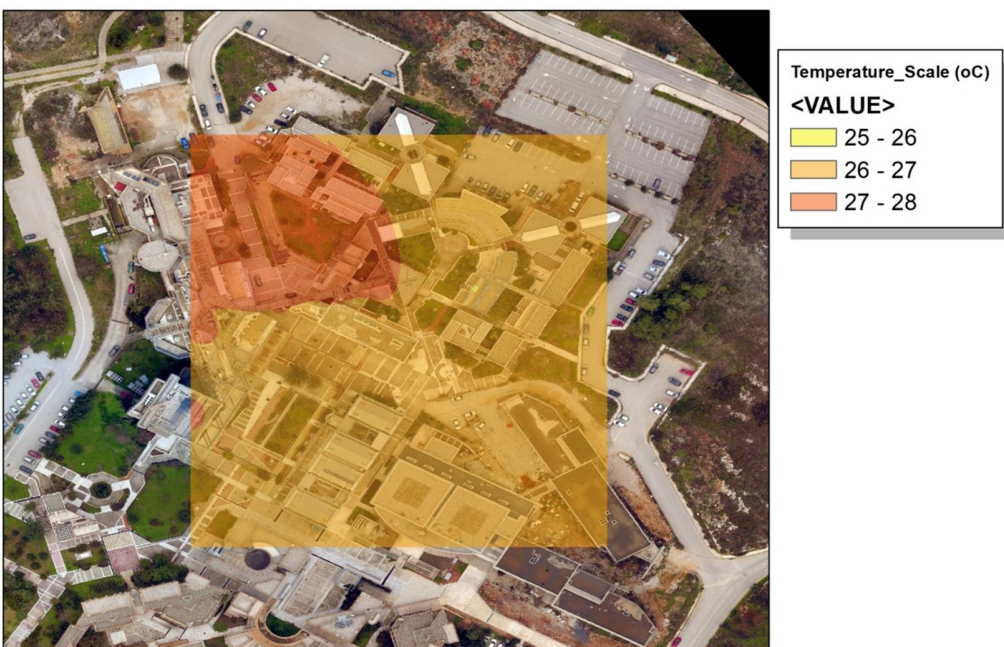


Figure 4.13: Temperature measurements at 30 meters



Temperature at 40 meters



Figure 4.14: Temperature measurements at 40 meters

Temperature

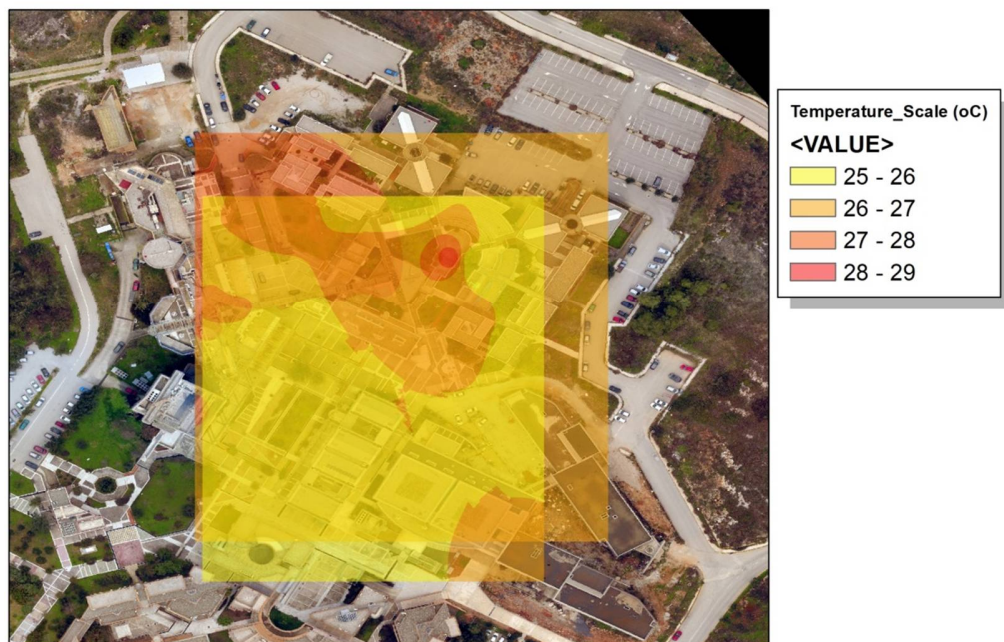


Figure 4.15: The two temperature layers attached

It is obvious, an approximately one degree difference of the temperature at two different heights.



➤ Humidity
Humidity at 30 meters

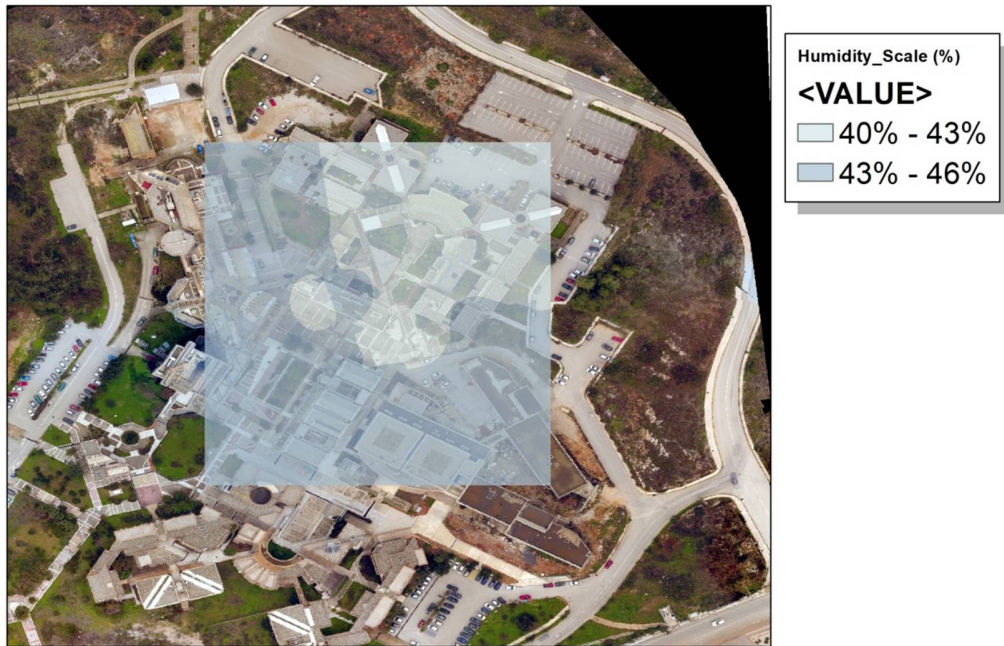


Figure 4.16: Humidity measurements at 30 meters

Humidity at 40 meters

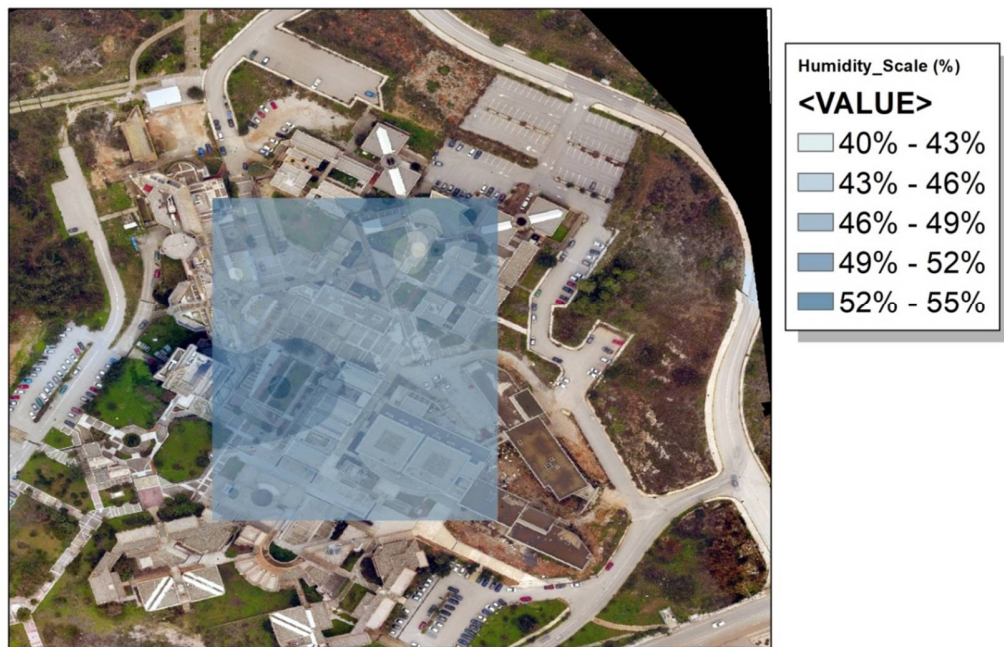


Figure 4.17: Humidity measurements at 40 meters



Humidity

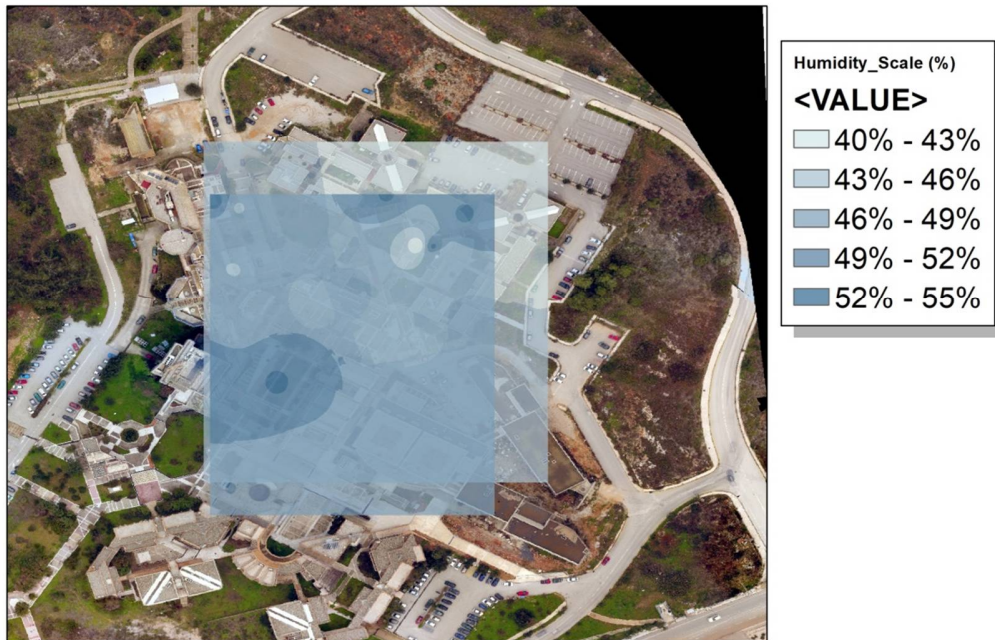


Figure 4.18: The two humidity layers attached

We can underline that, the highest humidity percentage was above the courtyard and trees, and it was increased at higher height.

- Atmospheric pressure data
Pressure at 30 meters



Figure 4.19: Atmospheric pressure measurements at 30 meters



Pressure at 40 meters

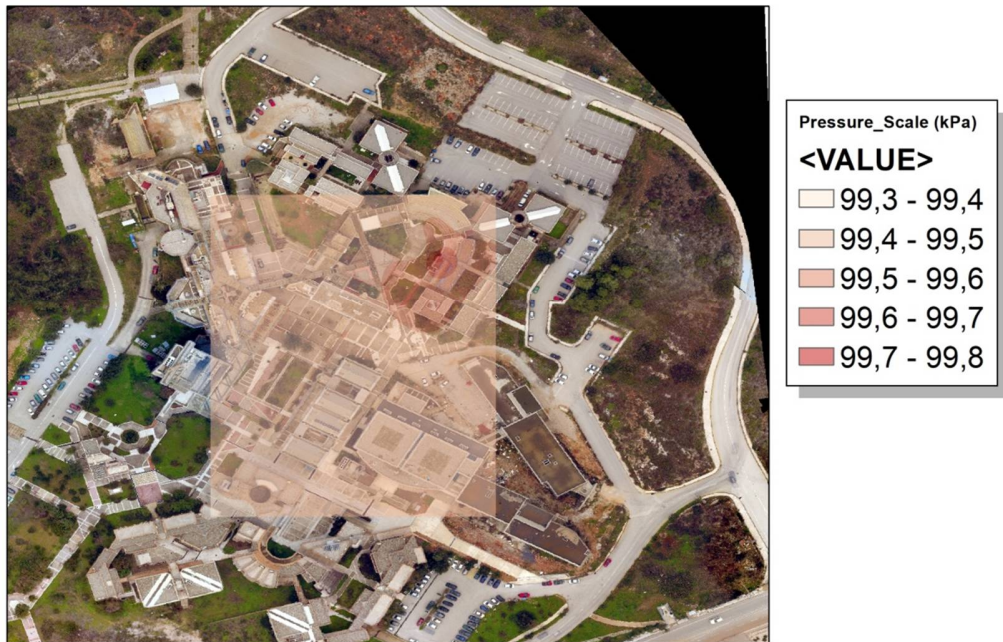


Figure 4.20: Atmospheric pressure measurements at 40 meters

Pressure

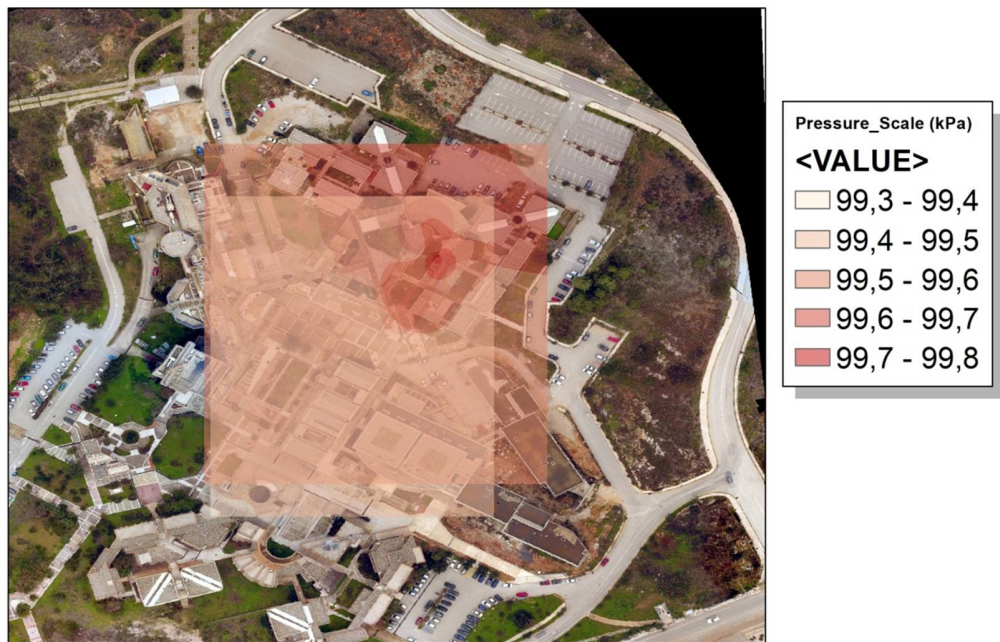


Figure 4.21: The two atmospheric pressure layers attached

We can easily denote the fact that the atmospheric pressure decreases at a higher height.



4.3 Geo-referencing junction of 3D model and 3D layers

The following figures show three different aspects of the 3D models.

- CO air emissions

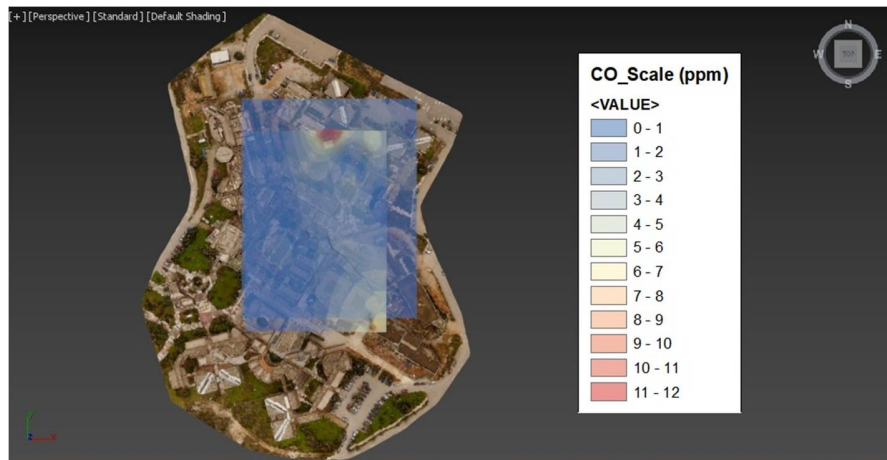


Figure 4.22: Top view of CO

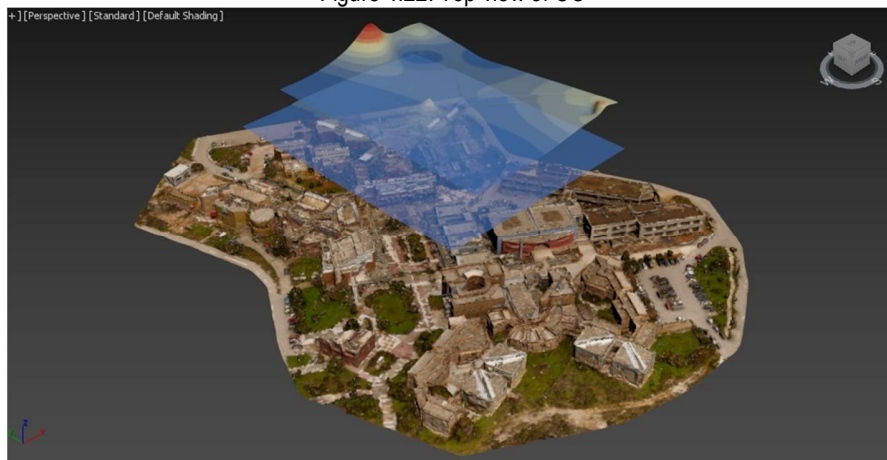


Figure 4.23: Angle view of CO

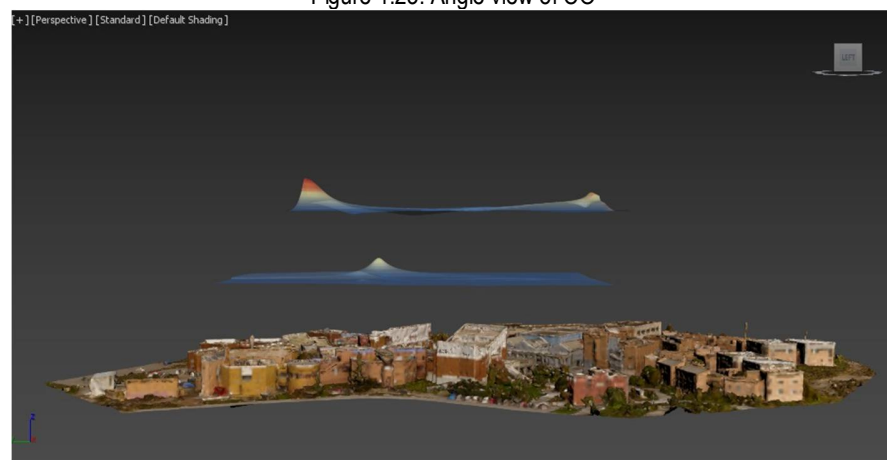


Figure 4.24: Left view of CO



➤ CO₂ air emissions

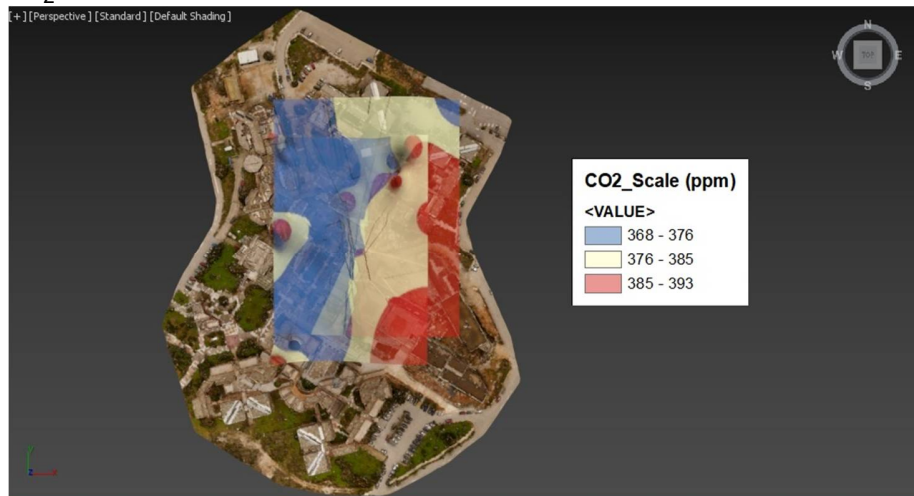


Figure 4.25: Top view of CO₂

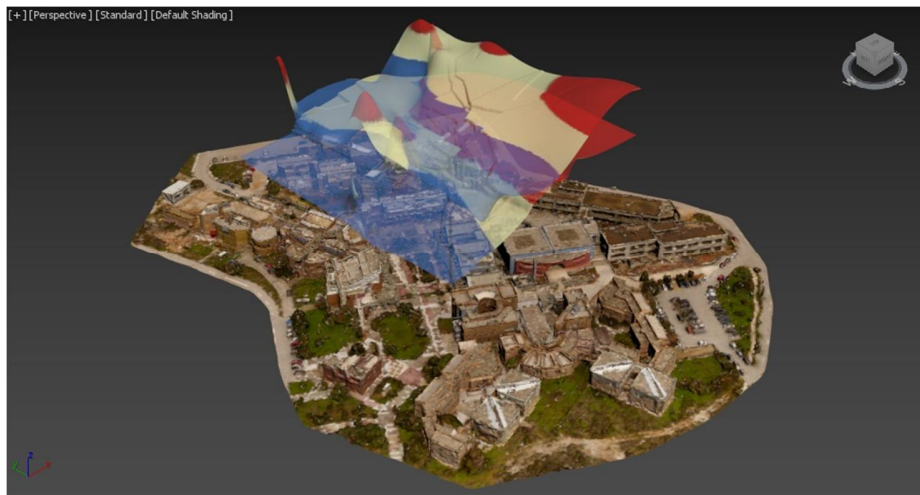


Figure 4.26: Angle view of CO₂

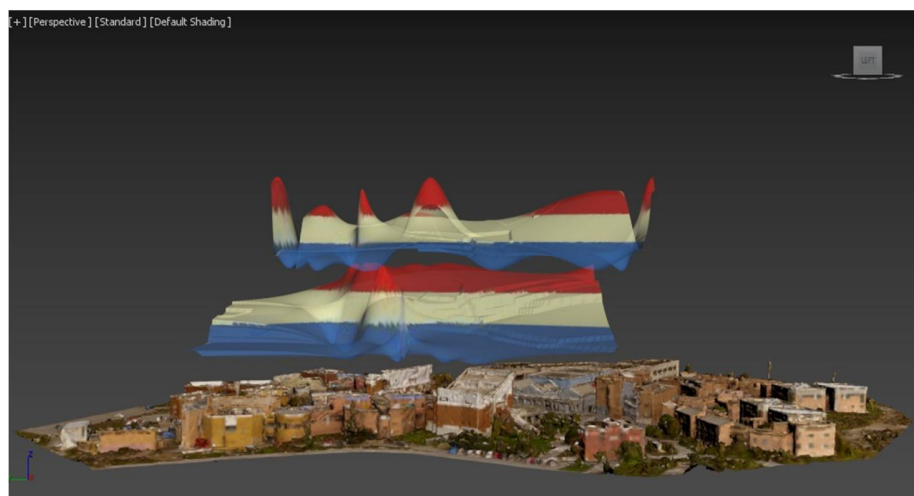


Figure 4.27: Left view of CO₂



➤ O₃ air emissions

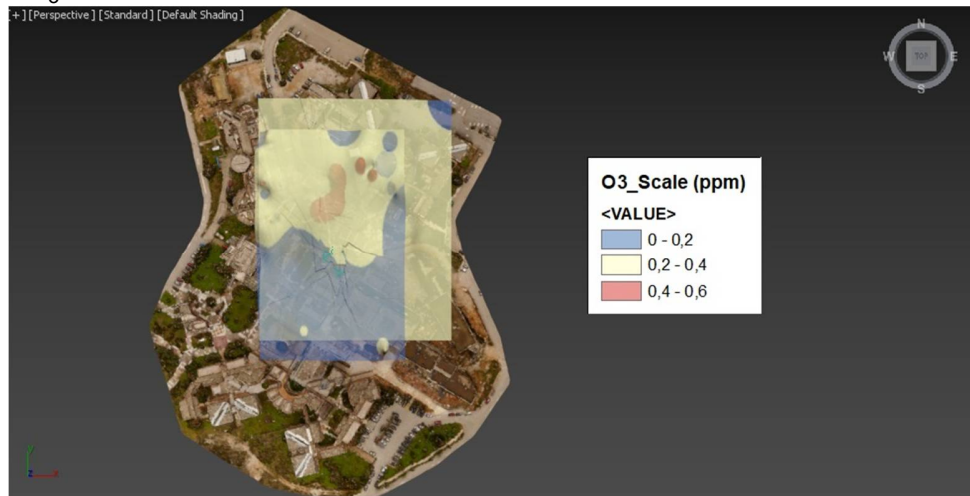


Figure 4.28: Top view of O₃

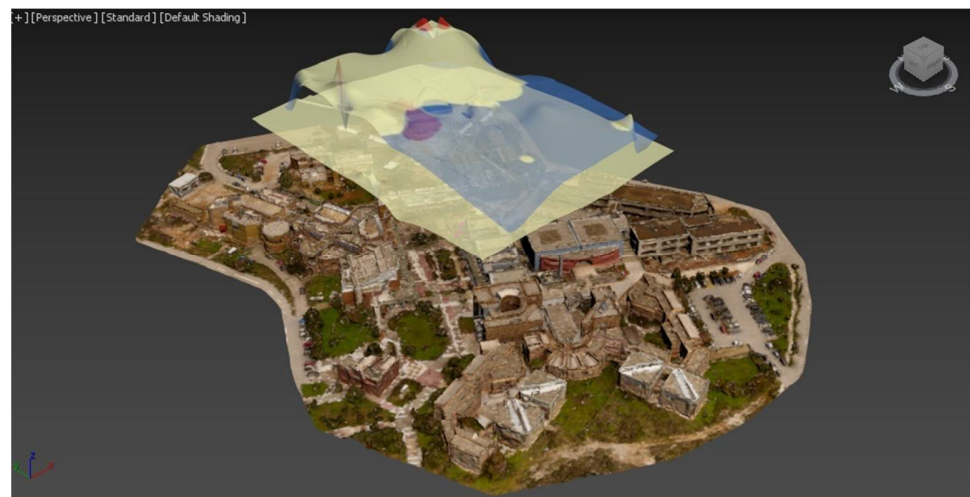


Figure 4.29: Angle view of O₃

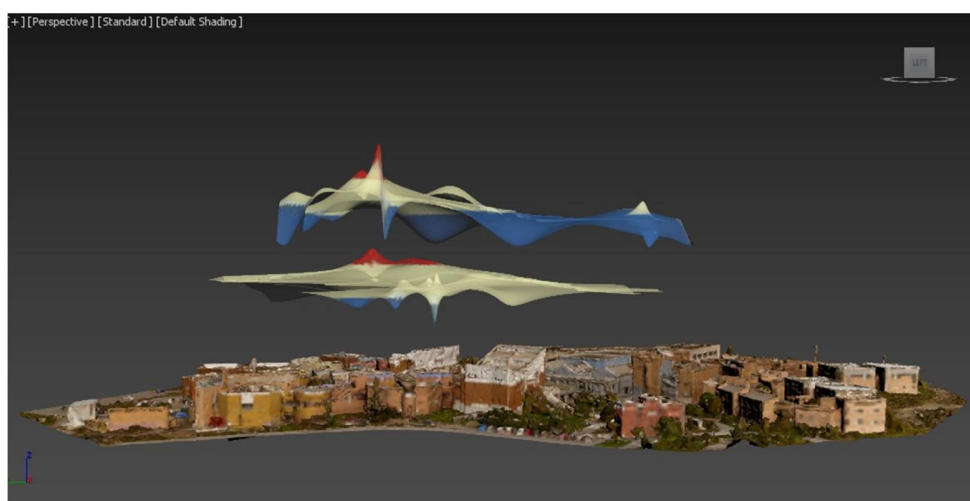


Figure 4.30: Left view of O₃



➤ Temperature

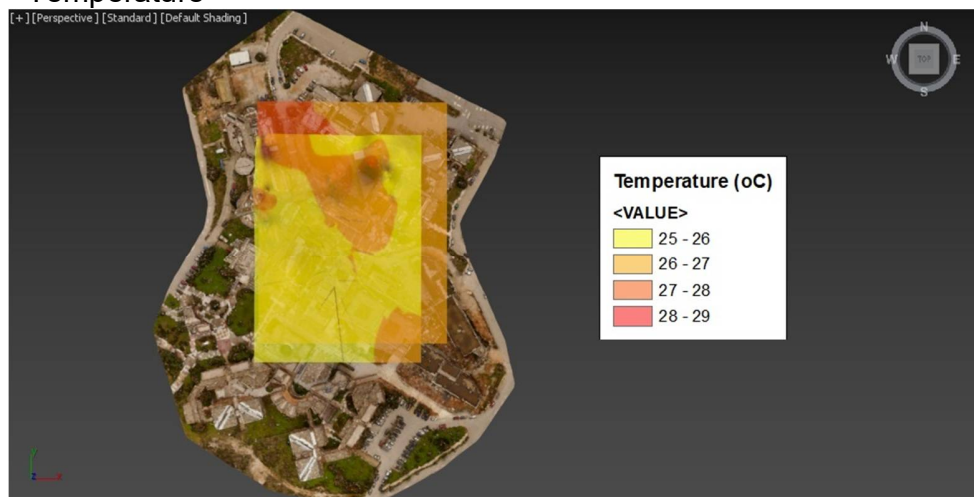


Figure 4.31: Top view of Temperature

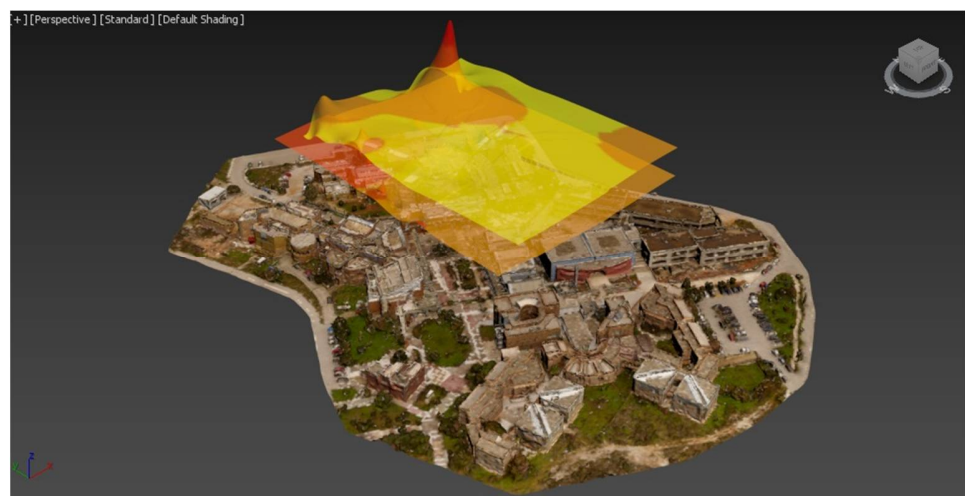


Figure 4.32: Angle view of Temperature

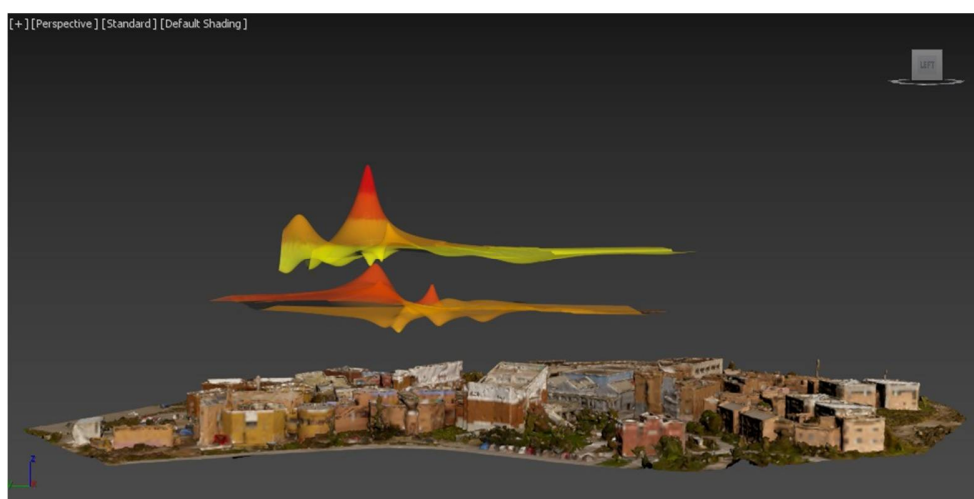


Figure 4.33: Left view of Temperature



➤ Humidity



Figure 4.34: Top view of Humidity

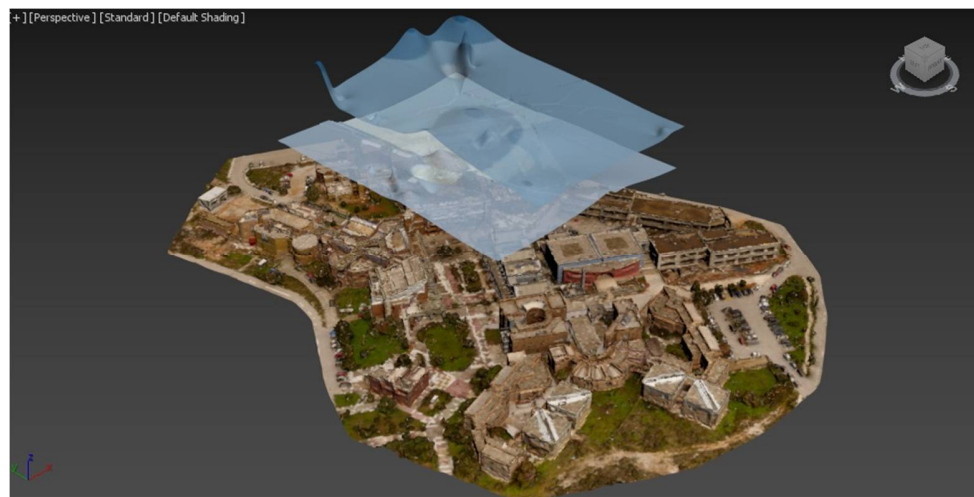


Figure 4.35: Angle view of Humidity

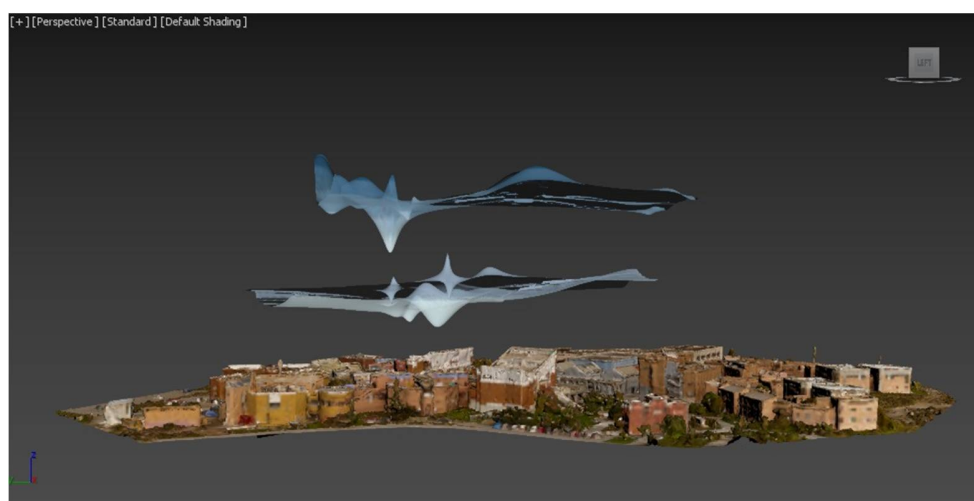


Figure 4.36: Left view of Humidity



➤ Atmospheric Pressure

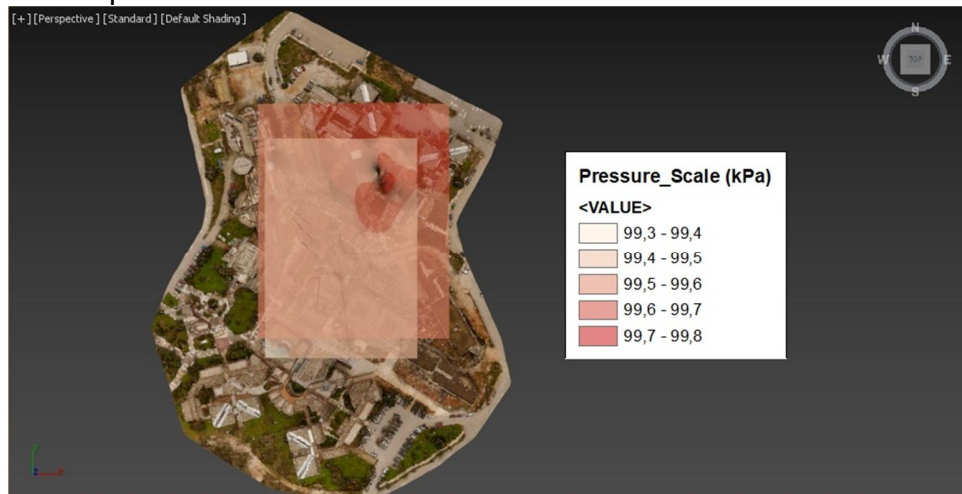


Figure 4.37: Top view of Pressure

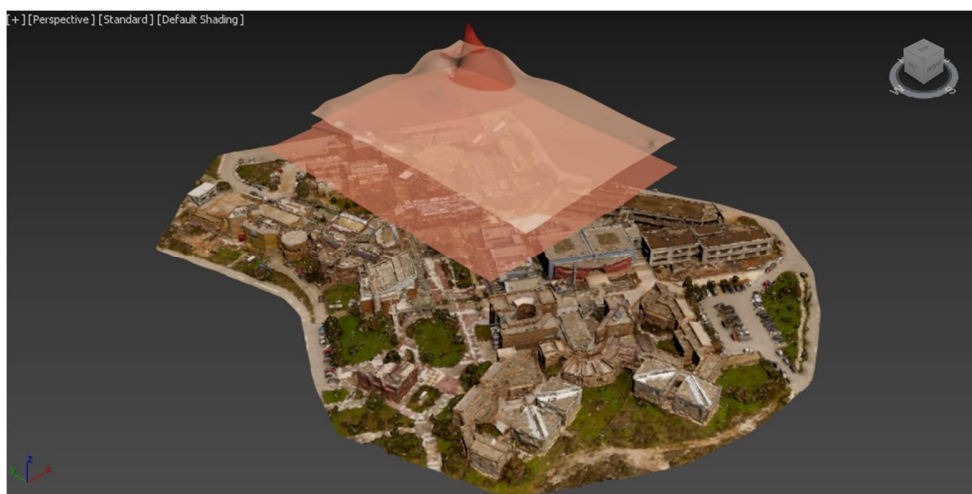


Figure 4.38: Angle view of Pressure

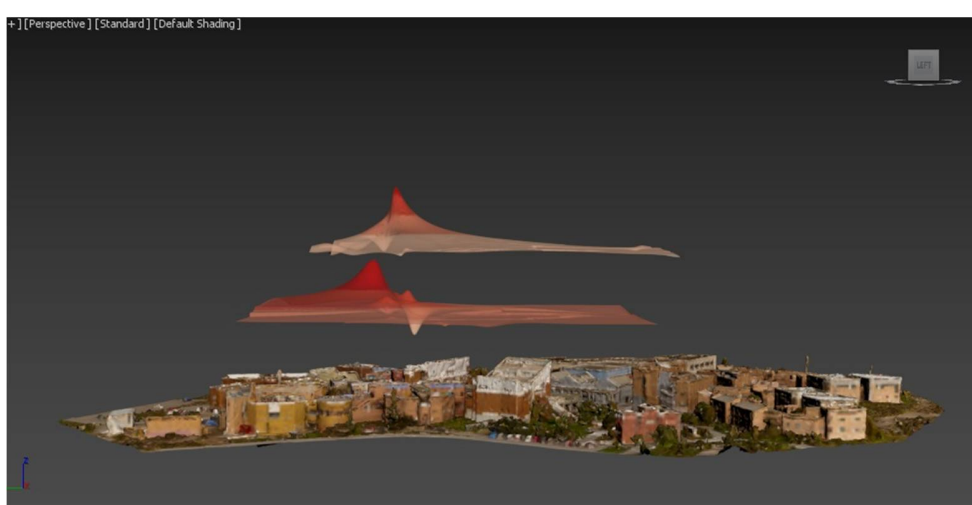


Figure 4.39: Left view of Pressure



Chapter 5

Discussion and Conclusions

This Chapter concludes this thesis by summarizing the content, proposing advances and suggests other areas of applications.

5.1 Conclusions

As it was shown from this thesis, UAVs can offer high resolution spatiotemporal sampling, which is not possible or feasible with manned aircrafts. The future of UAVs for use in air quality applications is promising, thanks to the capability and flexibility of these robotic platforms. The key factors in the new sensor development include: power, mass, and size, because these are intimately connected to the type of platform (rotary instead of fixed wings), engine (electrically or gas powered) and the type of mission (speed, longer distances with low altitude). The presented work has developed concepts and techniques for visualizing air gas emissions in 2D and 3D form. In particular, it has introduced a new way of measure air data, proposing the use of Unmanned Aerial Vehicles with onboard gas sensors. The platform selected in this thesis was the DJI's quadrotor drone, Phantom 4. In addition, the aerial photos captured by the drone, were processed through the photogrammetric software Pix4d, in order to create a three dimension model of the area of investigation. On the drone was mounted also a gas sensor board that measured air data. Furthermore, the data were transmitted and saved into a data-base, where they were processed afterwards. The main purposes of this thesis, apart from suggesting a new approach for gas measurements, was to visualize these air emissions in 2D and 3D, create a 3D mesh of the study area and visualize the data above the geo-referenced 3D model for better understanding the distribution of the air pollutants. Moreover, the Technical University of Crete, to be more precise the buildings of the School of Production and Management Engineering, was chosen as the area of study. As regards the results of this study, it was more a confirmation of the expected results without noticing any anomaly in the air quality above the University's campus. Some of the major importance results of this thesis were the emissions of CO₂ from the chimney of the University's restaurant and from the parking lot. This thesis can be used as the base for further investigation, since this methodology can be applied in areas



with high concentrations of air pollutants like industrial zones and harbors were the air quality monitoring is necessary.

5.2 Future Work

Apart from applying this study at other areas of interest, this methodology can be advanced in many ways. First and foremost, the use of more than one Unmanned Aerial Vehicles could be useful, since more data at the same time and at different locations and heights could be collected, giving the opportunity to investigate at a bigger scale the air quality. Secondly, it is proposed a real-time 3D visualization of the measured data above a 3D model of the area of interest. This application requires high programming skills as it is more complicated than processing the data manually, nevertheless it could be an effective tool for acquiring directly information about air pollutants. Lastly, apart for monitoring the quality of air at the atmosphere above an area, the survey of gas emissions from ships or airplanes when they are operating, is suggested in order to investigate how much they encumber the environment. Nowadays, UAVs have the ability to lock at a target and follow it for some time period from a distance. This feature could be used to monitor, for example, the emission of pollutants from a ship's smokestack.

5.3 Other areas of application

The basic theory underlying this thesis was the principles of remote sensing. In this study, the remote sensing was used in order to investigate, with the use of UAVs, gas emissions through sensors. Another innovative methodology introduced in order to observe the air composition would be through the use of Biosensors. The increasing number of potentially harmful pollutants in the environment requires fast and cost-efficient analysis to be used in extensive monitoring programs. The need for disposable systems or tools for environmental applications, in particular for environmental monitoring has encouraged the development of new technologies and more suitable methodologies. Furthermore, the use of UAVs gives the opportunity to reach remote areas and gather the data of interest. Moreover, with the living biosensors, which are engineered to glow a particular color in response to a given pollutant, we could easily detect dangerous gas emissions and interfere directly with high accuracy taking preventive measures. Nevertheless, the application of remote sensing could be applied in a variety of areas, like agriculture. An innovative idea is applying remote sensing for monitoring Honey Bee Colonies. Bees are very important for terrestrial ecosystems and above all, for the subsistence of many



crops, due to their ability to pollinate flowers. Currently, honey bee populations have seen a significant fall due to Colony Collapse Disorder (CCD). The nature of this disorder has not yet been determined and as a result, it is essential to acquire all possible information on the environmental conditions surrounding the beehives. By the same token, it is important to obtain such information as non-intrusively as possible to avoid modifying the bees' working environment and gather more trustworthy data. Based on all the above it is critical to construct an easily deployable system with regard to the number and types of sensors, the number of hives and simultaneously their geographical distribution. It is also essential to monitor in real time a hive and measure temperature and relative humidity data in order to intervene as quickly as possible in case of any disorder.



References

1. Monks, P.S.; Granier, C.; Fuzzi, S.; Stohl, A.; Williams, M.L.; Akimoto, H.; Amann, M.; Baklanov, A.; Baltensperger, U.; Bey, I.; et al. Atmospheric composition change—Global and regional air quality. *Atmos. Environ.* 2009, 43, 5268–5350. Available from: <http://www.sciencedirect.com/science/article/pii/S1352231009007109>
2. Lim, S.S.; Vos, T.; Flaxman, A.D.; Danaei, G.; Shibuya, K.; Adair-Rohani, H.; AlMazroa, M.A.; Amann, M.; Anderson, H.R.; Andrews, K.G.; et al. A comparative risk assessment of burden of disease and injury attributable to 67 risk factors and risk factor clusters in 21 regions, 1990–2010: A systematic analysis for the global burden of disease study 2010. *Lancet* 2012, 380, 2224–2260. Available from: [http://www.thelancet.com/journals/lancet/article/PIIS0140-6736\(12\)61766-8/abstract](http://www.thelancet.com/journals/lancet/article/PIIS0140-6736(12)61766-8/abstract)
3. Hansen, J.; Nazarenko, L. Soot climate forcing via snow and ice albedos. *Proc. Natl. Acad. Sci. USA* 2004, 101, 423–428. Available from: <http://www.pnas.org/content/101/2/423>
4. Jacobson, M.Z.; Kaufman, Y.J. Wind reduction by aerosol particles. *Geophys. Res. Lett.* 2006, 33. Available from: <http://onlinelibrary.wiley.com/doi/10.1029/2006GL027838/abstract;jsessionid=FB87B47097461593439322C50D33016D.f03t02>
5. Ramanathan, V.; Crutzen, P.J.; Lelieveld, J.; Mitra, A.P.; Althausen, D.; Anderson, J.; Andreae, M.O.; Cantrell, W.; Cass, G.R.; Chung, C.E.; et al. Indian ocean experiment: An integrated analysis of the climate forcing and effects of the great Indo-Asian haze. *J. Geophys. Res. Atmos.* 2001, 106, 28371–28398. Available from: <http://onlinelibrary.wiley.com/doi/10.1029/2001JD900133/abstract>
6. Lelieveld, J.; Berresheim, H.; Borrmann, S.; Crutzen, P.J.; Dentener, F.J.; Fischer, H.; Feichter, J.; Flatau, P.J.; Heland, J.; Holzinger, R.; et al. Global air pollution crossroads over the mediterranean. *Science* 2002, 298, 794–799. Available from: <http://science.sciencemag.org/content/298/5594/794>



7. Seinfeld, J.H.; Pandis, S.N. *Atmospheric Chemistry and Physics: From Air Pollution to Climate Change*, 2nd ed.; Wiley: Hoboken, NJ, USA, 2012.
8. Karion, A.; Sweeney, C.; Wolter, S.; Newberger, T.; Chen, H.; Andrews, A.; Kofler, J.; Neff, D.; Tans, P. Long-term greenhouse gas measurements from aircraft. *Atmos. Meas. Tech.* 2013, 6, 511–526. Available from: <http://www.atmos-meas-tech.net/6/511/2013/>
9. Wich, S.; Koh, L.P. Conservation drones. *GIM Int.* 2012, 26, 29–33.
10. Miller, D.J.; Sun, K.; Zondlo, M.A.; Kanter, D.; Dubovik, O.; Welton, E.J.; Winker, D.M.; Ginoux, P. Assessing boreal forest fire smoke aerosol impacts on U.S. Air quality: A case study using multiple data sets. *J. Geophys. Res. Atmos.* 2011, 116. Available from: <http://onlinelibrary.wiley.com/doi/10.1029/2011JD016170/abstract>
11. Corrigan, C.E.; Roberts, G.C.; Ramana, M.V.; Kim, D.; Ramanathan, V. Capturing vertical profiles of aerosols and black carbon over the Indian ocean using autonomous unmanned aerial vehicles. *Atmos. Chem. Phys.* 2008, 8, 737–747. Available from: <http://www.atmos-chem-phys.net/8/737/2008/>
12. Levy, R.C.; Remer, L.A.; Kaufman, Y.J. Effects of neglecting polarization on the modis aerosol retrieval over land. *IEEE Trans. Geosci. Remote Sens.* 2004, 42, 2576–2583. Available from: <http://ieeexplore.ieee.org/document/1356070/?reload=true>
13. Curry, J.; Maslanik, J.; Holland, G.; Pinto, J. Applications of aerosondes in the arctic. *Bull. Am. Meteorol. Soc.* 2004, 85, 1855–1861. Available from: <http://journals.ametsoc.org/doi/abs/10.1175/BAMS-85-12-1855>
14. Soddell, J.R.; McGuffie, K.; Holland, G.J. Intercomparison of atmospheric soundings from the aerosonde and radiosonde. *J. Appl. Meteorol.* 2004, 43, 1260–1269. Available from: [http://dx.doi.org/10.1175/1520-0450\(2004\)043<1260:IOASFT>2.0.CO;2](http://dx.doi.org/10.1175/1520-0450(2004)043<1260:IOASFT>2.0.CO;2)
15. Sandvik, Kristin Bergtora, and Maria Gabrielsen Jumbert. "The Good Drone." Google Books. Routledge, 22 Aug. 2016. Web. 02 May 2017.
16. European Commission. Commission Regulation (EU) 2105/1536. *Off J Eur Union.* 2015 ;(1321):16–48.
17. Gentile, Paul -. "Rise of Multicopter." *Rise of the Multicopter | Model Aviation.* -, - Dec. 2012. Web. 05 May 2017. Available here: <http://modelaviation.com/riseofmulticopter>



18. Juul M. Civil drones in the European Union. 2015 ;(October):1–8.
19. Yuhas C. Civil UAV. Assessment [Internet]. 2004;(December):1–7. Available from:
<http://scholar.google.com/scholar?hl=en&btnG=Search&q=intitle:Civil+UAV+Capability+Assessment#0>
20. Lozano, Sharon. "First Steps toward Drone Traffic Management." NASA. NASA, 19 Nov. 2015. Web. 05 May 2017. Available from:
<https://www.nasa.gov/feature/ames/first-steps-toward-drone-traffic-management>
21. EASA. "Civil Drones (Unmanned Aircraft)." Civil Drones (Unmanned Aircraft) EASA. European Aviation Safety Agency, -. Web. 05 May 2017. Available from:
<https://www.easa.europa.eu/easa-and-you/civil-drones-rpas>
22. Brooke-Holland L. Overview of military drones used by the UK armed forces. House Commons - Brief Pap. 2015;(6493):54.
23. Federal Aviation Administration. State and Local Regulation of Unmanned Aircraft Systems (UAS) Fact Sheet. 2015;40103(1):1–7.
24. Ben-Bassat Avi and Dahan Momi. Election Law Journal: Rules, Politics, and Policy. September 2015, 14(3): 190-206. Available from:
<http://online.liebertpub.com/doi/abs/10.1089/elj.2014.0296>
25. Carey, Bill. "Amazon Wins Exemption From FAA to Test Fly Small Drone." Aviation International News. Ainonline, 10 Apr. 2015. Web. 05 May 2017. Available from: <http://www.ainonline.com/aviation-news/aerospace/2015-04-10/amazon-wins-exemption-faa-test-fly-small-drone>
26. Greece, AIP -. "Airspace Restrictions and Hazards." Airspace Restrictions and Hazards (1982): n. pag. Civil Aviation Authority. AIP Greece, -. Web. 05 May 2017. Available from: http://hellasga.com/downloads/RAC_5.pdf
27. Αεροπορίας, Υπηρεσία Πολιτικής. "Υπηρεσία Πολιτικής Αεροπορίας - Νέα." Ypa.gr. Υπουργείο Υποδομών Μεταφορών και Δικτύων, 4 Oct. 2016. Web. 05 May 2017. Available from: <http://www.hcaa.gr/news/kanonismos-systhmatwn-mh-epandrwmewn-aeroskafwn-smhea-apo-thn-ypa>
28. Pai, Shalini Govil. "Principles of Computer Graphics." Google Books. Springer, -. Web. 17 May 2017. Available from:
https://books.google.gr/books/about/Principles_of_Computer_Graphics.html?id=d7Hd3A0bEx0C&redir_esc=y
29. Agency, Environmental Protection. "U.S. EPA Methods for Air Analysis." Handbook of Environmental Analysis (2010): 691-96.
30. Frangoul, Anmar. "Around 2.2 Million Deaths in India and China from Air Pollution: Study." CNBC. CNBC, 14 Feb. 2017. Web. 21 May 2017. Available



from : <http://www.cnbc.com/2017/02/14/around-22-million-deaths-in-india-and-china-from-air-pollution-study.html>

31. Rinkesh. "Causes, Effects and Solutions of Air Pollution." Conserve Energy Future. Conserve Energy Future, 03 Jan. 2017. Web. 21 May 2017.
32. Agency for Toxic Substances. "Toxic Substances Portal - Sulfur Dioxide." Centers for Disease Control and Prevention. Centers for Disease Control and Prevention, 21 Jan. 2015. Web. 21 May 2017. Available from: <https://www.atsdr.cdc.gov/phs/phs.asp?id=251&tid=46>
33. Green Facts. "Air Pollution Nitrogen Dioxide." How Does Nitrogen Dioxide (NO₂) Affect Human Health? -, -. Web. 21 May 2017. Available from: <https://www.greenfacts.org/en/nitrogen-dioxide-no2/level-3/02-health-effects.htm>
34. Scottish Environment Protection Agency. "Carbon Dioxide." Pollutant Fact Sheet. SEPA, n.d. Web. 21 May 2017. Available from: <http://apps.sepa.org.uk/spripa/Pages/SubstanceInformation.aspx?pid=2>
35. Shochat, Guy N., and Michael Lucchesi. "Carbon Monoxide Toxicity." Background, Pathophysiology, Epidemiology. -, 28 Dec. 2016. Web. 28 June 2017. Available from: <http://emedicine.medscape.com/article/819987-overview>
36. "Air Pollution Ozone." Ozone: 2. How Does Ozone (O₃) Affect Human Health? Greenfacts, n.d. Web. 28 June 2017. Available from: <https://www.greenfacts.org/en/ozone-o3/l-2/2-health-effects.htm>
37. Hoffmann, Gabriel M., et al. "Helicopter Flight Dynamics– an Introductory Tour." Helicopter Flight Dynamics, pp. 9–86., Available from: <https://pdfs.semanticscholar.org/f6a9/522225a98956d390f3d342244868867c472c.pdf>
38. DJI. Phantom 4 Series Intelligent Flight Battery. DJI Man. 2016;4–7.
39. HELIBOSS. Phantom 4. 2016;4–6. Available from: <http://heliboss.co/DJI-Drones/phantoms/Drone-phantom4/phantom4>
40. Libelium, "Waspmove", tech. rep., University of Zaragoza, Spain, March 2011.
41. D. Gascon, 12km zigbee link with waspmote. Research Article, 2010
42. Libelium, "Meshlium", tech. rep., University of Zaragoza, Spain, 2011
43. Libelium. "Smart Gases Pro Technical Guide." Smart Gases Pro Technical Guide, pp. 40–69 Available from: www.libelium.com/downloads/documentation/gases_sensor_board_pro.pdf
44. Childs, Collins. "Interpolating Surfaces in ArcGIS Spatial Analyst." (2004): 1–4.



ESRI Education Services, July 2004. Web. 1 July 2017.
<https://www.esri.com/news/arcuser/0704/files/interpolating.pdf>

45. Datasheet of MICS-4514, CO and NO₂ gas sensor from e2v, A1A-MiCS-4514 Version 2, July 2008, Available from:
http://www.e2v.com/assets/media/files/sensors_datasheets/Metal_Oxide/mics-4514.pdf
46. Datasheet of SO₂-BF Sulfur Dioxide Sensor, Available from:
<http://www.alphasense.com/pdf/SO2BF.pdf>
47. Alphasense Application Note AAN 104, How electrochemical gas sensors work, Available from: http://www.alphasense.com/pdf/AAN_104.pdf
48. Alphasense Application Note AAN 107-06, INTRINSIC SAFETY INFORMATION FOR APPROVALS, Available from: http://www.alphasense.com/pdf/AAN_107-06.pdf
49. Alphasense Application Note AAN 201-05, NDIR: Gas Concentration Calculation Overview, Available from:
http://www.alphasense.com/pdf/NDIR/AAN_201-05.pdf



Appendix A

This Section presents an approach to locate the disastrous “tristeza” virus using an RGB camera of an Unmanned Aerial Vehicle. In order to successfully locate the affected trees in a citrus field, two different photogrammetric software have been used, Pix4D and DroneDeploy.

Use of UAVs for locating the “Tristeza” virus in the citrus trees

1 Introduction

Early and accurate detection and diagnosis of plant diseases are key factors in plant production and the reduction of both qualitative and quantitative losses in crop yield. Optical techniques, such as RGB imaging, multi- and hyper spectral sensors, thermography, or chlorophyll fluorescence, have proven their potential in automated, objective, and reproducible detection systems for the identification and quantification of plant diseases at early time points in epidemics. Recently, 3D scanning has also been added as an optical analysis that supplies additional information on crop plant vitality. Different platforms from proximal to remote sensing are available for multi-scale monitoring of single crop organs or entire fields. Accurate and reliable detection of diseases is facilitated by highly sophisticated and innovative methods of data analysis that lead to new insights derived from sensor data for complex plant-pathogen systems. Tree growth and survival depends on climatic conditions, which influence processes like photosynthesis and respiration. Thus, change in climate and weather conditions will inevitably influence forest health and growth. As temperature and moisture affect pathogen growth, reproduction and infection, climate changes will also indirectly affect the distribution and abundance of forest pathogens, as well as the severity of tree diseases. The pathogens requiring moist conditions will have an increased impact on host trees where wetter future conditions are predicted. These pose a significant risk to forests worldwide, having the potential to cause the death of many trees. As regards the Tristeza virus, is a chronic problem for oranges-mandarin growers in the prefecture of Chania. As mentioned above, the problem of Tristetsa has been harassing the producers for many years and is only dealt with by the eradication of the diseased trees. The problem is mainly located in the geographical limits of the Municipality of Platanias Chania and east of the artificial lake of Agia. The detection and monitoring of affected trees is



therefore crucial for allowing management interventions to reduce the spread of infections. Symptoms of tristeza infection are highly variable and depend on several factors including host, virulence of the particular virus strain, and environmental conditions. The three most common groupings of symptoms are decline (quick and slow), stem-pitting, and seedling yellows. Decline is generally exhibited with sweet orange, mandarin, or grapefruit when they are grafted on infected sour orange rootstock. This decline includes chlorotic leaves and general dieback of the infected tree. Decline may be slow, lasting several months to years after the first symptoms are noticed. In this case the infected tree will also show a bulge above the bud union and honeycombing on the inner face of the original sour orange root stock bark. The decline may also be quick, resulting in host death just days after the first symptoms are noticed. Stem-pitting is another symptom of tristeza that manifests in most host types under the proper conditions, and especially in Citrus trees grafted onto sour orange rootstock. The host will develop pits in the trunk and stem. This result is decreased tree vigor and reduced fruit yield. The third major symptom of tristeza infection is seedling yellows. Symptoms include yellowing of foliage and general dieback.

2 System Specifications

UAV platform

The unmanned aerial vehicle used for this study was the quad-rotor DJI's Phantom 4 (Figure 1) capable of performing 28 minute long flights. It has 10m/s maximum wind speed resistance and take-off weight of 1380 g. It was developed to carry a RGB (red, green and blue) and is equipped with gimbals minimizing cameras movements in the roll axis during the flight.

Sensors

The RGB camera used for this study is a 4k camera, featuring video capture at 30 frames per second and Full HD 1080p at 120 frames per second for smooth slow motion. An aspherical lens with a 94° field of view (FOV) reduces distortion by 36% and chromatic aberration by 56% when compared to previous models. In addition, a hyperfocal length of one meter allows getting closer to objects while keeping them in pin-sharp focus. The camera has a resolution of 4000×3000 pixels (VGA) and automatically provides video feedback on a screen (e.g., smartphone). Moreover, an advanced 3-axis gimbal takes out unwanted vibration and movement in-flight. This gimbal is accurate to a highly precise $\pm 0.03^\circ$,



coupled with custom designed dampers enabling the camera to capture smooth and fluid footage even during complex maneuvers.



Figure A1: The DJI's Phantom 4

Ultrasonic sensors combine with advanced computer vision and processing to give the ability to Phantom to provide altitude measures for automatic altitude stabilization and assisted vertical speed control. If due to environmental conditions the distance from the terrain changes, the acquired point cloud should be scaled accordingly. Several software solutions are freely available for download over the Internet for the automatic navigation control of drones. In this study, the app of Pix4D, Pix4Dcapture, was used to create the flight plan and fly autonomously the UAV.

3 Data Acquisition

The study was located at Kofou , a village near the city of Chania.



ΕΘΝΙΚΟ ΚΤΗΜΑΤΟΛΟΓΙΟ
& ΧΑΡΤΟΓΡΑΦΗΣΗ Α.Ε.



Figure A2: Area of study

Kofou is approximately 14,6 km away from Chania and it is near the artificial lake of Agia.

Ground Images

To accompany the remote sensing data acquisition, for each of the sample trees, extensive ground images of the infected trees were collected. Furthermore, we extracted the GPS of the grounded images in order to visualize the position of the infected trees. We used the “Photo GPS Extract” software, which gave our data to a .kml form. The following figures show the position of the stressed trees, through Google Earth pro.



Figure A3: Infected trees

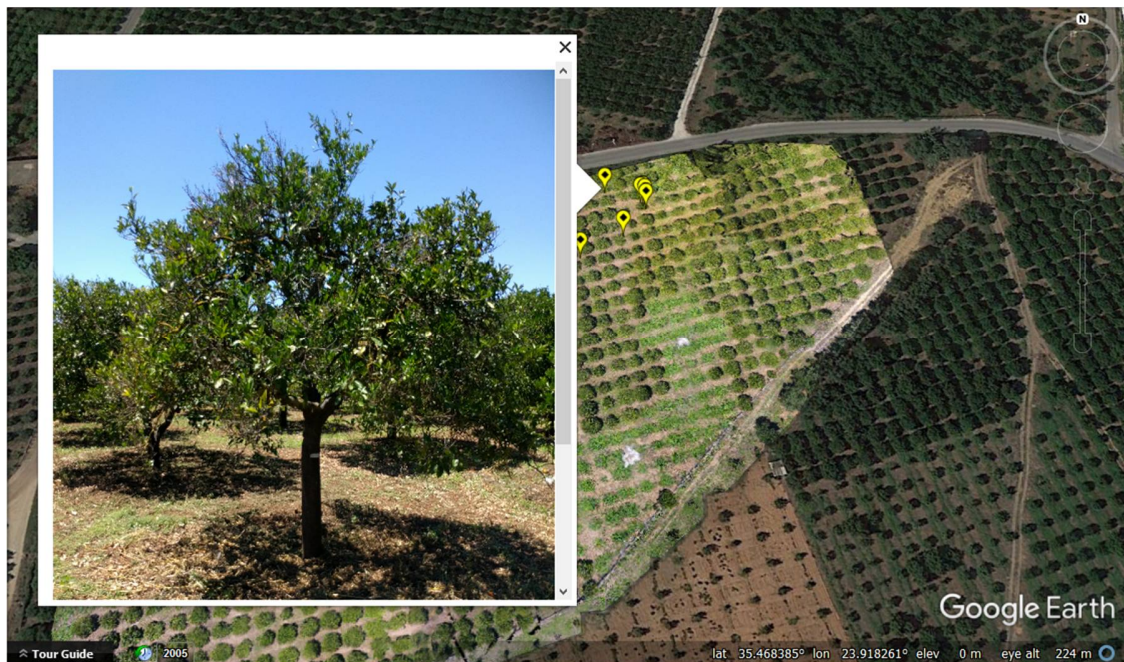


Figure A4: The infected trees through Google Earth



Tristezza trees

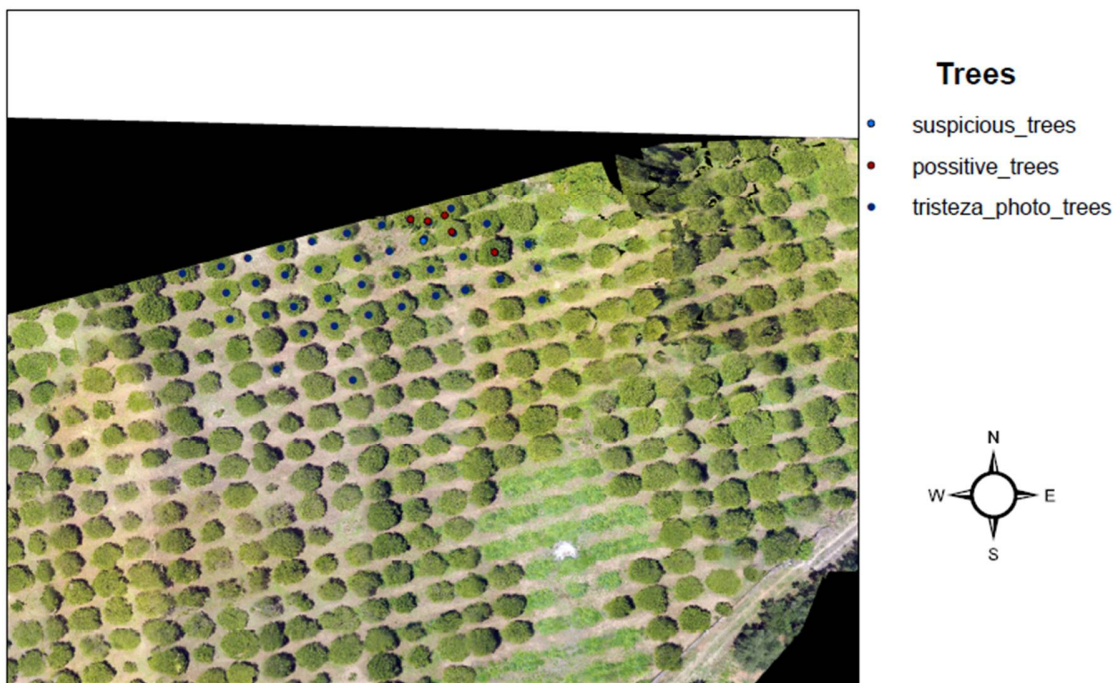


Figure A5: The stressed trees on the map

Remote Sensing

The flight of the quad-rotor UAV was, late in the noon, a dataset from the UAV system was collected for two of the research plots. The data was collected at the height of 40 m. The following figure shows the flight plan above the field.



Figure A6: The flight plan



4 Data Processing

In total 167 images were taken and were processed in Pix4Ddeskop. The outputs were a 3D mesh of the field, an orthomosaic and a digital surface model (DSM). We observed that some trees could not be illustrated 3D. After locating these trees, we figure out that they were stressed ones.

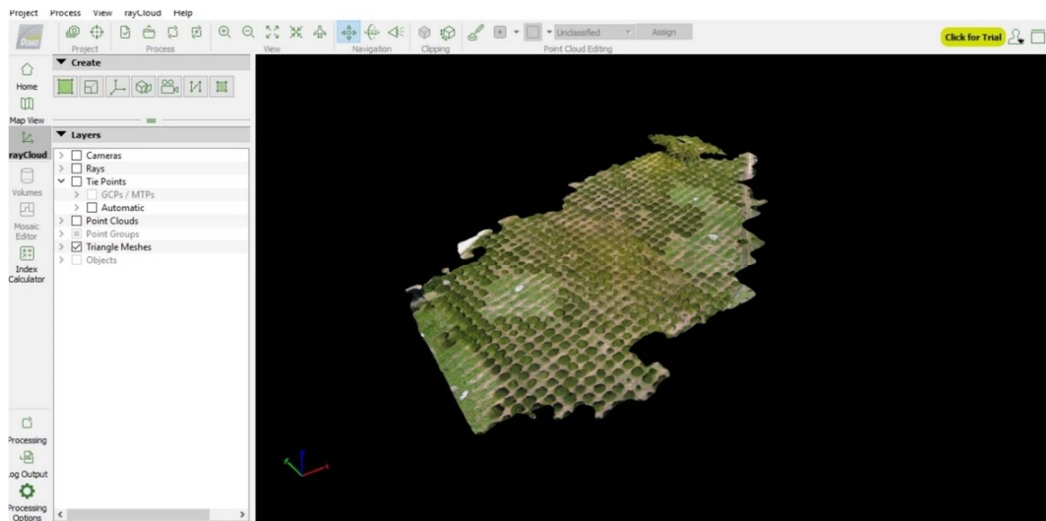


Figure A7: The 3D mesh

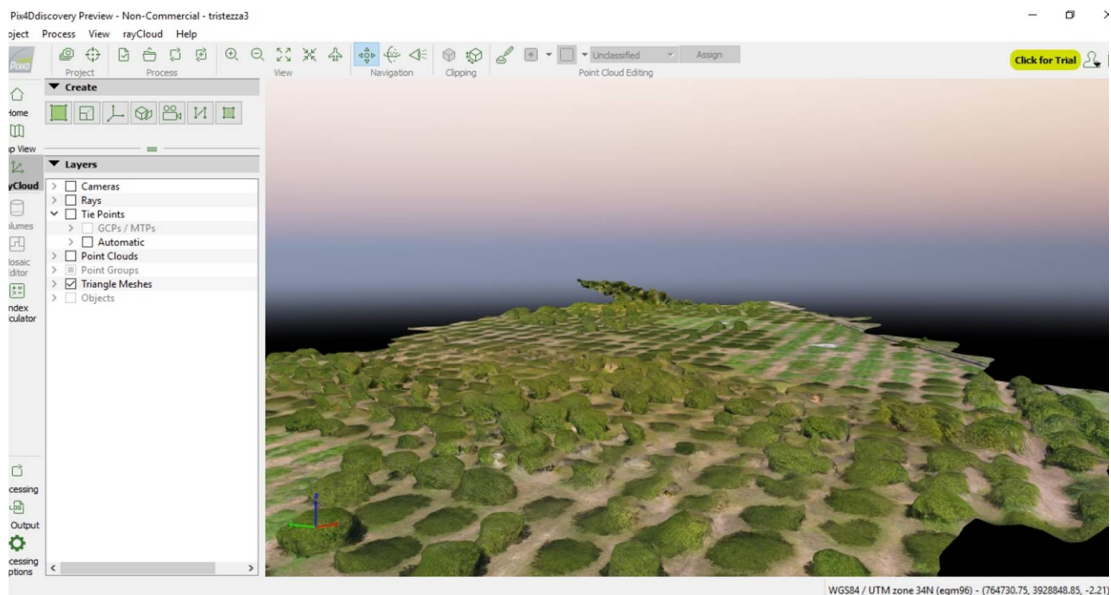


Figure A8: The trees that couldn't illustrated in 3D

After the 3D mesh outputs, the mosaic models were exported both at .jpg and .kml format.



Figure A9: The orthomosaic

Furthermore, the DroneDeploy online software was used in order to apply algorithms, which investigate the plant health. The first algorithm was the Visible Atmospherically Resistant Index (VARI) algorithm. VARI was designed and tested to work with RGB data rather than near-infrared (NIR) data. It is a measure of "how green" an image is. VARI is not intended as a substitute for a NIR camera, but it is meaningful when working with non-NDVI imagery.



Figure A10: The result of the VARI algorithm

Moreover, the second algorithm was the Enhanced Normalized Difference Vegetation Index (ENDVI). ENDVI includes a comparison of Green light in



addition to NIR, Red, and Blue in order to give a more sensitive result. This isolates the indicators of plant health, and can be used to assess the presence and health of a crop.



Figure A11: The result of the ENDVI algorithm

Comparing the two algorithms ENDVI gave more accurate results about the location of the stressed trees. In addition, the GPS from the ground pictures was extracted to locate the known infected trees. Using ArcMap software, a map of the known infected trees was constructed. The blue dots show the affected trees by the tristezza virus.

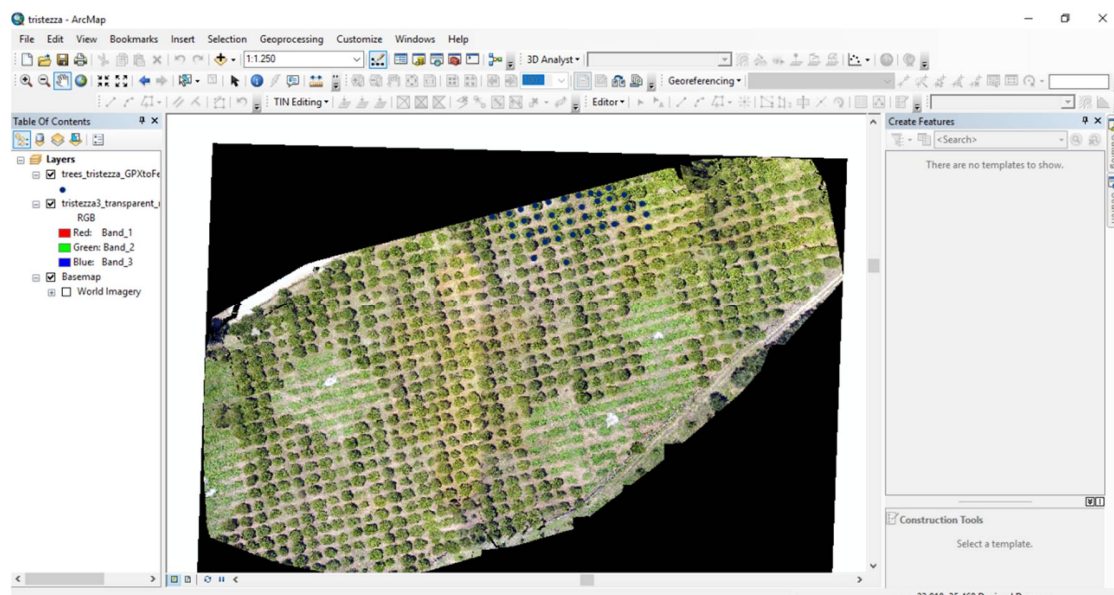


Figure A12: The constructed map with the known infected trees



Furthermore, an algorithm from Matlab that isolates the green color of an image was applied. The idea behind this application was that, if it was possible to isolate only the green pixels of an image, then it should be possible to locate, not necessarily the infected trees, but the “suspicious” ones.

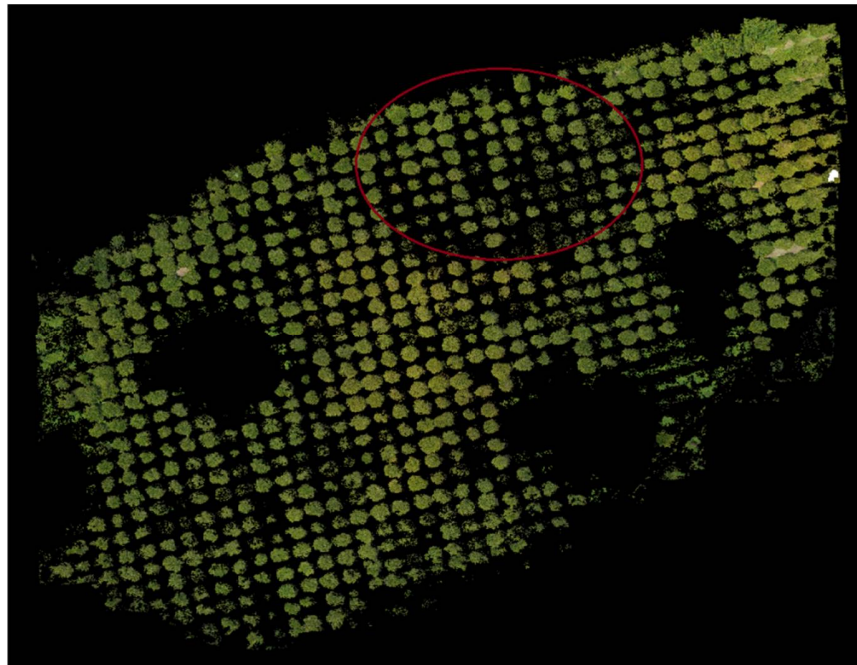


Figure A13: The result after isolating only the green pixels

As the results show, trees with high density of green pixels seem to be healthier in contrary with trees with low density of green.

5 Conclusions

Remote Sensing is a useful tool that applies in many areas. In this study we used an RGB (Red, Green, Blue) Camera of an Unmanned Aerial Vehicle in order to locate the “Tristeza” virus on a field. Unfortunately, the equipment wasn’t the best for an application such as this, since the crop health needs to be investigated with multi-spectrum and thermal cameras. Nevertheless the results were efficient, since we could locate the area, and in cases the exact trees, which carry the tristeza virus. The 3D model of the field, gave us the opportunity to do a spatial analysis of the crop and the applied algorithms gave us a first view of the health of the trees. However, further investigation with more accurate tools is suggested.